ANALYSIS AND DESIGN OF NANOANTENNAS

WU YU-MING

B. ENG. , HARBIN INSTITUTE OF TECHNOLOGY

A THESIS SUBMITTED
FOR THE DEGREE OF DOCTOR OF PHILOSOPHY
DEPT. OF ELECTRICAL & COMPUTER ENGINEERING
NATIONAL UNIVERSITY OF SINGAPORE
2010

Abstract

The focus of this thesis is put on the investigations of single and multiple metallic nanoparticles for their near-field optical and far-field radiation properties. In particular, we elaborately design and carefully analyze such structures to perform their functions as the nanoantennas operating in the optical range. Nanoantennas have been found capable of producing strong enhanced and highly localized light fields. Existing research on them has shown their considerable applications in diverse fields such as the near-field optical microscopy, spectroscopy, chemical-, bio-sensing, and optical devices. Thus the useful results prompt us to implement a more systematic and further exploration on nanoantennas of some specific configurations of interest.

In our present work, the nanoantenna's operating mechanisms of nanometric localized surface plasmon resonances are demonstrated through the material's characterization. A study on the accurate description of dispersive dielectric constant is conducted to successfully overcome the limitations by utilizing classical models in previous research. In addition, some theoretical methods suggested for characterizing nanoantennas are discussed together with comparisons. An appropriate numerical approach is developed for a more effective calculation of nanoantennas covering the broad frequency range including visible and infrared region. Compared with the conventional methods, the results show important improvement in enhancing the efficiency of nanoantenna applicable frequency band.

Comprehensive investigations are carried out and presented in detail on various factors which have significant impacts on the nanoantenna's performance in the optical range. The nanoantenna designs explored in this thesis cover the single nanoparticles and closely placed coupling nanoparticle pairs of a few different shapes, and the nanoparticle chain and array consisting of consistent or varying components. Sufficient number of factors influencing these nanoantennas' optical properties are

adequately described and determined. Some of them are innovatively proposed for the first time to conduct a comprehensive study on tunable features of the nanoantennas, such as the nanospheroid pair and bow-tie aperture nanoantenna. Under certain restriction conditions, the comparisons among the designs with varying parameters are provided for intuitionistic understanding. In this way, the nanoantenna performance becomes controllable by changing the values of these specifications and the optimization design can be theoretically implemented by further adjustment. Compared with current studies on the nanoantennas, this study contributes to a more effective and helpful guidance for the nanoantena's design. This is of great practical design importance.

Instead of nanoantenna studies demonstrated by the near-field optics background of common research concern, the specific study based on the engineering electromagnetics' theory to describe their far-field radiation characteristics is conducted in this work. Some design specifications for the conventional radio frequency antenna such as the radiation patterns, gain and directivity are computed for our nanoantennas in quantity. Such a study extends current research topics by providing more valuable insight.

Further fabrication and measurement of our designed nanoantennas with desirable performance are considered as a future research topic.

to my parents

Contents

List of Figures

List of Tables

Acknowledgements

First and foremost, my deepest gratitude goes to my supervisors, Prof. Le-Wei Li and Dr. Bo Liu for their invaluable guidance, constant supports, and kindness throughout my postgraduate program. Without their advice and encouragement, this thesis would not have been possible.

I would also like to express my heartfelt gratitude to Dr. Wei-Bin Ewe, Mr. Chun Tong Chiang, Dr. Hailong Wang for their valuable suggestions and helpful discussion. I would also be grateful for Prof. Xudong Chen, Prof. Minghui Hong for their attention and suggestions on my research.

I also owe my sincere gratitude to the members of Radar Signal Processing Laboratory: Dr. Haiying Yao, Dr. Fei Ting, Miss Yanan Li, Dr. Chengwei Qiu, Dr. Tao Yuan, Dr. Kai Kang, Dr. Hwee Siang Tan, Dr. Haoyuan She, Mr. Li Hu, Mr. Kai Tang, Miss Huizhe Liu, Miss Pingping Ding, Miss Dandan Liang, and Mr. Jack Ng. They have helped me a lot in the past four years.

Special thanks should go to my friends Dr. Xiaolu Zhang, Dr. Guang Zhao, Dr. Fugang Hu, Miss Jing Zhang, Miss Hanqiao Gao, Mr. Tianfang Niu, Mr. Zheng Zhong, and Dr. Yu Zhong, who shared with me a pleasant life in Singapore.

Importantly, I am grateful to my beloved parents for their love and great support all through these years. Thank goes to my father because he led me into the fantasy world of research as my teacher and model. Thank goes to my mother for her selfless care as my intimate friend. I am also grateful to my passed grandfathers and grandmothers for their love and support forever.

List of Publications

Journal Papers

[1] **Yu-Ming Wu**, Le-Wei Li, and Bo Liu, "Gold Bow-tie Shaped Aperture Nanoantenna: Wide Band Near-field Resonance and Far-field Radiation", *IEEE Trans. Magn.*, vol. 46, No. 6, pp. 1918-1921, 2010.

[2] **Yu-Ming Wu**, Le-Wei Li, and Bo Liu, "Optical Resonance of Nanoantenna consists of Single Nanoparticle and Couple Nanoparticle Pair ", submitted to *Opt. Express*.

[3] **Yu-Ming Wu**, Le-Wei Li, and Bo Liu, "Effects in Designing Nanometer Scale Antennas with Coupling Structures", submitted to *Opt. Express*.

[4] Qun Wu, Yue Wang, **Yu-Ming Wu**, Lei-Lei Zhuang, Le-Wei Li, and Tai-Long Gui, "Characterization of the radiation from single-walled zig-zag carbon nanotubes at terahertz range", Chin. Phys. B Vol. 19, No. 6, pp. 067801, 2010.

[5] C. Y. Chen, Q. Wu, X. J. Bi, **Y. M. Wu**, and L. W. Li, "Characteristic Analysis for FDTD Based on Frequency Response", *J. Electromagn. Waves Appl.*, vol. 24, no. 2-3, pp. 283-292, 2010.

Conference Papers

[6] **Yu-Ming Wu**, Le-Wei Li, and Bo Liu, "Geometric Effects in Designing Bow-tie Nanoantenna for Optical Resonance Investigation", in Prof. of *APEMC'10*, Beijing, China, Apr. 12-16, 2010.

[7] **Yu-Ming Wu**, Le-Wei Li, and Bo Liu, "Gold Bow-tie Shaped Aperture Nanoantenna: Wide Band Near-field Resonance and Far-field Radiation", in Proc. of the *11th Joint MMM Conference"*, Washington, DC, USA, Feb. 2010.

[8] **Yu-Ming Wu**, Le-Wei Li, and Bo Liu, "Optical Resonance of Nanometer Scale Bow-tie Antenna and Bow-tie Shaped Aperture Antenna", in Proc. of *APMC'09*, pp. 543-546, Singapore, Dec. 2009.

[9] **Yu-Ming Wu**, "Resonance of Coupled Gold Nanoparticles as Effective Optical Antenna", *IEEE R10 student paper contest'09*.

[10] **Yu-Ming Wu**, Le-Wei Li, and Bo Liu, "Light Scattering by Arrays of Gold Nanospheres and Nanoellipsoids", in Proc. of *APEMC'08*, pp. 586-589, Singapore, May 2008.

[11] **Yu-Ming Wu**, Le-Wei Li, and Bo Liu, "Nanoantennas: From Theoretical Study of Configurations to Potential Applications", in Proc. of *ISAP'07*, pp. 908-911, Niigata, Japan, Aug. 2007.

[12] Yue Wang, **Yu-Ming Wu**, Lei Lei Zhuang, Shao-Qing Zhang, Le-Wei Li, and Qun Wu, "Electromagnetic Performance of Single Walled Carbon Nanotube Bundles", Proc. of *APMC09*, Singapore, Dec. 2009.

[13] Qun Wu, Lu-Kui Jin, **Yu-Ming Wu**, Kai Tang, and Le-Wei Li, "RF Performance of rec-BCPW and arc-BCPW DMTL Millimeter-Wave Phase Shifters", in Proc. of *APMC09*, Singapore, Dec. 2009.

[14] Shao-Qing Zhang, Lu-Kui Jin, **Yu-Ming Wu**, Qun Wu, and Le-Wei Li, "A Novel Transparent Carbon Nanotube Film for Radio Frequency Electromagnetic Shielding Applications", in Proc. of *APMC'09*, Singapore, Dec. 2009.

[15] Yue Wang, Qun Wu, **Yu Ming Wu**, Lei Lei Zhuang and Le Wei Li, "Performance Predictions of Carbon Nanotubes Loop Antenna in the Terahertz Region", in Proc. of *International Conference on Nanoscience and Technology*, Beijing, China, Sept. 2009.

[16] Kai Tang, **Yu-Ming Wu**, Qun Wu, Hai-Long Wang, Huai-Cheng Zhu and Le-Wei Li, "A Novel Dual-Frequency RF MEMS Phase Shifter", in Proc. of *APEMC'08*, pp. 750-753, Singapore, May 2008.

List of Abbreviations

RF	radio frequency
EM	electromagnetic
VLF	very low frequency
LF	low frequency
MF	medium frequency
HF	high frequnecy
VHF	very high frequency
UHF	ultra high frequency
mm	millimeter
IR	infrared
NIR	near infrared
NSOM	near-field scanning optical microscope
SERS	surface enhanced Raman scattering
SP	surface plasmon
SPP	surface plasmon polariton
SPR	surface plasmonic resonance
LSPR	localized surface plasmonic resonance
FDTD	finite difference time domain
FEM	finite element method
MWS	Microwave studio

FIT	finite integration technique
LSP	localized surface plasmon
IE	integral equation
MOM	method of moments
BEM	boundary element method
FMM	fast multipole method
PDE	partial differential equation
MMP	multiple multipole program
BC	boundary conditions
AFM	atomic force microscopy
FIB	focused ion beam
3D	three-dimensional
2D	two-dimensional
PSTM	photon scanning tunneling microscope

Notations

When dealing with the electromagnetic field analysis and characterization of material, some of our notations and some constants are given here.

- E electric field
- H magnetic field
- J electric current density
- M magnetic current density
- ϵ_0 permittivity of free space ($8.854 \times 10^{-12} F/m$)
- μ_0 permeability of free space ($4\pi \times 10^{-7} H/m$)
- n refractive index
- k extinction coefficient, when appearing together with n; propagation constant, when appearing together with r or a
- N complex index of refraction
- λ wavelength
- ω radian frequency, equal to $2\pi f$

Upright letters like $\mathbf{E}$ are used to denote vector. On the contrary, ordinary italic letters like E are used to denote scalar. Those letters with a cap such as $\hat{r}$ and $\hat{x}$ mean they are unit vector in that direction. In antenna design applying specifications, some parameters are illustrated as follows:

- $U(\theta, \phi)$ radiation intensity

- P power
- R resistance

Chapter 1

Introduction

The antenna is a transducer designed to transmit or receive electromagnetic waves. As a commonly used device in the modern society, antennas have been widely used in the systems such as the radio and television broadcasting, radar, and space exploration. To evaluate the performance of an antenna, its specifications are very important in both its design and its measurement. The antenna specifications of interest generally include the radiation pattern, gain, efficiency, and bandwidth. These specifications can be adjusted during the design process. In addition, the performance of an antenna can be tested in the measurement to ensure that the antenna meets the required specifications in the design. The antenna's measurement involves the regions of near field and far field. These two regions are defined for research convenience to identify the field distribution of the antenna. In the near field region, the antenna does not radiate all the energy to infinite distances; rather, some energy remains trapped in the area near the antenna. Therefore the angular field distribution is very much dependent upon the distance from the antenna. In the far field region, however, the energy is radiated to the infinite distance from the source, so that the angular field distribution is independent of this distance. The antenna's performance in the

far field region is of main concern, because the antenna is conventionally studied for its radiation performance in the radio frequency (RF) or microwave range.

Antennas are very helpful in the communications and have been continuously demanded over the last several decades. Various theories have been well established to analyze their properties and considerable experiments have been extensively conducted to improve their performances and designs. The existing investigations on the traditional antennas have shown many useful applications. However, the applications of most popular antennas are mainly restricted to the radio/microwave frequency in the electromagnetic (EM) spectrum particularly for wireless communications. The whole EM spectrum covering different frequencies/wavelengths is given in Fig. 1.1. The visible light forms a small part of the spectrum. Inside the EM spectrum, the radio frequency band is further divided into small sub-bands with different names allocated for different applications, which can be seen from Fig. 1.2. These frequency bands with increasing sequence are respectively the very low frequency (VLF), low frequency (LF), medium frequency (MF), high frequnecy (HF), very high frequency (VHF), ultra high frequency (UHF), microwave (including L-, S-, C-, X-, K_u-, K- and K_a- bands), and millimeter (mm) wave band. The radio frequency spectrum has been allocated so intensively that few resources of the RF range remain for study. On the contrary, sufficient resources of infrared (IR) and visible light range are left for further exploration. As a result, researchers have been attempting to find the optical antennas with higher performance applicable for optical communications.

The optical antenna, also known as nanoantenna, is a light coupling device con-

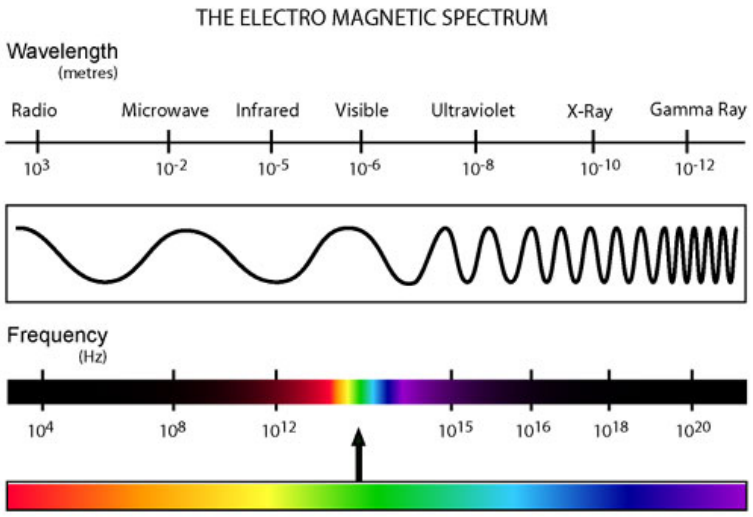

Figure 1.1. The whole electromagnetic spectrum.

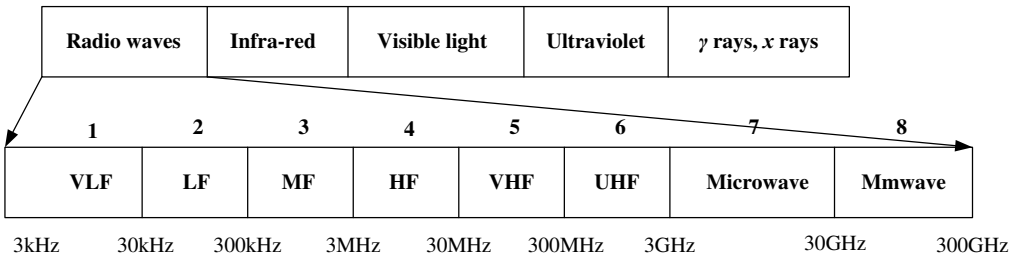

1. submarine communications, time signals, storm detection
2. broadcasting (long wave), navigation beacons
3. broadcasting (medium wave), maritime communications, analogue cordless phones
4. broadcasting (short wave), aeronautical, amateur, citizen band
5. FM broadcasting, business radio, aeronautical
6. TV broadcasting, mobile phones, digital cordless phones, military use
7. point to point links, satellites, fixed wireless access
8. point to point links, multimedia wireless systems

Figure 1.2. The applications for sub-bands of RF inside electromagnetic spectrum.

sisting of nanometer scale metallic particles, which operates in the optical range. The nanoantenna's study is of great significance. On one hand, the utilization of nanoantennas solves the problem of insufficient usage of EM spectrum in the optical communications. They can serve as the far-field radiation devices. Nanoantennas successfully take full advantage of the available resources of the IR and visible ranges in terms of considerable sophisticated designs. By exploiting the nanoantenna counterparts as those conventional RF antennas based on the same referential antenna theories, potential similar or even updated properties can be found and more helpful applications can be developed in the optical range. Nanoantennas may be used and integrated into the high density optical circuits. In addition to possessing the properties of the conventional antennas, the nanoantennas also benefit from wider bandwidth compared with the traditional antennas. That is because the optical frequency is much higher than the frequency used in the wireless communications. Above considered meaningful nanoantenna research for optical communication purpose closely relates to the antennas' radiation performance in the far-field, which is more of researchers' concern regarding the conventional antenna design. On the other hand, the nanoantennas are able to produce promising results over the traditional antenna, especially in the near-field applications. They are found to be capable of producing giant concentrated and highly localized fields with the size as small as tens of nanometers, thus improving the size mismatch between the diffraction limited light spot excited by light source and fluorescent molecules which are much smaller than the excitation wavelength [1]. So another importance of the nanoantennas lies in the fact that they can act as the bridge for the coupling between the microstructure

of small-sized particles and the macrostructure of continuous medium. However, so far all these attractive nanoantenna applications have not been fully explored yet. In a word, the increasing advances in nanoscience and nanotechnology, the improvement of fabrication techniques and the developments of optical measurement devices prompt the further development of optical antennas, thus making the theoretical study of optical antennas desirable to uncover their underlying mechanism and unknown characteristics.

Compared with the conventional antenna in RF, the nanoantenna in optical frequency is an innovative concept worth of further analysis. Nanoantennas have various unique properties mainly in the material, dimensional and methodological aspects. In the material aspect, metals are no longer ideal conductors with all charges on their surfaces in the optical range. Instead, they turns to exhibit dielectric properties. To describe such changed material properties, the dielectric constant is actually frequency-dependent, which needs special characterization. In the dimensional aspect, as the particles' size decreases to the nanometer scale, the continuous band structures of the bulk materials transit to the discrete localized energy level and the quantum effects become apparent. However, insufficient knowledge is known in this nanophase material for antenna design. Though the measurements seem to be an important characterization approach for understanding the quantum effects, they are limited by current machining precision and testing condition. In the methodological aspect, nanoantenna generally applies direct light excitation instead of power guided from the matching or feeding devices. Therefore most present studies of the nanoan-

tennas are based on the background of optics and microscopy. More investigations based on the electromagnetic theory and engineering fundamentals are needed. In this thesis, we focus our study on the electric properties of the nanoantenna, particularly on discovering the efficient designs for satisfactory performance and on conducting detailed analysis of its resonance properties in the near-field.

1.1 Review of the Studies on Nanoantennas

The concept of the "nanoantenna" was firstly proposed for the nanoparticles' resonant characteristics as the resonators for local field enhancement [2], and once seemed innovative. The extraordinary effects of surface plasmon of metallic nanoparticles induced by light and the interaction between them have drawn extensive research interest over past few years. The nanoparticles is capable of focusing and confining visible and near infrared (NIR) lights into nanometer scale dimensions by employing surface plasmon resonance, thus generating local enhanced fields with considerable magnitude [1; 3]. In view of the local field concentration and enhancement effects, these metallic nanoparticles have been proposed to be used as the optical nanoantennas or plasmonic resonant antennas [4; 5; 6] and investigated extensively [7; 8]. In particular, the nanoantenna is famous for their ability to provide sub-diffraction limit resolution in near-field optics and photonics, which results in great improvement over the other near-field probes. In the conventional optical imaging system like the optical lenses, the resolution of standard optical microscopy is limited by a diffraction limit which is related to the wavelength. This diffraction limit originates

from the fact that it is impossible to focus the light to a spot smaller than half of its wavelength. In practice, this means that the maximal resolution in the optical microscopy is ∼250-300 nm in the optical range. However, the nanoantennas can create sub-wavelength enhanced fields even confined to region ∼20 nm in size, which significantly defeating the diffraction limit. Thus the confined light spot generated by the nanoantenna can be used as an advantage to selectively illuminate the samples in a near-field scanning optical microscope (NSOM) to examine more detailed features [9]. Recently the nanoantennas are specifically designed to produce intense optical fields confined to subwavelength spatial dimensions when illuminated at the resonant wavelength. Nanoantennas based on surface plasmon resonance have diverse applications in the near-field sample or molecule detection/emission [10; 11; 12; 13; 14], surface enhanced Raman scattering (SERS) [15], optical microscopy [16; 17; 18] or imaging [19; 20], spectroscopy [21], high-density optical data storage [22], photonic devices for chemical and bio-sensing [23; 24; 25; 26], and optical circuits [27].

Currently investigated nanoantennas include various designs in terms of different material constitutions, configurations, and arrangements. Firstly, the nanoantenna designs involve different material constitutions: there are the designs which were partially loaded with diverse kinds of materials like the multi-layered materials [19; 28; 29] and the sectional materials [30] and there are also the designs which were entirely filled with a single material like gold, silver and copper [31]. While the antennas with the structures partially loaded with different kinds of materials are very difficult to fabricate in practice, those with the structures fully filled with one kind of material

show a lot of promise. Among the various materials used for nanoantennas, gold has the obvious advantage of suffering from less oxidation than the other materials in the optical range. Secondly, the nanoantenna designs have different configurations which consist of particles of many shapes. For a single particle, the shapes of sphere [10; 32], ellipsoid [33], cylinder (including wire [34; 35; 36; 37], monopole [38; 39; 40], elliptical and triangular cylinder [41], triangle [42], pentagon [43] have been studied. For two coupling particles, the shapes of sphere [44], dipole [5], nanorod [45; 46], disks [47; 48], elliptical pairs [49], and triangles (*i.e.* bowtie) [1; 50] have been explored. A range of plasmon resonances for a variety of particle morphologies can be found in [51]. In fact, it is found the optical properties of nanoantennas are very sensitive to the nanoparticle size, shape, and local dielectric environment [25; 52]. However, these shapes were studied separately or only some limited kinds of shapes were studied together. So far there has been no comprehensive study of the shape effects on the light intensity. One exception was that in [43], which studied the effect of shape on the spectral response. But in their study, silver was used for the material, which is not as good as gold. Similarly, another exception was the study conducted in [2], which conducted a systematic investigation of the shape, length, sharpness effects on light intensity. However, this study did not examine comparable measurements of the light intensity spectrum. At the same time, in this paper, the simulation band was limited to the infrared range, thus a broadband study containing the visible range needs to be considered. Thirdly, the nanoantenna designs possess different arrangements from single antenna component to antenna particle-chain [16; 53] and array [54; 55; 56; 12; 29]. Among these designs, the nanoantennas which can be

successfully fabricated are considered more practical than those which can only be analyzed in theory, so the practical nanoantenna designs will be focused on with more research interest for referential purpose.

1.2 Optical Properties of Metals and Surface Plasmon Resonances

In order to understand various new properties of the nanoantenna, it is essential to understand the nanoantenna's radiation mechanism. Nanoantennas can produce strong focused fields around them, depending on their structures. The field confining structures include the holes or apertures in the metal films, or at the apex of metal-coated fiber probes, as well as the noble metal nanoparticles and their sharp tips. Surface plasmon plays an important role in describing the local fields that occur in such structures. In fact, the function of the nanoantenna is performed through the localized surface plasmon resonance.

The surface plasmons (SPs) are coherent electron oscillations which exist at the interface between metal and dielectric. The surface plasmon phenomena can occur in many situations: the energy loss of electrons propelled through thin metal foils; the colorful appearance of suspensions of small metallic particles (see Fig. 1.3, the ruby color is probably due to the embedded gold nanoparticles.); and the dips in the intensity of light reflected from metal coated diffraction gratings. When excited by the light, such SPs will couple with the photons and result in a collective electron

charge oscillation in the visible and NIR portion of the spectrum. This is equivalent to the surface electromagnetic waves propagating parallel to metal/dielectric interface direction, which is called surface plasmon polariton (SPP).

Figure 1.3. "Labors of the Months" (Norwich, England, ca. 1480).

For the planar surface between metal and dielectric, the SPP is denoted as a surface plasmonic resonance (SPR). The waves yielded by planar interface are evanescent in the perpendicular direction to the interface. While for the system of nanometer-sized metallic structures and dielectric, the SPP is called localized surface plasmonic resonance (LSPR). The electromagnetic field is localized at the nanoparticles and decay away from the nanoparticle/dieletric interface into the dielectric background. The confined fields will dramatically enhance the near field at resonance and thus the light intensity enhancement is a very important aspect of the LSPR. Localization

properties of the LSPR mean very high spatial resolution restricted by the size of nanoparticles and they have various potential useful applications [57]. LSPR's properties are usually dictated by the the metal, geometry and surrounding environment.

One important condition for surface plasmon's existence is that: the two materials should have different signs for the real part of their dielectric functions. This condition is met in the IR and visible wavelength region for metal/dielectric interfaces. In the optical range, metal will exhibit different properties as those in the normal frequencies. Their dielectric constant is a complex value with a negative real part, which magnitude is greater than that of the dielectric, and a small imaginary part. The negative real part is important for the optics of small particles, which can absorb and scatter (*i.e.* the extinction) strongly at certain frequencies which are also dependent on their shapes. In particular, the strong absorbtion by spheres in air occurs at the frequency where its real part of dielectric constant is equal to 2 [58]. This kind of complex values supports strong surface plasmon as well as minimize the loss. Typical metals that support the surface plasmons are silver and gold. But the metals such as copper, titanium, or chromium can also support surface plasmon generation. Surface plasmons have been used to enhance the surface sensitivity of several spectroscopic measurements including the fluorescence, Raman scattering, and second harmonic generation. For the nanoparticles, the localized surface plasmon oscillations can give rise to the intense colors of their solution and cause the very intense scattering of them. The nanoparticles of noble metals exhibit strong ultraviolet to visible absorption properties that are not present in the bulk metals.

Regarding the nanoantennas, the resonances inside the nanoparticles can be explained in terms of different ways. To simplify this problem, a rather straight forward way is to treat the nanoantenna as a simple electric dipole resonator. The nanoantenna's resonant function can be briefly illustrated as the following process to understand. As the metal is confined in all three dimensions for the nanoparticles' case, the plasmon resonance becomes confined as well. During the light illumination, the free electrons inside the metal particles will be induced. These electrons will oscillate in turn with the incident light and create corresponding changing surface charges which accumulate on the opposite sides of the particle. Such charges are resonant in phase with the incident electric field (light) like a polariton and the shift in changing charges results in electromagnetic fields generated in the near-field zone of the metallic nanoparticle. The process of nanoparticles producing electromagnetic waves (light) assembles the RF antenna's radiation properties very much. In this sense, the nanoparticles can be considered as the antennas operating in the optical range. In view of the nanoantenna's radiation mechanism, the concepts of antenna theory can be transferred from the radio frequency region to the optical frequencies. The nanoantennas can be optimized to efficiently collect electromagnetic radiation and confine it to subwavelength dimension.

The resonances of nanoparticles can be solved either by the Maxwell's equations with an electrostatic approximation, or by a full-wave electromagnetic solution with the analytic solution like the Mie theory as well as the numerical methods such as the finite difference time domain (FDTD) method and finite element method (FEM). Take

the case for a small metallic sphere embedded in a dielectric medium as an example. Using quasistatic approximation, the fields inside and outside the sphere are obtained and the polarizability with resonance effects was calculated in [59]. The factors which are mainly responsible for LSPR are found to be size, shape, and dielectric function of the metallic particles. Thus these aspects will be intensively investigated in our work.

1.3 Dielectric Constant Characterization and Dispersion of Metals

During the numerical calculation of the EM fields, the frequency dependent material properties should often be specified by an appropriate formula. For the present problem, in order to describe the existence and properties of the surface plasmons, the simplest way is to treat each material as a homogeneous continuum, characterized by a dielectric constant. For metals at optical frequencies, their dielectric constant ε is frequency dependent and has negative real part as illustrated. In addition, this negative value is of special significance for the small particles because it can result in the local enhanced absorbing and scattering at certain frequencies depending on their shapes and sizes. In particular, the strong absorption occurs when $\varepsilon = -2$ if the first order resonance is considered [58].

In the characterization of the dielectric constant, some classical models have been widely adopted, such as the quantum, Drude, Debye and Lorentz models [60]. The

values of the dielectric constant derived from these models can be applied to the computational EM algorithms for nanoantenna analysis. Currently, one of the popular electromagnetic computational algorithms FDTD has been employed to solve the optical scattering problem of nanoantenna (for a detailed description of the FDTD method, see Chapter 2, Section 2.2). Recent studies have shown the Drude, Debye and Lorentz models are useful to set the dielectric constant in FDTD [61; 62; 63]. Among them, the Drude model has been widely utilized to describe some properties of several metals in the NIR region [58; 64; 65]. In the Drude model, the relative permittivity $\varepsilon_r(\omega) = \varepsilon' + i\varepsilon''$ is expressed in the following formula by

$$\varepsilon_r(\omega) = \varepsilon_\infty - \frac{\omega_p^2}{\omega(\omega + iv_c)}, \tag{1.1}$$

where ε_∞ is the infinity constant, ω_p stands for the plasma frequency, τ denotes the interband relaxation time, and $v_c = \tau^{-1}$. This model describes the dielectric constant in terms of an electrically conducting collective of free positive and negative charge carriers, where the thermal movement of electrons is neglected. For most metals, their plasma frequency is in the ultraviolet range. For copper, it has ω_p in the visible range. For doped semiconductors, ω_p is usually within the IR region. Hence both the real and imaginary parts can be obtained in terms of the plasma frequency. In fact, $\omega_p = \left(\frac{4\pi n_{eff}^2}{m_e}\right)^{1/2}$, where n_{eff} is the effective number density of electrons participating in the intraband transitions. m_{e} and e are free-electron mass and charge respectively. However, there is large sum of variables and each variable's inaccuracy will accumulate in the calculation for final results. Another classical model is the Lorentz model, which

is characterized by the resonance process expressed as

$$\varepsilon_r(\omega) = \varepsilon_\infty + \frac{(\varepsilon_s - \varepsilon_\infty)\omega_0^2}{\omega_0^2 - \omega^2 - i\omega\delta}. \tag{1.2}$$

This formula contains the resonance frequency ω_0 and the damping factor δ.

Besides the Drude and Lorentz models, there is the Debye model described by the relaxation process, which is characterized as

$$\varepsilon_r(\omega) = \varepsilon_\infty + \frac{\varepsilon_s - \varepsilon_\infty}{1 - i\omega\tau}. \tag{1.3}$$

As discussed above, the accuracy of these models is especially important, because these models specify the frequency dependent dielectric constant and influence the final results obtained from the numerical computation method.

Although the Drude, Debye and Lorentz models can describe some aspects of the properties of metallic particles (such as the DC and AC conductivities, the Hall effects, and the thermal conductivities in metals), these models are derived from simple physical models. Therefore they are not sufficiently accurate for the description of all the optical properties of actual metals over a wide frequency range due to their lack of consideration for interband effects [66]. For example, Drude model fails around 1.24-2.48 eV (equivalent to 500-1000 nm in wavelength). This problem of inaccuracy will become even more severe when these models are applied to the numerical EM algorithms like FDTD. To address this problem, some improved approaches have been proposed in recent studies [67; 68; 69; 70]. One approach is to modify a certain model to fit the experimental data in [71; 72; 73] and improve its applied range. For example, a modified Debye model with appropriate parameters has been proposed

in [68] . In this new model, some additional variables were assumed and a gradient optimization was used to decide the values of the variables to achieve a minimum error in comparison with the measured data. At the same time, another modified Debye model was provided in [70]. In this modified model, a large-scale nonlinear optimization algorithm was applied to optimize the parameters to agree with the experimental values over a broad frequency band (effective for 700-1200 nm). Apart from the modified models, a hybrid model like Lorentz-Drude model is also developed in [67; 69], which takes into account the interband transitions. This hybrid method becomes necessary and effective when the wavelength of interest is below 700 nm [74].

Even through these improved approaches are, to some extent, capable of expanding the previously limited band restricted by the classical models, several deficiencies still exist. This influences the reliability of the data of the dielectric constant. Firstly, some variables suggested in the optimization approach [68; 70] are determined by the optimization algorithm instead of being derived from any physical quantity. Although these values of the dielectric constant can better fit the experimental data, the variables assumed in the formulation of the dielectric constant are only applicable for the mathematical operation. Such variables actually have neither rigorous theoretical support nor reasonable physical explanation. Secondly, the hybrid model like the Lorentz-Drude model has unfortunately failed to fit very well the experimental values, for example, $\sim$2 eV for gold [75; 76]. Thirdly, the experimental data used as the reference for the improved models to fit with were dated back to around the 1970's. These data are out of date when compared with the recently obtained experimental

data [77]. Old data's accuracy may be limited by the insufficient machining precision in the fabrication or the poor laboratory condition in the measurement, making the validity of the data questionable. Fourthly, both the modified models and the given data of the dielectric constant are not user friendly to some currently employed commercial 3D electromagnetic simulation software. On the one hand, the software with model setting functions generally only accepts the classical models rather than the modified models. Accordingly further post-processing of the modified models is necessary, but it can be very complicated. For instance, in order to use the modified Debye model in the software of RemCom XFDTD 5.3 using the FDTD algorithm, complex operation process is required to change from the modified model to the Debye model, because only the Debye model can be acceptable by the XFDTD [61]. On the other hand, some software which directly inputs the data of the dielectric constant without the model setting function still requires inconvenient data manipulation for a refined calculation. For example, if the software of Comsol Multiphysic based on the algorithm of FEM is to be used, the experimental data need to be fitted to a polynomial expansion in terms of $1/f$ and this expansion process is very complicated [78] (for details of the FEM method, see Chapter 2, Section 2.2).

In our work, more recent and actual data of the dielectric constant in the handbook [79] collected from the experimental results are adopted. The data are sufficient, effective and convincing for a broad band calculation. In [79], the author selected to tabulate refractive index n and extinction coefficient k. We note that the complex

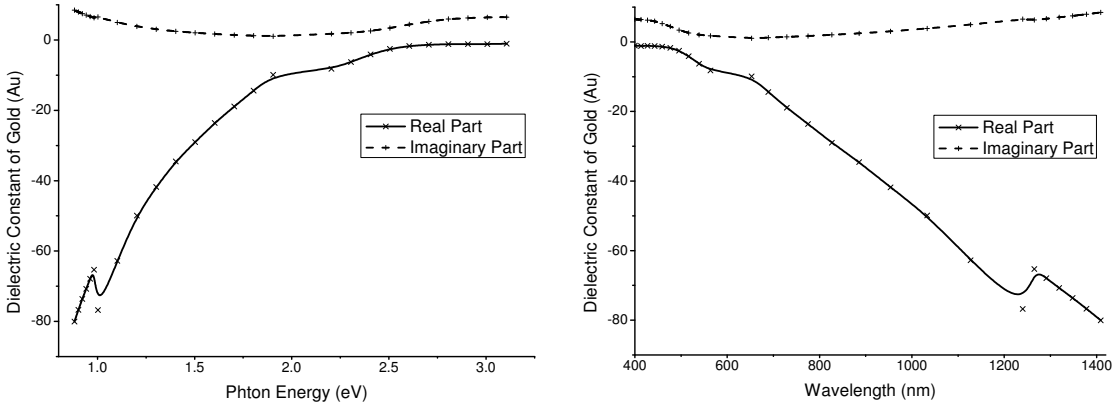

(a) (b)

Figure 1.4. ε of gold in terms of photon energy and wavelength.

dielectric function ε and complex index of refraction N are defined as

$$\varepsilon = \varepsilon' + i\varepsilon'' = N^2 = (n + ik)^2 \tag{1.4}$$

So it is straightforward to obtain the real part by $\varepsilon' = n^2 - k^2$ and the imaginary part by $\varepsilon'' = 2nk$.

The real part and imaginary part of the frequency dependent complex dielectric constant ε of gold, silver, copper and aluminum calculated using the data in [79] are shown in Fig. 1.4, Fig. 1.5, Fig. 1.6, and Fig. 1.7 respectively. Fig. 1.4 (a)- Fig. 1.7 (a) are plotted in terms of the photon energy, while Fig. 1.4 (b)- Fig. 1.7 (b) are plotted in terms of the wavelength of light. It is noted that the visible light's wavelength range is from 390 nm to 780 nm. Its corresponding photon energy range is from 3.19 eV to 1.16 eV.

In addition to the algorithms of FDTD and FEM, another helpful numerical electromagnetic computation algorithm applicable for the nanoantenna is adopted, which

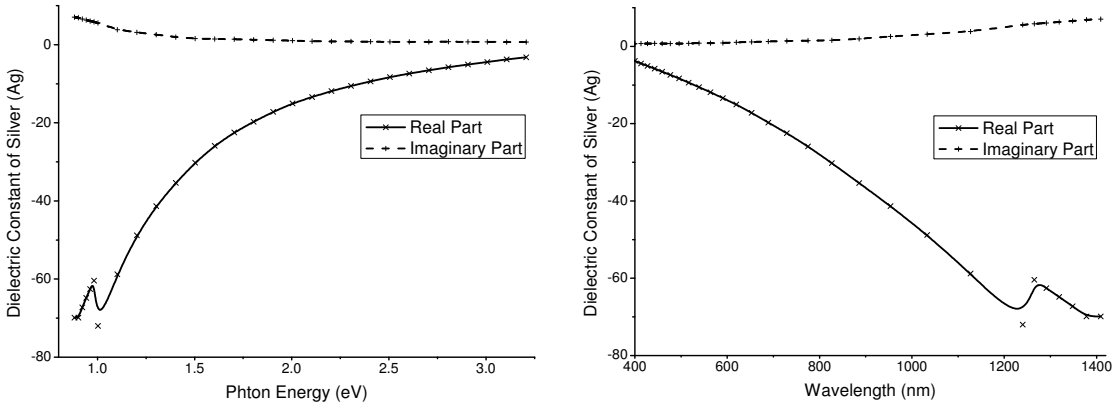

(a) (b)

Figure 1.5. ε of silver in terms of photon energy and wavelength.

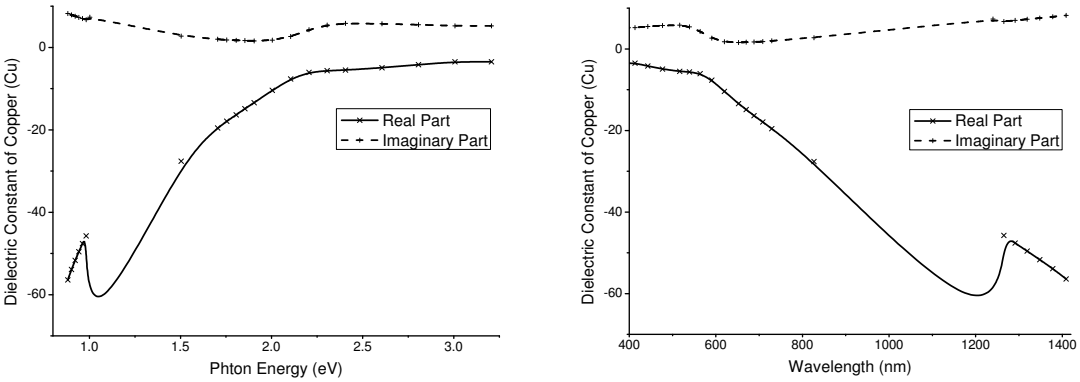

(a) (b)

Figure 1.6. ε of copper in terms of photon energy and wavelength.

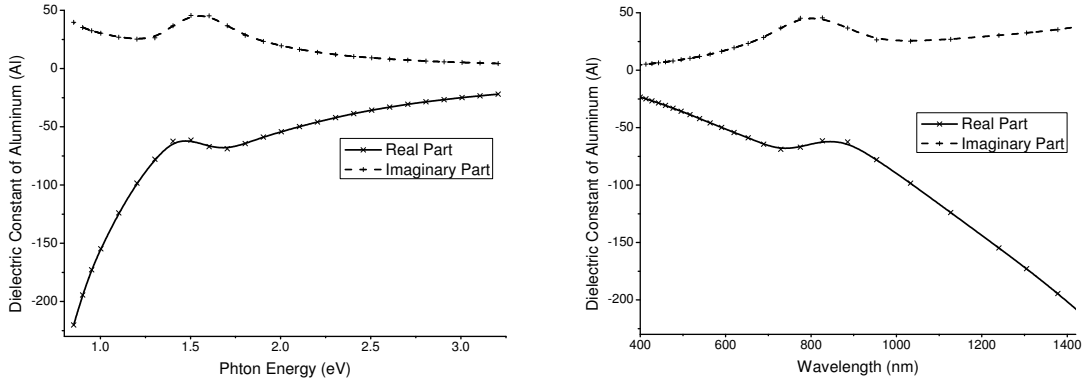

(a) (b)

Figure 1.7. ε of aluminum in terms of photon energy and wavelength.

is the finite integration technique (FIT) (for details of the FIT method, see Chapter 2, Section 2.2). Software of CST Microwave studio (MWS) based on this FIT algorithm has been reported to successfully simulate the properties of nanoantenna [40; 80] (For the details of CST, see Chapter 2, Section 2.3). In addition, this software has the advantage of directly importing the given data to customize the dielectric constant curve as a function of frequency. Therefore, instead of using any model discussed above which has errors, updated experimental data are directly input to CST to obtain more acceptable numerical results.

1.4 Structure of this Dissertation

In summary, although the nanoantennas have the promising applications in the visible and infrared range, they cannot be simply designed by directly transferring their counterparts in the RF range to the optical range. This is due to three main rea-

sons: Firstly, the metals constituting nanoantenna change to be dispersive in optical range. The dielectric constant of metals requires further characterization. Although some models have been proposed to express the dielectric constant, they still have some deficiencies. The problem remains on how the metals' dielectric constant can be accurately characterized. Secondly, not all the numerical methods for calculating the conventional antennas in the RF are always suitable for computing the nanoantennas. Some methods are only effective in a limited frequency band. The broadband calculation through a proper method is needed. Thirdly, the studies of the conventional antennas in the RF range have not focused on their near-field performance as much as on their far-field performance. The nanoantennas' near-field performance is in need of systematic investigations. It is found that the nanoantennas' near-field performance in the optical range is dependent on many factors, such as the antenna configurations, excitation conditions and substrate dimension. These factors can be controllable by adjusting corresponding nanoantenna parameters so that an desirable design can be obtained before the fabrication. However, so far there has been no comprehensive study of such factors' influences on nanoantennas' performance.

In consideration of various nanoantenna designs and the existing problems, we will focus our study on the design procedure of the nanoantennas before their fabrication process. More specifically, we aim at designing a practically feasible nanoantenna with proper configuration and appropriate material. The structure of the dissertation is organized as follows:

Chapter 2 concentrates on the theoretical and computational methods for solving

the nanoantennas in the optical range. Based on the specifications' study for the conventional antennas in the RF frequencies, special properties of the nanoantenna and related antenna parameters in controlling the nanoantenna performance are explored. Recent effective calculation approaches including both analytical solution and numerical methods are discussed. Useful simulation tools applying proper numerical methods are also considered for a referential purpose in studying the possible performance before the practical application.

In Chapter 3 and Chapter 4, the nanoantenna designs of single nanoparticles and coupled nanoparticle pairs are investigated in terms of various kinds of structures. To examine each influencing factor, considerable numbers of designs are tested together under some restrictive conditions to provide comparable results, which are not shown in previous research. It is found that the coupling pairs provide much better enhancement than a single nanoparticle. In particular, Chapter 5 focus on the pair designs of the bow-tie nanoantenna and the bow-tie aperture nanoantenna, because they exhibit predominant characteristics than other kinds of pair structures. In addition, Chapter 6 extends the study of the nanoantennas from one single particle component to the multiple particles' chain and array, which is a worthwhile trial.

Finally, in order to achieve a more completed work, future plans in detail are provided in Chapter 7. Directions of research prospect and several problems still to be solved are explained here. Based on the analysis of the potential difficulties, the possible schemes for overcoming some limitations or difficulties are proposed briefly.

Chapter 2

Methodologies

2.1 Design Specifications of Conventional Antenna in Radio Frequency

To describe the performance of a nanoantenna, some popular parameters necessary for the RF antenna design will be briefly introduced in this section, such as the radiation pattern, gain, efficiency, resonant frequency and bandwidth. The definitions provided below are from the IEEE standard Definitions of Terms for Antennas (IEEE Std 145-1983) [81].

2.1.1 Resonant Frequency and Bandwidth

Typically, an antenna can effectively operate at a range of frequencies centered by a specific resonant frequency. Instead of a single resonant frequency, some antennas

have multiple resonant frequencies. This resonant frequency is related to the electrical length of an antenna, which is the physical length divided by the velocity factor (the ratio of the speed of wave propagation in the antenna to that in the vacuum). Antennas can be made resonant on harmonic frequencies with lengths that are fractions of the target wavelength. When at resonance, the antenna will provide much better coupling of the EM waves to radiate. The bandwidth of an antenna is defined as "the range of frequencies within which the performance of the antenna, with respect to some characteristic, conforms to a specified standard". Usually, it means that within the bandwidth, the antenna characteristics such as the input impedance, pattern, bandwidth, polarization, gain, efficiency, etc. are within an acceptable value of those at the center frequency. Wider bandwidth is able to lead to more sufficient usage of the frequencies, so it has been a common goal of extensive research works to devote to. Some antennas are relatively effective over a very broad range of frequencies. The most commonly known type of wide band antenna is the logarithmic or log periodic antenna, but its gain is usually much lower than that of a specific or narrower band antenna. There are kinds of techniques to increase the bandwidth of an antenna as the frequency is changed. That may include proper adjustments of critical dimensions of the antennas and the feeding networks. Small antennas are usually preferred for convenience, but there is a fundamental trade-off relating bandwidth, size and efficiency.

2.1.2 Radiation Pattern

An antenna radiation pattern is defined as "a mathematical function or a graphical representation of the radiation properties of the antenna as a function of space coordinated". In particular, the radiation pattern is determined in the far-field region and is typically represented as a function of the coordinates. It is more intuitionistic to plot the pattern as a three dimensional graph or two dimensional polar plots of the horizontal and vertical cross sections. The radiation property of most concern is the radiated energy spatial distribution. The power pattern and field pattern are also the often considered specifications. For the ideal isotropic antenna, this is a sphere. For a typical dipole, this is a toroid.

2.1.3 Gain

Another usually considered antenna design parameter is the gain. The absolute gain of antenna (in a specific direction) is defined as "the ratio of the intensity, in a given direction to the radiation intensity that would be obtained if the power accepted by the antenna were radiated isotropically". The radiation intensity $U(\theta, \phi)$ corresponding to the isotropically radiated power is equal to the power accepted (input) P_{in} by the antenna divided by 4π. This is expressed as the following equation form:

$$\text{Gain} = 4\pi \frac{U(\theta, \phi)}{P_{\text{in}}}. \tag{2.1}$$

While for a more common case, the relative gain is used, which is defined as "the ratio of the power gain in a given direction to the power gain of a reference antenna in its referenced direction". Such reference antenna with the known gain is usually a dipole or horn antenna and it is also the lossless isotropic source. The power gain is usually taken in the direction of maximum radiation when the direction is not stated. As seen from the illustration, the gain closely related to the directivity. It is a measure that takes into account both antenna efficiency and directional capabilities. An antenna with a low gain emits radiation with about the same power in all directions, whereas a high-gain antenna will preferentially radiate in particular directions.

An antenna designer must take into account the application for the antenna when determining the gain. High-gain antennas have the advantage of longer range and better signal quality, but must be aimed carefully in a particular direction. Low-gain antennas have shorter range, but the orientation of the antenna is relatively inconsequential.

2.1.4 Efficiency

The total radiated power P_{rad} is related to the total input power P_{in} by

$$P_{\text{rad}} = e_{cd} P_{\text{in}},$$

where e_{cd} is the antenna radiation efficiency (dimensionless). The efficiency is the ratio of power actually radiated to the power put into the antenna terminals. The radiation of an antenna is caused by radiation resistance R_r which can only be measured as

part of total resistance including loss resistance R_L. Loss resistance usually results in heat generation rather than radiation, and reduces efficiency. Mathematically, the efficiency is calculated as

$$e_{cd} = \frac{R_r}{R_L + R_r}.$$

2.1.5 Directivity

The directivity is defined as "the ratio of the radiation intensity in a given direction from the antenna to the radiation intensity averaged over all directions". If the direction is not specified, the direction of maximum radiation intensity is implied. That means the nonisotropic directivity is equal to the ratio of its radiation intensity in a given direction over that of an isotropic source. It is written as

$$\mathrm{D} = \frac{U}{U_0} = 4\pi \frac{U}{P_{\mathrm{in}}}.$$

The directivity is a measure that describes only the directional properties of the antenna, thus it is controlled only by the pattern.

2.2 Analytical and Numerical Methods for Nanoantennas

2.2.1 Qualitative and Theoretical Analysis of Localized Surface Plasmon Resonance Mode

As discussed in Section 1.1 of Chapter 1, recently the surface plasmons of metallic nanoparticles induced by light have drawn extensive research interest. The excitation of plasmonics in these nanoparticles is the localized surface plasmons (LSP), which are the non-propagating excitations of the conductions electrons inside the metallic nanostructures coupled to the EM field. It is necessary for us to study the basic nanoantenna components' scattering characteristics in response to the applied EM field, because they are helpful for the perception of arose normal modes of the nanoparticles during LSPR.

- Oscillator model for a small metallic nanoparticle

We begin the discussion of LSP mode with the explanation of a small metallic nanoparticle upon excitation by light to arrive at the resonance condition. The case considered is a small nanoparticle with its dimension in the penetration depth of applied EM field, which is about 10 nm order for noble metals in the optical frequency range. Fig. 2.1 shows the interaction of the small nanoparticle with the incident light (*i.e.* the applied EM field). The external EM field can penetrate into nanoparticle's volume and lead to the shift of free conduction electrons with respect to the nanopar-

ticle's lattice. As seen form the figure, the surface charges oscillate in phase with the oscillating external field (at time $t = t_1$ and $t = t_2$). Accordingly the positive and negative charges are induced and accumulated on both sides of the particle surface, allowing for a restoring local field to exist within the nanoparticle. The more the electron gas shifts relative to the ion background, the stronger this restoring field is. This process produces an oscillator like resonance by the coherently shifted electrons in response to the oscillation field. By this model, LSPR can be qualitatively described. This behavior is defined by the electron's effective mass and charge, the electron density and the geometry of the particle. It should be noted that for bigger nanoparticles, in addition to a single oscillation mode, there are also the higher order mode. These different modes differ in their charge and field distribution. For the lowest LSPR mode, the distributions are dominated by a dipolar character; for the higher LSPR modes, those are combined with the multipolar charge distributions of higher order [82].

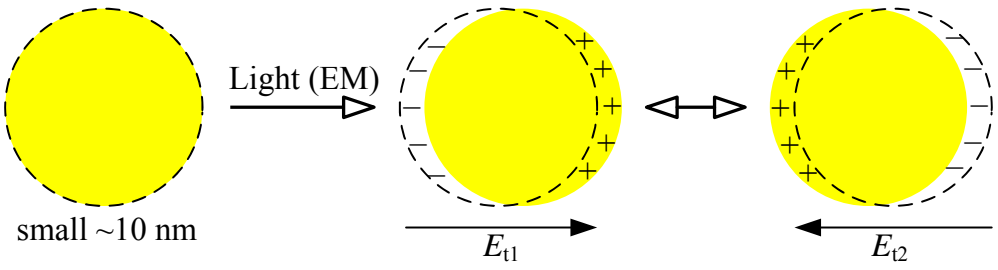

Figure 2.1. Resonant oscillations of the electrons of a small metallic nanoparticle upon excitation by light.

- Quasistatic approximation for subwavelength metallic nanopaticles

For particles much smaller than the radiation wavelength ($2r \ll \lambda$), they can be analyzed through the quasistatic approximation because their dimension is relative small compared to the local variations of the incident EM fields. In this regime, the excitation field is assumed to be homogeneous and the retardation effects over the particle's volume are neglected. Such approximation has achieved good agreement with the experiments. For simple particle under plane wave excitation case, the oscillating dipole moment will be induced, thus leading to the scattering of the plane wave by the sphere caused by the dipole radiation. This can be represented as the radiation by a point dipole [83]. The extinction (the sum of both scattering and absorption) spectra of the nanoparticles can be calculated [84]. The extinction cross-section C_{ext} for a spherical particle with size much smaller than the wavelength (its dielectric constant $\varepsilon_s = \varepsilon' + i\varepsilon''$) surrounded by the medium with the dielectric constant ε_m can be expressed as

$$C_{\text{ext}} = \frac{24\pi^2 a^3 \varepsilon_m^{\frac{3}{2}}}{\lambda} \frac{\varepsilon''}{\left(\varepsilon' + 2\varepsilon_m\right)^2 + \varepsilon''^2}.$$

From this equation, a resonance enhancement in metallic nanoparticles' extinction occurs whenever the condition of $\varepsilon' = -2\varepsilon_m$ is satisfied [85]. This relationship is associated with LSPR mode in an oscillating field. The LSPR peaks can account for the brilliant colors of various metal nanoparticles. This is because some metals like copper and gold have electronic interband transitions in the visible range, where some specific light energies (colors) are absorbed, thus yielding their distinct colors. In addition, the condition also implies the dependence of the resonance frequency on the dielectric environment. The resonance will red shift with bigger value of ε_m.

For a more general case instead of the spherical particle, the research in [59] also applied the quasi-static approximation to investigate the polarizability of the elliptical particlemetallic nanosphere embedded in a dielectric medium using the theories in [83; 58; 85]. It has been shown that the LSPR is mainly influenced by the size and shape of the metallic particle along with the dielectric function of the metal.

- Mie theory in solving scattering from spherical nanoparticles

In this part, taking a simple case of the scattering from a spherical scatterer as an example, we start our investigation of nanoantennas. The Mie theory is a well known analytical solution of the Maxwell's equations for the electromagnetic scattering by spherical particles [86; 87]. In contrast to the Raleigh scattering, which describes the elastic scattering of light by spheres only valid when the radius of the sphere is much smaller than the wavelength of light, the Mie solution to the scattering problem is valid for all possible ratios of diameter to wavelength. For more details about the Mie theory, one can find related information in [58; 85; 88]. Here, for a typical case, the problem for a plane wave incident to a sphere located at the origin of the coordinate is discussed for the study of the Mie theory. We assume that this sphere is of radius a, permittivity ε, and permeability μ, respectively. The plane wave has the following expression in rectangular coordinates

$$\mathbf{E}_{\mathrm{i}} = \hat{x} E_0 e^{ikz} = \hat{x} E_0 e^{ikr\cos\theta}$$

$$\mathbf{H}_{\mathrm{i}} = \hat{y} \frac{1}{\eta} E_0 e^{ikr\cos\theta}.$$

In order to match the boundary conditions (BC) on the sphere's surface, the incident wave is expanded in terms of spherical harmonics by using the wave transformation [88]

$$e^{ikr\cos\theta} = \sum_{n=0}^{\infty} (-i)^{-n}(2n+1)j_n(kr)P_n(\cos\theta).$$

To solve the scattering problem in our case with more ease, the Debye potentials π_e and π_m are introduced. Under their help, the spherical waves will be decomposed into TE component $\mathbf{A}$ and TM component $\mathbf{F}$ corresponding to $\hat{r}$ components, which are expressed as

$$\mathbf{A} = \hat{r}\pi_e$$

$$\mathbf{H} = \nabla \times \mathbf{A} = \hat{\theta}\frac{1}{\sin\theta}\frac{\partial}{\partial\phi}\pi_e - \phi\frac{\partial}{\partial\theta}\pi_e$$

$$\mathbf{F} = \hat{r}\pi_m$$

$$\mathbf{E} = \nabla \times \mathbf{F} = \hat{\theta}\frac{1}{\sin\theta}\frac{\partial}{\partial\phi}\pi_m - \phi\frac{\partial}{\partial\theta}\pi_m,$$

where π_e and π_m satisfy the Helmholtz equation in spherical coordinates:

$$(\nabla^2 + k^2)\left\{ \begin{array}{c} \pi_e \\ \\ \pi_m \end{array} \right\} = 0$$

with$\nabla^2 = \frac{1}{r}\frac{\partial^2}{\partial r^2 r} + \frac{1}{r^2\sin\theta}\frac{\partial}{\partial\theta}\sin\theta\frac{\partial}{\partial\theta} + \frac{1}{r^2\sin^2\theta}\frac{\partial^2}{\partial\phi^2}$. The Maxwell equation is solved via this equation. After lengthy manipulation procedure, the electric and magnetic fields' components in the spherical coordinates are expressed in the following forms:

$$E_r = \frac{i}{\omega\varepsilon}\left(\frac{\partial^2}{\partial r^2}r\pi_e + k^2 r\pi_e\right) \tag{2.2}$$

$$E_\theta = \frac{i}{\omega\varepsilon}\frac{1}{r}\frac{\partial^2}{\partial r\partial\theta}r\pi_e + \frac{1}{\sin\theta}\frac{\partial}{\partial\phi}\pi_m \tag{2.3}$$

$$E_\phi = \frac{i}{\omega\varepsilon}\frac{1}{\sin\theta}\frac{\partial^2}{\partial r\partial\phi}r\pi_e - \frac{\partial}{\partial\theta}\pi_m \tag{2.4}$$

$$H_r = -\frac{i}{\omega\mu}\left(\frac{\partial^2}{\partial r^2}r\pi_m + k^2 r\pi_m\right) \tag{2.5}$$

$$H_\theta = -\frac{i}{\omega\mu}\frac{1}{r}\frac{\partial^2}{\partial r\partial\theta}r\pi_m + \frac{1}{\sin\theta}\frac{\partial}{\partial\phi}\pi_e \tag{2.6}$$

$$H_\phi = -\frac{i}{\omega\mu}\frac{1}{\sin\theta}\frac{\partial^2}{\partial r\partial\phi}r\pi_m - \frac{\partial}{\partial\theta}\pi_e. \tag{2.7}$$

To determine the Debye potentials for the incident wave, it is noted that

$$E_r = E_0\sin\theta cos\phi e^{ikr\cos\theta} = \frac{-E_0\cos\phi}{ikr}\frac{de^{ikr\cos\theta}}{d\theta} \tag{2.8}$$

$$= \frac{-iE_0\cos\theta}{kr}\sum_{n=1}^{\infty}(-i)^{-n}(2n+1)j_n(kr)P_n^1(\cos\theta) \tag{2.9}$$

$$= \frac{-iE_0\cos\theta}{kr}\sum_{n=1}^{\infty}(-i)^{-n}(2n+1)\hat{J}_n(kr)P_n^1(\cos\theta), \tag{2.10}$$

where $\hat{J}_n(kr) = krj^n(kr)$. $\hat{J}_n(z)$ and $\hat{H}_n^{(2)}(z)$ (which appears later) are all Riccati-Bessel functions, the solution of the Riccati-Bessel equation $(\frac{d^2}{dz^2}+1-\frac{n(n+1)}{z^2})w_n(z) = 0$. Because π_e (corresponding to the incident wave) satisfies the Helmholtz equation, it can be expressed by $\pi_e^i = \sum_{n=1}^{\infty} C_{1,n}j_n(kr)P_n^1(\cos\theta)\cos\phi$, where $C_{1,n}$ denotes coefficients to be determined. Substituting this Debye potential to Eq. (2.2) and comparing with Eq. (2.8), we can obtain $C_{1,n}$ as

$$C_{1,n} = \frac{-E_0(-i)^{-n}(2n+1)}{n(n+1)\sqrt{\frac{\mu}{\varepsilon}}}.$$

So $\pi_e^i = -\frac{E_0 \cos\phi}{\omega\varepsilon r} \sum_{n=1}^{\infty} \frac{(-i)^{-n}(2n+1)}{n(n+1)} \hat{J}_n(kr) P_n^1(\cos\theta)$, and π_m can be obtained by duality

$$\pi_m^i = \frac{E_0 \sin\phi}{kr} \sum_{n=1}^{\infty} \frac{(-i)^{-n}(2n+1)}{n(n+1)} \hat{J}_n(kr) P_n^1(\cos\theta).$$

The scattered field can be expressed in terms of Debye potentials:

$$\pi_e^s = \frac{-E_0 \cos\phi}{\omega\mu r} \sum_{n=1}^{\infty} a_n \frac{(-i)^{-n}(2n+1)}{n(n+1)} \hat{H}_n^{(2)}(kr) P_n^1(\cos\theta)$$

$$\pi_m^s = \frac{E_0 \sin\phi}{\omega\mu r} \sum_{n=1}^{\infty} b_n \frac{(-i)^{-n}(2n+1)}{n(n+1)} \hat{H}_n^{(2)}(kr) P_n^1(\cos\theta).$$

The total field outside the sphere is equal to the sum of the incident and scattered fields. The field inside the sphere can be also obtained in terms of the Debye potentials as

$$\pi_e^{in} = \frac{-E_0 \cos\phi}{\omega\mu r} \sum_{n=1}^{\infty} c_n \frac{(-i)^{-n}(2n+1)}{n(n+1)} \hat{J}_n(k_s r) P_n^1(\cos\theta)$$

$$\pi_m^{in} = \frac{E_0 \sin\phi}{\omega\mu r} \sum_{n=1}^{\infty} d_n \frac{(-i)^{-n}(2n+1)}{n(n+1)} \hat{J}_n(k_s r) P_n^1(\cos\theta).$$

The BCs at $r = a$ require that E_θ, E_ϕ, and H_ϕ be continuous. In view of Eqs. (2.2), (2.3), (2.4), (2.5), (2.6), and (2.7), the coefficients can be determined as

$$\begin{aligned}
a_n &= \frac{\sqrt{\frac{\varepsilon\mu_s}{\varepsilon_s\mu}} \hat{J}_n(ka)\hat{J}_n'(k_s a) - \hat{J}_n'(ka)\hat{J}_n(k_s a)}{\hat{H}_n^{(2)'}(ka)\hat{J}_n(k_s a) - \sqrt{\frac{\varepsilon\mu_s}{\varepsilon_s\mu}} \hat{H}_n^{(2)}(ka)\hat{J}_n'(k_s a)} \\
b_n &= \frac{\sqrt{\frac{\varepsilon_s\mu}{\varepsilon\mu_s}} \hat{J}_n(ka)\hat{J}_n'(k_s a) - \hat{J}_n'(ka)\hat{J}_n(k_s a)}{\hat{H}_n^{(2)'}(ka)\hat{J}_n(k_s a) - \sqrt{\frac{\varepsilon_s\mu}{\varepsilon\mu_s}} \hat{H}_n^{(2)}(ka)\hat{J}_n'(k_s a)} \\
c_n &= \frac{\hat{J}_n(ka)\hat{H}_n^{(2)'}(ka) - \hat{J}_n'(ka)\hat{H}_n^{(2)}(ka)}{\hat{H}_n^{(2)'}(ka)\hat{J}_n(k_s a) - \sqrt{\frac{\varepsilon\mu_s}{\varepsilon_s\mu}} \hat{H}_n^{(2)}(ka)\hat{J}_n'(k_s a)} \\
&= \frac{\hat{J}_n(ka) i\hat{N}_n'(ka) - \hat{J}_n'(ka) i\hat{N}_n(ka)}{\hat{H}_n^{(2)'}(ka)\hat{J}_n(k_s a) - \sqrt{\frac{\varepsilon\mu_s}{\varepsilon_s\mu}} \hat{H}_n^{(2)}(ka)\hat{J}_n'(k_s a)} \frac{i}{\hat{H}_n^{(2)'}(ka)\hat{J}_n(k_s a) - \sqrt{\frac{\varepsilon\mu_s}{\varepsilon_s\mu}} \hat{H}_n^{(2)}(ka)\hat{J}_n'(k_s a)} \\
d_n &= \frac{i}{\hat{H}_n^{(2)'}(ka)\hat{J}_n(k_s a) - \sqrt{\frac{\varepsilon_s\mu}{\varepsilon\mu_s}} \hat{H}_n^{(2)}(ka)\hat{J}_n'(k_s a)}.
\end{aligned}$$

Then the scattered fields outside the sphere from Eqs. (2.2), (2.3), (2.4), (2.5), (2.6) and (2.7) become

$$E_r = -iE_0 \cos\phi \sum_{n=1}^{\infty} a_n (-i)^{-n} (2\mathrm{n}+1) \frac{\hat{H}_n^{(2)}(kr)}{(kr)^2} P_n^1(\cos\theta)$$

$$E_\theta = -iE_0 \cos\phi \sum_{n=1}^{\infty} \frac{(-i)^{-n}(2n+1)}{n(n+1)} \left[a_n \frac{\hat{H}_n^{(2)'}(kr)}{kr} \frac{dP_n^1(\cos\theta)}{d\theta} + b_n i \frac{\hat{H}_n^{(2)}(kr)}{kr} \frac{P_n^1(\cos\theta)}{\sin\theta} \right]$$

$$E_\phi = iE_0 \sin\phi \sum_{n=1}^{\infty} \frac{(-i)^{-n}(2n+1)}{n(n+1)} \left[a_n \frac{\hat{H}_n^{(2)'}(kr)}{kr} \frac{P_n^1(\cos\theta)}{\sin\theta} + b_n i \frac{\hat{H}_n^{(2)}(kr)}{kr} \frac{dP_n^1(\cos\theta)}{d\theta} \right]$$

$$H_r = i\frac{E_0}{\eta} \sin\phi \sum_{n=1}^{\infty} b_n (-i)^{-n} (2\mathrm{n}+1) \frac{\hat{H}_n^{(2)}(kr)}{(kr)^2} P_n^1(\cos\theta)$$

$$H_\theta = -i\frac{E_0}{\eta} \sin\phi \sum_{n=1}^{\infty} \frac{(-i)^{-n}(2n+1)}{n(n+1)} \left[a_n i \frac{\hat{H}_n^{(2)}(kr)}{kr} \frac{P_n^1(\cos\theta)}{\sin\theta} + b_n \frac{\hat{H}_n^{(2)'}(kr)}{kr} \frac{dP_n^1(\cos\theta)}{d\theta} \right]$$

$$E_\phi = -i\frac{E_0}{\eta} \cos\phi \sum_{n=1}^{\infty} \frac{(-i)^{-n}(2n+1)}{n(n+1)} \left[a_n i \frac{\hat{H}_n^{(2)}(kr)}{kr} \frac{dP_n^1(\cos\theta)}{d\theta} + b_n \frac{\hat{H}_n^{(2)'}(kr)}{kr} \frac{P_n^1(\cos\theta)}{\sin\theta} \right].$$

Because of the spherical Hankel functions' asymptotic behavior $\hat{H}_n^{(2)'}(kr) \rightarrow (-i)^{n+1} e^{ikr}$, $\hat{H}_n^{(2)}(kr) \rightarrow (-i)^n e^{ikr}$, the explicit expressions for the scattered fields in the far-field can be identified. Since the longitudinal fields decrease as $(kr)^2$, it can be neglected as compared with the transverse fields. Accordingly, the far fields are

$$E_\theta = -iE_0 \cos\phi \frac{e^{ikr}}{kr} \sum_{n=1}^{\infty} \frac{(2n+1)}{n(n+1)} \left[a_n \frac{dP_n^1(\cos\theta)}{d\theta} + b_n \frac{P_n^1(\cos\theta)}{\sin\theta} \right]$$

$$E_\phi = iE_0 \sin\phi \frac{e^{ikr}}{kr} \sum_{n=1}^{\infty} \frac{(2n+1)}{n(n+1)} \left[a_n \frac{P_n^1(\cos\theta)}{\sin\theta} + b_n \frac{dP_n^1(\cos\theta)}{d\theta} \right]$$

$$H_\theta = -\frac{E_\phi}{\eta}$$

$$H_\phi = -\frac{E_\theta}{\eta}.$$

If the radius of the sphere is much small than the wavelength with $ka \ll 1$ and $k_s a \ll 1$, for a small quantity z ($|z| \ll 1$), the following approximations can be assumed:

$$\begin{aligned} j_n(z) &\approx \frac{z^n}{(2n+1)!!} \\ \hat{J}_n(z) &\approx \frac{z^{n+1}}{(2n+1)!!} \\ h_n^{(2)}(z) &\approx -i\frac{(2n-1)!!}{z^{n+1}} \\ \hat{H}_n^{(2)}(z) &\approx -i\frac{(2n-1)!!}{z^n}. \end{aligned}$$

We calculate the coefficients as follows

$$a_n = i\frac{1+1/n}{(2n-1)!!(2n+1)!!}(ka)^{2n+1}\frac{\varepsilon_s - \varepsilon}{\varepsilon_s + (1+1/n)\varepsilon}$$

$$b_n = i\frac{1+1/n}{(2n-1)!!(2n+1)!!}(ka)^{2n+1}\frac{\mu_s - \mu}{\mu_s + (1+1/n)\mu}.$$

If only n=1 is considered for the dielectric $\mu_s = 1$ and a perfect conducting sphere ($\varepsilon_s \to \infty$ and $\mu_s = 0$) case, we find that

$$a_1 = \frac{2}{3}(ka)^3 \frac{\varepsilon_s - \varepsilon}{\varepsilon_s + 2\varepsilon}$$

$$b_1 = \frac{2}{3}(ka)^3 \frac{\mu_s - \mu}{\mu_s + 2\mu}.$$

They are exactly the same as the expressions for the Rayleigh scattering.

According to the Mie theory, the spherical particles have different eignmodes including dipolar or multipolar characteristics. When the particles are bigger beyond the quasistatic approximation due to the retardation effects, researchers have explored the fist TM mode of Mie theory for the sphere case [89; 90]. The extinction cross-section C_{ext} of the spheres can be obtained as a series of multiple oscillations [91]. The generated higher LSPR mode with quadratic term results in an energy shift towards the lower level: the spectral position of the dipole resonance red-shifts with increasing particle size because of the retardation of the depolarization field.

In summary, the metallic nanoparticles much smaller than the wavelength of light (like ∼10 nm) tend to absorb more, so the extinction is dominated by the absorption in the metallic nanoparticles. In this case, only single dipolar mode is supported. As the nanoparticle size increases (like ∼100 nm), the extinction is dominated by the scattering. The increasing nanoparticle size leads to increased retardation effects and higher order multipole excitation modes like dipolar and quadrupolar may be supported as well, thus decreasing the efficiency of the scattering process [92; 93].

Another example of analyzing the nanoantennas is a new theory based on the RLC circuit analogy developed to produce the analytical values for the EM field enhancements within a two-dimensional metal nanoparticle arrays [54]. This draws our interest of constructing appropriate equivalent circuit of the problem we are concerned about. But because of the limitations in the knowledge of quantum physics

and electrical engineering for understanding the special effects occur in nanometer scale, the problem is worthy further work.

2.2.2 Computational Methods for Nanoantennas

In this section, the numerical computational methods for electromagnetic problems will be discussed in general and followed by a summary of recent attempts of applying them to the characterization of nanoantennas.

In fact, many electromagnetic problems cannot be analytically solved due to the multitude of irregular geometries designed. Such problems may include scattering, radiation, and waveguiding cases. These complex situations with various constitutive relations of media and BCs demand for computational numerical techniques. They have been shown to be able to overcome the problems [94]. In general, the governing Maxwell's equations or related equations in these problems can take the form of either a differential equation or an integral equation (IE). Accordingly, integral equation solvers involve the method of moments (MOM) or boundary element method (BEM), fast multipole method (FMM), and finite integration technique (FIT) etc.; while popular differential equation solvers include the finite difference time domain (FDTD) and finite element method (FEM) etc. As typical adopted methods, the FDTD, FEM, FIT and MOM will be briefly discussed as follows.

The FDTD is a popular computational electrodynamics modelling technique because it is easy to understand and implement in the software [95]. In FDTD, Maxwell' equations are discretized using the central-difference approximations to the space and

time partial derivatives. By dividing the domain of interest into a grid and time-stepping in the whole domain for each time instant, the resulting finite-difference equations are solved in either software or hardware in a leapfrog manner: the electric field vector components in a volume of space are solved at a given instant in time; then the magnetic field vector components in the same spatial volume are solved at the next instant in time; and the process is continuously repeated until the desired transient or steady-state electromagnetic field behavior was fully evolved [96]. Because FDTD is a time domain method, it has the advantage of obtaining wide frequency range coverage response with a single simulation run, especially for the case in which broadband pulse like a Gaussian pulse is used as the source. The FDTD is useful in the applications where resonant frequencies are not exactly identified, or anytime that a broadband result is desired.

The FEM is a method used for finding the approximate solution of partial differential equations (PDE) and integral equations. The approach of solution is through either eliminating the differential equation completely or rendering the PDE into an equivalent ordinary differential equation, which is later solved using standard techniques. The finite element analysis basically involves discretizing the solution region into a finite number of subregions or elements, deriving governing equations for a typical element, assembling of all elements in the solution region and solving the system of equations obtained [96]. In solving the PDE, the primary challenge is to create a numerically stable equation that approximates the equation to be studied. The FEM is a good choice for 1) solving partial differential equations over complicated domains

like cars and oil pipelines, 2) when the domain changes, 3) when the desired precision varies over the entire domain, or 4) when the solution lacks smoothness.

The FIT is a spatial discretization scheme to solve the electromagnetic field problems in time and frequency domains numerically. The basic idea of this approach is to apply the Maxwell's equations in integral form to a set of staggered grids. This method is predominant because of its high flexibility in geometric modelling and boundary handling as well as the incorporation of arbitrary material distributions and material properties, such as anisotropy, non-linearity and dispersion. In addition, the use of a consistent dual orthogonal grid in conjunction with an explicit time integration scheme can result in extremely high efficient algorithms referred to both computation time and memory requirements. These aspects are especially suitable for transient field analysis in the RF applications.

The MOM, as a computational method for solving linear PDE which have been formulated as integral equations, basically has the following steps in its solution procedure: (1) derivation of the appropriate integral equations; (2) conversion of the IE into a matrix equation using basis functions and weighting functions; (3) evaluation and filling of the matrix elements, and (4) solving the matrix equation and obtaining the parameters of interest. For discretized boundary, the MOM becomes the boundary element method (BEM). Because BEM only requires the calculation of the boundary values instead of those values throughout the space defined by a PDE, it is significantly more efficient in terms of computational resources for the problems where there is a small surface/volume ratio [97]. If we compare BEM with FEM, it has

some difference between their performances on computations. In theory, boundary element formulations typically give rise to fully populated matrices, thus the storage requirements and computational time tend to grow according to the square of the problem size. On the contrary, finite element matrices are typically banded and the storage requirements for the system matrices typically grow quite linearly with the problem size, which are better under certain circumstances.

It should be noted that a certain computational EM algorithm should be chosen according to the specific application circumstance, even if different techniques might converge to the same field and power distributions in the modelled domain. For example, as illustrated above, the transient response and impulse field effects are more accurately modelled by the computational electromagnetics in the time domain by FDTD. Moreover, curved geometrical objects are computed more accurately by using FEM, or non-orthogonal grids. As to the numerical methods for the nanoantennas, several algorithms have been reported in the applications including FDTD method [98; 99], FIT [38], multiple multipole program (MMP), semi-analytic boundary discretization method [100], BEM [101], and boundary integration equation [102]. For FDTD, this computational approach adopted for calculating the field distribution in the vicinity of the optical antennas is based on the time domain method, and it suffers from inadequate dielectric constant characterization problems as stated in Chapter 1, Section 1.3. Improvement needs to be done to modify the dielectric function's models used in the simulation. In MMP, EM fields are represented by a series expansion of known analytical solutions of Maxwell's equations. To determine the

unknown coefficients in the series expansion, BCs are imposed at discrete points on the interfaces between adjacent homogeneous domains. Once the resulting system of equations is solved and the coefficients are determined, the solution is represented by a self-consistent analytical expression. A difficult problem to face with for MMP is the requirement of very fine discretization due to the unique properties owned by optical antennas, such as strong material dispersion, loss, and plasmon-polariton effects. Because the MOM deals with the matrix, the memory requirements and computational time will grow much faster as the problem scale become even larger. This is a problem which needs further consideration.

2.3 Effective Electromagnetic Simulation for Nanoantennas

In order to understand the electromagnetic properties of antennas, it is usually necessary to perform some numerical simulations to solve the Maxwell's equations. The purpose of the simulation is to get a good visualization of the electric fields distribution, so that more detailed features can be characterized. By predicting these properties, time and space can be resolved more finely than the experiments. In addition, such calculation can target at specific problem, allowing for the solution to discrete questions of a system. Further more, numerical studies can supplement the measurement by providing important information which is essential be unavailable through experimental approaches alone. A good preparation for further fabrication

step can be made as well. Various numerical simulations tools may be used to analyze the EM effects in order to minimize the time-consuming and expensive experiments. However it is difficult for commonly used numerical simulation techniques to solve the problem because of the strong dispersion of metals at the optical wavelength with negative permittivity, non-negligible losses and plasmon-polariton effects of plasmonic nanoantennas. Fine discretization is required, which is difficult and extremely time-consuming.

To our knowledge, currently there have been some commercial software packages employed in simulating the properties of kinds of nanoantennas in the optical range, such as CST Microwave Studio (MWS) based on FIT, COMSOL MULTIPHYSICS based on FEM, and XFdtd, FullWAVE, MODE Solutions based on FDTD and other field-based software packages. They are present popular design tools which allow one to carry out accurate fullwave simulation and optimization of planar integrated circuits and antennas.

CST is capable of simulating the field distribution of a dielectric or metallic sphere around the tip of the microscope [103] early in the last century. Recently, in the study of the monopole antenna fixed on the apex of the aperture probe, insight in this nanoantenna characteristics is gained by the CST calculations of the local electromagnetic field distributions for both the driving field and the antenna response [38]. In addition to field distribution, the CST is also capable of exploring the radiation features of optical nanoantennas and analyze the impedance matching related concepts of the plasmonic nanodipoles [80].

As another common simulation tool, COMSOL can calculate the cases of gold elliptic nanoparticle pair array embedded in quartz [104], reduced symmetry core-shell nanoparticles [105] and metallic wire array [106].

MODE Solutions has also been reported in the study of the optical nanocircuit consisting of a receiving and an emitting nanoantenna connected by a two-wire optical transmission line [107] and the plasmon-enhanced fluorescence calculations [108]. FullWAVE is helpful in simulating the optical profile of the bow-tie nanoantennas [20].

In view of the examples, CST has promising features of successful calculation the electromagnetic behaviors of frequency dependent materials. It is particularly preferable for our nanoantennas' designs in the consideration of wide band properties. So we choose it as the simulation tool in the present work. On one hand, several built-in dispersive material models for utilizing in the transient solver are provided for us to choose; On the other hand, "user's list" function is available for inputting the individual interested data in the frequency domain solver. The principle of the former computation is that, a dispersion curve is formed, either by defining the property's parameters under a certain chosen model, or by fitting the data through a general polynomial formulation; while the latter solver will take into account every single dispersive value in the calculation. Because the problems discussed before attribute to the inaccurate dielectric constant used and the inappropriate conditions assumed, we choose to import the appropriate data to customize the dielectric constant values at different frequencies and adopt the frequency domain solver instead.

2.4 Summary

In this chapter, the theoretical approaches for studying the electromagnetic scattering problems of nanoparticles are presented. Fundamental principles of nanoantenna theory are significant as they can be further applied to our depiction of nanoantenna analysis, design and measurements hereinbelow. A key benefit of the methodology exploration of the nanoantenna is the better explanatory power for the nanoantenna features. This chapter has provided important sights into this problem with theories from not only the practice background in engineering but also the abstract basis in physics. On one hand, from the engineering's point of view, the common specifications of the conventional RF antenna are introduced in the beginning. More emphasis is placed on the usage of the typical parameters of bandwidth and resonant frequency, radiation pattern, gain, efficiency, and directivity. As a result, we can take them as a reference for nanoantennas design to evaluate their performance or make a comparison with the existing RF antennas in practice. On the other hand, from the theoretical point of view, both the analytical and numerical EM computational methods are provided targeting at solving our specific nanoantenna topics. Nanoantenna's mechanism performed are discussed by analysis of localized surface plasmon resonance mode. As a famous analytical solution of the scattering problem for spherical particles, the Mie theory is demonstrated wherever it is necessary. Moreover, in addition to the analytical methods, numerical methods are also proposed and discussed. Current applied numerical methods especially for the nanoantennas are listed and compared together. For a better understand of the practical nanoantenna

problem, it is also interesting to compare several popular simulation tools on the basis of different computational methods, such as the FIT, FEM and FDTD. CST based on the FIT has been found to be more suitable for a nanoantenna, because it is more appropriate for a broad band calculation. It is also preferable in the aspect of convenient configuration/setting of parameters and precise characterization of the dispersion relationship of the metallic particles in the optical range as well. Based on the study, the idea of using the resonant plasmonic nanoparticles as the optical antenna components will be further developed in terms of different designs in the following chapters.

Chapter 3

Single Nanoparticle as the Nanoantenna Component

3.1 Characterization of Nanoparticles in Modeling Nanoantennas

In this section, we begin our investigation with the discussion of the single nanoparticle's modelling. There are several important aspects about the characterization of the nanoparticles in the nanoantennas' design procedure, which needs further illustration. In general, except for the basic indices (for example, the boundary conditions and the frequency range), they involve the configuration, dimension, material for the antenna and the excitation setup for the source. Among various factors, the helpful properties of metallic nanoparticles are found to be intimately related to their

geometries. One of the key features of these nanoparticles is that their resulting SPRs with predominant properties can be geometrically tunable. Thus it enables one to set LSPR at a specific laser wavelength or certain spectral region to match a particular application. Focused on the geometric effects, some basic consideration regarding the characterization of the nanoparticles in the simulation is described point by point as follows.

- The configuration of the nanoparticles

As reviewed in Chapter 1, Section 1.1, the topics of light scattering from the nanoparticles and the plasmonic properties of nanoparticles had been widely studied even before the concept of "nanoantenna" and "optical antenna" was emerged. The investigated nanoparticles contain kinds of structures such as sphere, spheroid/ellipsoid, polygon, cylinder/wire/rod, shell and ring. Among all of these structures, the sphere, spheroid, triangle, cylinder and rod own the advantages of lower complexity in their configurations. They can be considered as the basic components for composing the nanoantennas or further antenna arrays. The nanoparticles of the polygon shape may lead to multiple scattering which may be a more complex case which is more suitable for a practical measurement purpose. Hence in our theoretical study, we prefer to use simple structures to investigate their potential of being used as the antenna components. Although there existed the studies about a single particle of various shapes and sizes fabricated and measured in the microscopy, they are basically investigated for the extinction spectra over a limited range from the solid physics point of view. In addition, there was no comprehensive study on the

geometric effects influencing the optical properties of the nanoparticles under certain geometric restrictions such as the same volume and cross-section. Those necessary studies are included in our work for a systematic study. In our later modelling, the nanoparticles will be placed in the Cartesian coordinates with their geometric center located at the origin and their longitudinal direction aligned along the x-direction for the asymmetric structures.

- The dimension effects of the nanoparticles

In addition to the structures, the proper dimension chosen for the nanoparticles in antenna design is equally essential. The plasmonic properties of the nanoparticles are extremely sensitive to the small variation in dimension [25; 52]. Despite of the fact that the size of the nanoparticles should be certainly in the nanometer scale, it does not necessarily mean the smaller the scale the better the performance. Too small dimensions, say, less than 10 nm, cannot satisfy the classical Maxwell's equations any more. In previous studies, the spheres with radii of 50 nm have been successfully fabricated [46] and those of 30 nm have been theoretically analyzed [109]. In view of these cases reported in the literature, we set our structure's one dimensional sizes in the order of 10 nm to 100 nm for single spheres, spheroids and cylinders.

- The material effects of the nanoparticles

The noble metal is able to exhibit the LSPR in the optical range. The problem arose accordingly is the choice of the material among available noble metals for a

better performance. The metals usually considered and applied in recent nanoantenna research involve gold (Au), silver (Ag), aluminum (Al) and copper (Cu) [10; 110; 111; 20; 112]. The choice of the metals depends on the application wavelength, because the wavelength is dependent on the dielectric constants of metals. It is better for the dielectric constant of the metal has a high absolute value for the real part and a small imaginary part, which determines the absorption of the metal. These conditions support strong surface plasmon fields along the surface and simultaneously minimize the losses, as stated in Chapter 1, Section 1.3. Ag is suitable due to its advantage to obtain high transmission in the visible part of the spectrum. When the wavelength is above 600 nm, Au is even better, because it benefits from little oxidation. In the IR, metals such as Ni or Cu can also be applicable [113]. In our work, we suggest gold as a typical metal appropriate for modelling. We will consider the other common noble metals as well for a comparison in the following discussion.

- The excitation of the nanoantennas

For the excitation source, available literature seems to support the view that a plane wave is usually adopted. A pulsed laser of 532 nm [10] and a ring dye laser of 600 nm [17] have been respectively used to propagate in the optical fiber and illuminate uniformly to the local sample. Moreover, a monochromatic plane wave of 830 nm free-space wavelength has also been utilized as the excitation source for nanorod structures in [46]. In our computation, we are interested in the optical antenna calculation covering a broadened frequency band. So theoretically we implement our study in the visible range and extend it to the IR range for the excitation frequency.

The detailed wavelength range is from 400 nm to 1360 nm with even frequency step samples at every 10 THz. In addition, this plane wave in our simulation is polarized in the x-direction with an electric vector of 1 V/m and propagates in the z-direction in the Cartesian coordinate. So its polarization is along the longitudinal direction of the nanoparticles and incident to them from the lateral direction. It is noted that in different research works, scientists expressed the abscissa of their spectra in terms of different measures including the wavelength, frequency and electron energy. In fact, there is some relationship between them and they can be converted to each other as needed. The frequency v is related to the wavelength λ through $c = \lambda v$, where c is the speed of light in vacuum, 3×10^8 m/s; the photon energy E is related to the frequency v through the Einstein equation, where h denotes the Plank constant with the value of 6.626×10^{-34} J $\times$ s or 4.136×10^{-15} eV $\times$ s. For example, the light at the frequency of 600 THz is equivalent to the wavelength of 500 nm and 2.48 eV if expressed in the photon energy. However, it should be noted that in a practical measurement, only certain wavelengths of the incident laser are available in the laboratory for testing in the visible range, such as 458 nm, 514 nm, 532 nm and 633 nm [114; 38; 3; 115], and some major laser wavelengths like 1064 nm are available in the near IR range [116; 59]. Here it is again shown to be meaningful that the nanoantenna can be specifically designed with carefully adjusted parameters to allow them to be resonant to match the wavelength required for a particular application. It is noted that in additional to the plane wave, the other sources can be also utilized in the present research. For example, high-order modes such as Hermite-Guassian

and Laguerre-Gaussian beams are applied through phase adjustment to control the optical near field of the gold nanowire antenna in [117].

- The environment around the nanoantenna

In view of the realistic environment, our proposed nanoantennas are supported by a substrate with a refractive index of 1.5, which can be considered as the silicon dioxide. The substrate thickness is 200 nm in the initial design. Such a system is placed in a medium that bears an analogy to vacuum with the refractive index of 1. The thickness of the substrate is initially set as 200 nm. In the subsequent study, its thickness is varied from 50 nm to 200 nm to examine its impact on the nanoantenna performance. Subsequent to these steps, the simulations of characterizing the nanoantenna are performed by using CST. The detailed scheme is shown in Fig. 3.1 for the single nanoparticle geometry. A gold spheroid nanoparticle placed on the silicon dioxide substrate is shown here as an example. The excitation details is also given in this figure. The simulation is carried out with a fine tetrahedral mesh and locally condensed at the metallic particle area in order to achieve more accurate results.

3.2 Optical Resonant Properties of Nanoparticles Dependent on Several Design Parameters

In this section, we provide an integrated approach for the demonstration of the optical properties of a single nanoparticle under the influence by various geometric

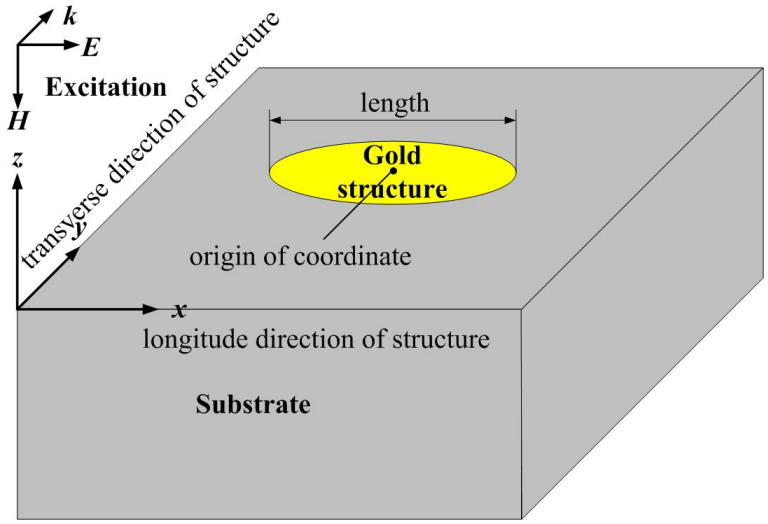

Figure 3.1. Scheme of single particle.

effects. Two parameters of our concern are the light intensity and the enhancement factor. The light intensity is an important specification for measuring the optical properties of the nanoparticles in the near-field. It is considered as the square of the magnitude of E-Field in optical microscopy. In our simulation, the E-field value is collected and the corresponding light intensity is calculated through this relationship at a position of research interest. This procedure of exploring the field distribution at a desired point is implemented by the convenient function supported by different solvers in CST. On one hand, if the transient solver is employed, its associated "probe" function are applied, which is exactly like the probe of a practical microscope in samples scanning and signal detection. On the other hand, if the frequency solver is utilized, alternatively the post processing function is performed to evaluate the field at specific coordinates. The enhancement factor describes the capacity of magnification in the E-field of light at the light focused position normalized to the incident value. If upon excitations with different frequencies, the maximum E-field remain at the

same position on the nanoantenna, this peak value is recorded and divided by the incident E-field value to obtain the enhancement factor. Different from previous research that is limited to the topics on the shape variation for different nanoparticles and the size variation for the same particle, it is our interest to compare various nanoparticles with the same volume and cross-section. Such a investigation on the factors responsible for the nanoantenna performance as a supplement to the present work is highly imperative for a new research extension. These factors are listed below and the results are presented with detailed analysis.

3.2.1 Optical Resonance of Spheres with Different Radii

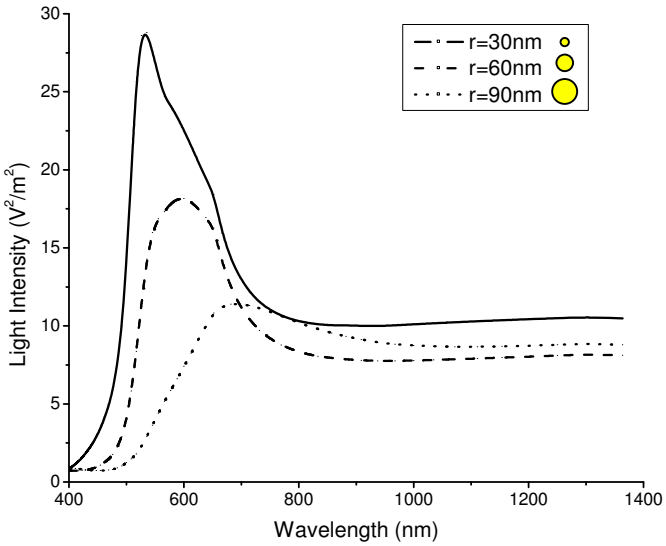

Figure 3.2. Light intensity spectra of spheres.

Fig. 3.2 shows the light intensity spectra of the spheres with the radii of 30 nm, 60 nm, and 90 nm respectively. In this part, the electric field value is calculated

at the end of the nanosphere along the incident polarization x-direction. The light intensity $|E|^2$ is then obtained with its unit V^2/m^2. As seen from this figure, for each spherical case, as the wavelength increases (*i.e.* approaches the red portion of the light spectrum), the sphere's light intensity's curve firstly rises, and then drops with a peak point in between. This resonant manner alike the resonance in an antenna response, which can be considered as the resonance point of the nanoantenna. Particularly, the maximum value is found to be located at opposite edges of the sphere along the longitudinal direction in the x-direction, with a value obviously enhanced compared with that of the incident light. Because the E-field's value of the excitation source is set as unit, the values in all the spectral figures in this paper are normalized to the incident light. In our calculation, these spheres' strong resonances are seen in the red portion of the visible light spectrum. For example, the resonance of the sphere with radius of 30 nm occurs at 535.7 nm, which is equivalent to 2.31 eV, this matches well with the result in [109]. Our result shows similar positions for resonance as those in [118; 109] including both theoretical and experimental studies. In addition, when comparing the spheres with different size in the order of tens of nanometer, we find that smaller sphere shows stronger enhancement of light intensity, which is expressed as a higher value in the figure. Moreover, when the sphere turns bigger, its resonance position in spectrum exhibits a red-shift phenomenon, which means the resonance frequency turns lower and the corresponding wavelength goes longer. The peak becomes broader as the wavelength increases as well. These findings are in a good agreement with those of present studies [84; 43]. In some research, it has been found that the resonance of Au particles with radii smaller than 10 nm occurs around

520 nm, regardless of their sizes [118; 84]. This is because the phase retardation effects and multiple modes can be neglected in this quasi-static regime. Mie theory gives a constant resonant frequency independent of particle size by using bulk dielectric constant. While when the radii are larger than 10 nm, the peak and the width of the spheres' spectra are dependent on the particles' size. For these larger particles, the quantum confinement effects becomes negligible, and the role of phase retardation effects comes into play. The peak red-shift observed in the experiments is attributed to the electrodynamic effects caused by the phase retardation [49]. In view of the characteristics of the nanosphere found above, we will use 30 nm as the transverse radius dimension for further investigation of other shapes of nanopartciles, because it is acceptably small and provides relative better enhancement at resonance as well.

3.2.2 Optical Resonance of Spheres, Spheroids and Cylinders with Constant Cross-section

In order to see the geometric effects on the antenna's performance, we tried the nanoparticles with several shapes while remaining their constant transverse cross-section in the *yoz*-plane. Their longitudinal dimensions are different with increasing lengths. That extension process correspondingly produces various shapes of sphere, spheroid with larger axial ratio, and cylinders with larger lengths respectively. Here, with the constant radius of 30 nm in the transverse plane, the spheroids are set with axial ratios of 2, 3, and 4 (*i.e.* their lengths are 120 nm, 180 nm and 240 nm, respectively) and the cylinders are set to have lengths 180 nm and 240 nm respectively.

These shapes considered are depicted in Fig. 3.3 and Fig. 3.4 for their light intensity and E-field spectra respectively. The data recorded for a single nanoparticle case is located at the end of this particle along the source polarization direction. In Fig. 3.3, a logarithmic scale is used to show the difference between the structures more clearly.

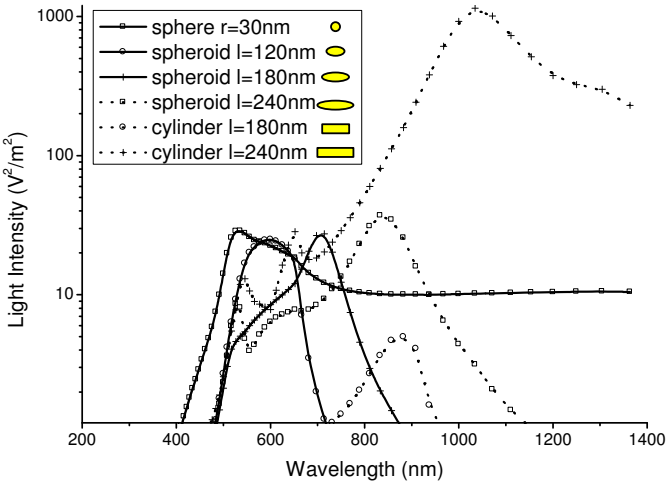

Figure 3.3. Light intensity spectra of particles with the same cross-section.

Our results indicate that, if the cross-section of the structures are kept constant, those structures with a longer dimension in the longitudinal direction (which is also the excitation polarized electric field's direction) generally show stronger resonance than the shorter ones. Among all the structures, the cylinder with length 240 nm has much more intensity value than other structures. For further physical insight, a quantitive analysis of the ratio of the peak value of the cylinder with length 240 nm to the sphere with radius 30 nm is conducted. That multiple is found to be 1009.7/28.8$\sim$35 times. Similar as the cases for the spheres, the resonances of the other structures are also found to lie at the ends along their longitudinal direction.

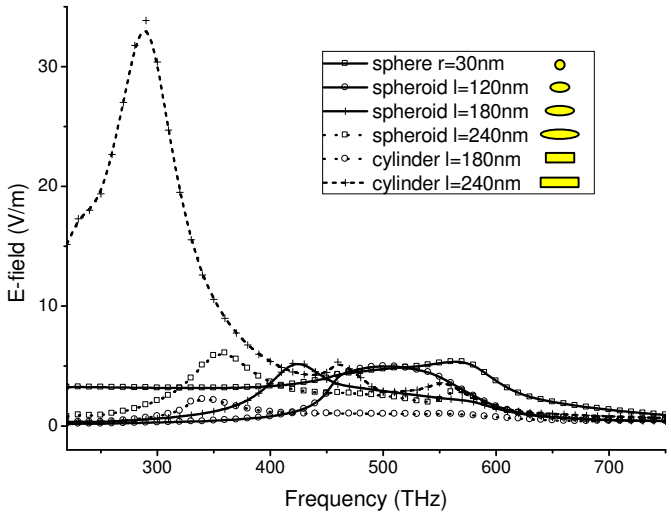

Figure 3.4. *E*-field spectra of particles with the same cross-section.

Particularly, for the cylinder, the peak's position is at the interface between the antenna and the substrate. Furthermore, longer structure results in a red-shift of the resonance in the spectrum. For example, the resonances respectively occur at 500 THz, 420 THz, and 360 THz for the spheroids with increasing lengths of 120 nm, 180 nm, and 240 nm respectively. Similarly, this finding is also true for the cylinders. This finding is in consistent with those in [119; 42] for the red-shift in resonances with increasing aspect ratio of (or more oblate) ellipsoids and cylinders. This can be explained by the increasing overall effective dielectric constant caused by longer structure. There are several aspects of the results that we need to highlight. Firstly, although the longer structure here gives better field enhancement, it leads to more amount of material to use. For the noble metal case like gold particles, this causes the increase in cost, which may be more obvious when a nanoparticle array is adopted. More over, the spheroidal shape's formation in the experiments

needs further consideration. In the practical nanosphere synthesis process, larger size particle deposited ont the substrate tend to lose their spherical property and look like ellipsoid, causing redshift of resonance frequency [92]. Thus spheroidal assembling particles will be formed alternatively in the evaporation process other than the ideal spherical shape due to the surface tension. Furthermore, oblate ellipsoidal shape was reported to be least sensitive to the surrounding dielectric medium in the extinction spectrum of the nanoparticles [120]. So the study of the spheroidal case may be a more general case for the antenna element in further nanoantenna design step. Accordingly we prefer to use the spheroids in the later coupling pairs' investigation instead of the spheres.

3.2.3 Optical Resonance of Spheres, Spheroids and Cylinders with Constant Volume

In this part, besides the constant cross-section, the case of the constant volume for different structures is also taken into account. Fig. 3.5 presents the results of the light enhancement factor for a sphere, a spheroid and a cylinder with the same volume of 1.1304×10^5 nm^3. The enhancement factor here is the maximum light intensity value for local field amplification in comparison with the incident light upon the excitations by different frequencies. For a fixed volume, the structures show different performance in the light intensity enhancement. Among them, the cylinder has stronger enhancement capability than the spheroid, followed by the sphere. This can be explained by the following two aspects. First, for a single nanoparticle configu-

ration, cylinder is shaper than end-rounded spheroid at the end cross-section, where the data are recorded. Shaper structure is better for accumulating field near their sharpest end due to lightning rod effects [121], which implies that any sharp geometrical feature like corner and edge can generate quasi-electrostatic "crowding" of many electric field lines, thus leading to a tremendous field enhancement. This effect occurs as long as the effective curvature of the sharp feature is much smaller than the wavelength. Second, the interaction area with substrate for the cylinder is bigger than that for the spheroid, which may results in stronger coupling and higher light enhancement. It is noted that, for the enhancement factor, the peak value of E-field is collected at each frequency. The positions where the peak values occur may slightly change as the frequency varies. It may be attributed to different mesh grids captured under different frequencies during the numerical calculations, which is inevitable but acceptable for a qualitative study. Our purpose is to find the best enhancement factor, so the values at different positions are recorded. In contrast to the enhancement factor, the E-field and light intensity are recorded at the same position. This can be adequately explained by the practical experiment case in microscopy. It is possible to locate the probe or the detector/sensor to observe at the fixed position around the particle's fringe.

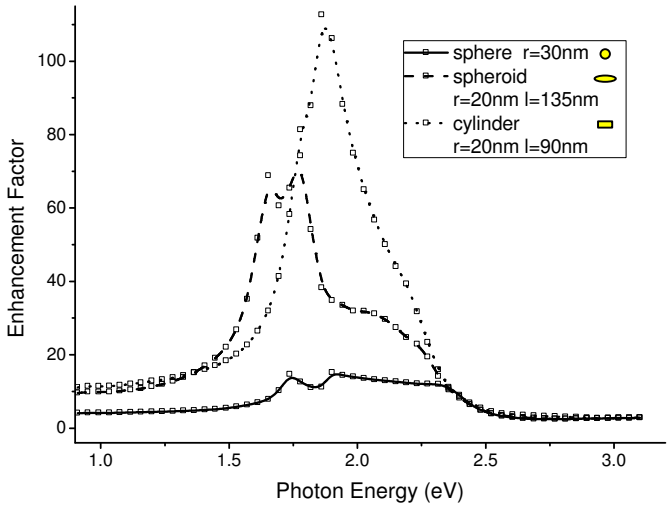

Figure 3.5. Enhancement factor of particles with the same volume.

3.2.4 Optical Resonance of Spheres, Spheroids, Cylinders, Rods, Triangles, and Fans with Constant Thickness in the z-direction

In order to understand the shape effects on the resonance, a comprehensive analysis is made among different structures which attracts most interests of researchers. The shapes include the spheres, spheroid, cylinders, rods, triangles and fans. For a comparative study, except for the sphere, the lengths of the other structures are set constant as 240 nm. Similarly, the thickness of the rod, triangle and fan are all 60 nm. To avoid singularity, the two ends of the rod and the apex of the fan are rounded with the radius of curvature 30 nm. Both the triangle and the fan have the same included angle of 60°. The final results of the optical properties of different shapes are given in Fig. 3.6. The logarithmic scale is again used to more obviously present

the data with differences. As seen from this figure, the light intensity at resonance is ordinal decreasing for the cylinder, rod, spheroid, sphere, fan, and triangle. The results for cylinder and rod achieve good agreements with those in [109]. In addition, strong enhanced field is found at the apexes of both triangles and fans. Because they have ununiformity in the geometries, their sharp ends cause the localized light concentration. Their field distribution is similar as that in [2]. Inside the spectra, multiple resonances are found for some strurctures. This is probably caused by the relatively sharp surface around the vertex. Further more, there's a redshift in resonance shown in the triangle case in comparison with the sphere case, it is due to the higher mode resonances excited which is resulted from the triangle's corner features. This explanations is supported by the experimental observation in [122].

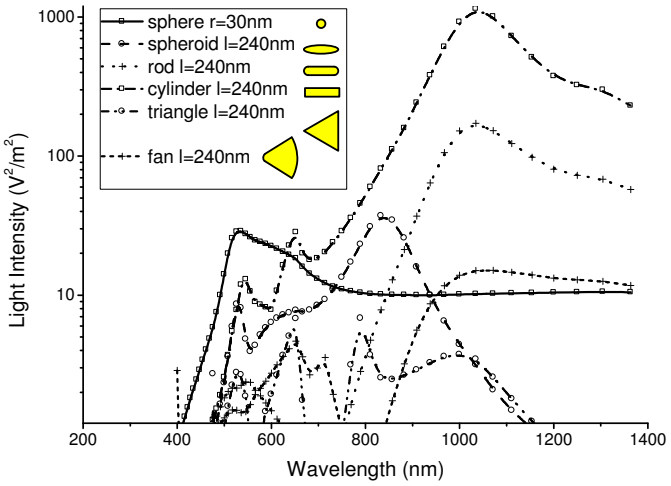

Figure 3.6. Light intensity spectra of particles with the same thickness.

3.3 Results and Discussion

In this section, the mechanisms behind the results and the reasons accounting for the observed optical properties of single nanoparticles as the nanoantenna components are considered after the detailed analysis data are presented. When induced by light, the metallic nanoparticles can produce the localized surface plasmon excitation due to their unique material properties in the optical range, which is closely related to their dispersive dielectric constant. The light intensity generated is confined at distinct region of the nanoparticles, depending on their detailed structures. These promising features can be taken as advantages of for diverse applications. This work evaluates the significance of the light intensity enhancement features of the single nanoparticles under the control by various factors. Some basic considerations for the simulation setup are also inclusive in this chapter. They provide the fundamentals for future discussions on the multiple particle case-studies in the subsequent chapters. For the noble metals available for calculation in the optical range, gold is the best choice with suitable performance. The configuration and dimension are elaborately set in view of both theoretical accessibility and present experimental feasibility. The size of the nanoparticles in our modelling is chosen to be around tens of nanometers to offer a reasonable performance. Moreover, the substrate and the excitation may also affect the nanoantenna performance in certain ways. These will be analyzed in the following chapter. In the method aspect, an adequate method is developed targeting at a broad band calculation involving the visible and near infrared range of the light spectrum. It appears that the geometric effects result in substantial differences in the performances

and optical properties of nanoantennas. The important factors identified in this chapter which are referred to are the size effects for spheres, the length effects for the spheres, spheroids, and cylinders with a constant cross-section or volume, the shape effects for the sphere, spheroid, rod, cylinder, triangle and fan with constant thickness. They have been investigated extensively and intensively based on the numerical calculations. Usually, strong field or light spot will be focused on the ends of a single particle with the strength which are much higher than the incident light. A dipole-alike resonant behavior is found in the light intensity spectrum. Within the acceptable small size range, smaller spheres offer higher light intensity than the bigger ones. They will also red shift the resonance as the radius of sphere increases. This is in consistent with the findings in previous research. The spheroidal shape is preferable in the practical application sense. Rather than the restrictive consideration of size, this study is the first to consider the nanoparticles with a constant cross-section and volume. Clearly, the findings indicate that the length has a positive effect on the light enhancement. A possible explanation is that higher polarizability can be obtained at a larger length. Similar to the smaller spheres with higher enhancement factor, the longer structure with higher enhancement factor at resonance also leads to a red-shift of the resonance in the spectrum. Regarding the shape effects among various nanoparticles, our results have provided conclusive evidence that the cylinder and rod have a better structural advantage to enable stronger light intensity in the considered frequency range. Although multiple resonances occur for the single triangle and fan due to the strong enhanced field found at the apexes, they are also of our interest in further studies to constrcut coupling structures. It should be noted that in addition to

the shape and size variations of nanoparticles, the variation of its surrounding medium also plays a role in plasmon resonance [120; 123; 124], which is quite amazing. That could be a further research direction.

Chapter 4

Nanoantennas Consisting of Coupled Nanoparticle Pairs

4.1 Introduction

Among diverse nanoantenna designs, closely placed particle pairs recently have attracted extensive research interest, and they are usually referred to as the nanoparticle dimmers. Early studies of the two interacting metal nanoparticles included a theoretical study in [125], an experimental observation of gold spherical particles in [126] and systematic studies of separation distance of gold nanodisks in [44] and elliptical pairs in [49]. These studies of nanoparticle pairs were important because their coupling effect will lead to stronger field enhancement as well as much more effective confinement compared with a single particle [46; 115; 127]. In particular, obvious concentrations of luminance were observed near the sharp tips or inside the gap between

the two particles of these dimmer nanoantennas [99]. The resonance can be further controllable by changing certain dimensional parameters and thus has potential engineering applications [128; 129]. The resonance's tuning characteristics depending on the gap are investigated in [130; 52]. Most intensively studied coupled particles structures include the bow-tie antenna, nanorods antenna and dipole antenna [99; 16; 3]. The simplified shapes of corresponding single particle are the triangles, cylinders and rectangular parallelepiped respectively. In this chapter, our study focuses on these coupling particles with specific shapes of the spheroid, cylinder, rod, triangle and fan to find their optical properties in the following aspects. Firstly, the optical properties of the single and coupling particles are illustrated together to make a comparison. Secondly, the light intensity as a function of the coupling structures' size and gap is numerically investigated for the nanoantennas with kinds of shapes. Thridly, these coupling pairs of different shapes are compared with the same lengths and spacing, so that the shape effects can be further evaluated. The scheme for the coupled particle pair's geometry is shown in Fig. 4.1 and Fig. 4.2. In the former figure, the top view is given for the spheroid, cylinder, rod, and triangle (bow-tie) shape. In the latter figure, a spheroid pair structure is taken as an example to explain the geometric parameters such as the gap and length. In the initial designs, the the parameters for coupling structures are set as follows: their lengths are changed from 180 nm to 240 nm; and their spacing are changed from 10 nm to 20 nm. Rod's ends and fan's facing apexes have the same radius of curvature of 30 nm. The apex angles for triangle and fan are both set as 60°.

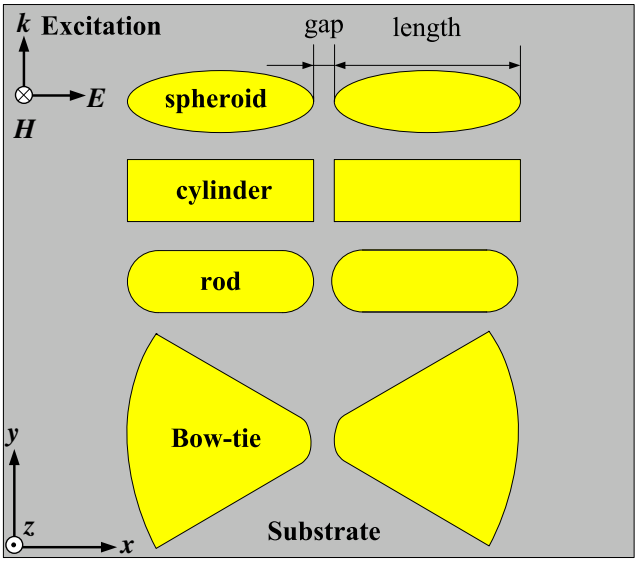

Figure 4.1. Scheme of coupling particle pairs.

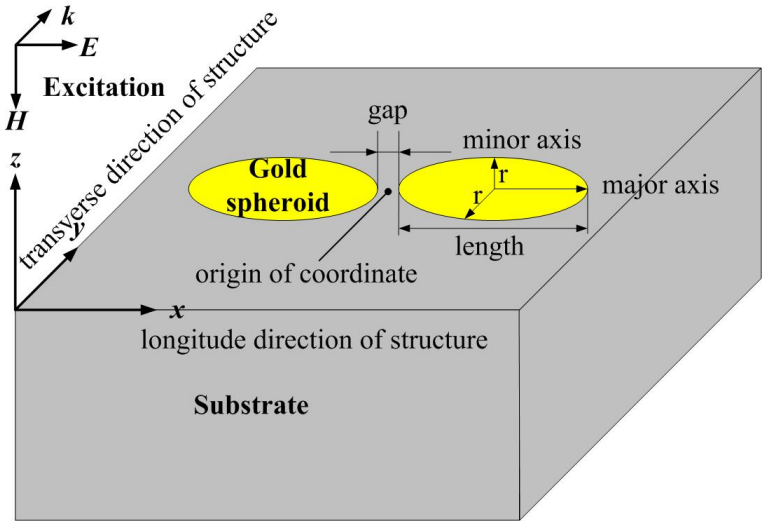

Figure 4.2. Scheme of the spheroid particle pair.

4.2 Optical Resonant Properties of Nanoparticle Pairs of Different Shapes

4.2.1 Optical Resonance of Single Nanoparticle and Nanoparticle Pairs

First of all, the spheroid is studied as a typical shape for coupling nanoparticle pair. The characterization and modelling in the simulation setup for the nanoparticle pairs are similar to those for a single nanoparticle in Chapter 3. In our computation, the localized strong enhanced field is found inside the gap of such particle pairs. The peak values at the position between the pair are recorded. In order to make a comparison, those values for a single particle case (at the particle end along X-direction)is also provided. The light intensity spectrum is plotted in Fig. 4.3 for both a single spheroid and two spheroid pair with length 180 nm and gap length 10 nm. In the following figures for two nanoparticle pair cases, the data is also recorded at the coordinates origin between two particle components. For the distinction between the single particle and couple particle pair cases, it can be seen that the coupling spheroid pairs are much more effective in the intensity's enhancement than the single spheroid. The ratio of the peak light intensity achieved by the nanoparticle pair to that of an individual nanoparticle is about 228, much better than 2, which is the simple sum of two single particles. This obvious better enhancement can be adequately explained by the enhanced lightning rod effect. Because both ends of a single spheroid can give

rise to strong field, the two ends facing together in a closed placed spheroid pair case tend to enhance such light concentration and confine sufficient light in the narrow gap between them. Moreover, the resonance in the nanoparticle pair case red shifts from 714.29 nm to 769.23 nm in the single nanoparticle case. The shift can be analyzed in this way. For a single nanoparticle upon excitation by the incident light, the movement of conduction electrons inside leads to the buildup of polarization charges, allowing a restoring force to occur with the direction opposite to the applied field direction. When two nanoparticles are placed together, these polarization charges on the facing ends of adjacent particle with different polarities will generate a induced field. This induced local field on the particle is along the applied filed but against the restoring field, thus decreasing the LSPR frequency. This is equivalent to a redshift in the wavelength. Above is the explanation for two spheroids case. In fact, the same is also true for the other shapes of particle pairs, which will be demonstrated and shown later. Besides, the light intensity spectra of four geometrically related coupled spheroid pairs are given in Fig. 4.4 to see the influences of length and gap size through the comparison among them. Four cases are proposed with different lengths and gap distances. This figure shows that both single particles with different lengths exhibit relative much lower light intensity than the pairs, so the curves for them seem like straight lines compared with those of pairs with obvious variation of intensive values. In fact, there is still some kind of fluctuation (*i.e.* resonances) for the single particle case even though it is not so apparent. It is simply hard to distinguish them in Fig. 4.4. The finding for enhanced light intensity of couple nanospheroids is also true for the coupling pairs of the other shapes shown in the following discussions.

The figure also reveals that the resonance is located at the near-infrared range of the light spectrum. Especially noteworthy is the finding that the spheroidal pair with narrower gap and larger length provides higher intensity at resonance among different designs. This conclusion is in consistent with those findings of the elliptical pairs in [49]. According to our computed results, the structure of 240 nm length and 10 nm gap distance reaches the best performance of E-field enhancement. The strongest intensity can achieve as 100 times stronger as that of the incident field. The detailed E-field distribution along the curve between the gap of the pairs with length 180 nm and gap distance 10 nm is also studied. At a frequency of 330 THz, where this structure is found to be resonant, the field distribution is plotted in Fig. 4.5.

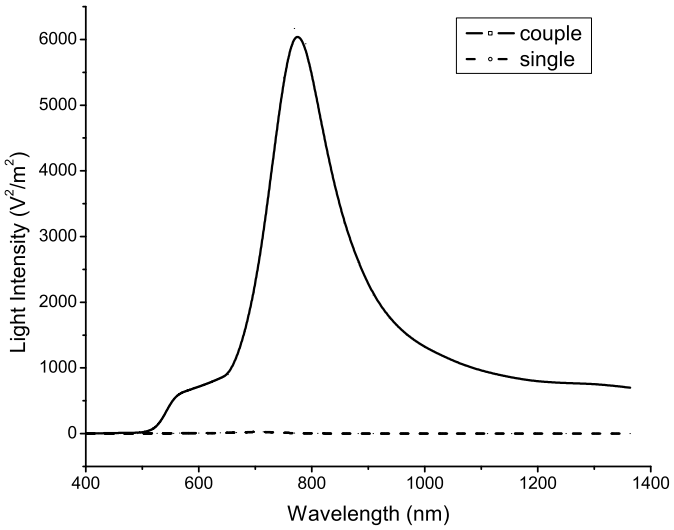

Figure 4.3. Light intensity spectra of single spheroid and couple spheroid pair.

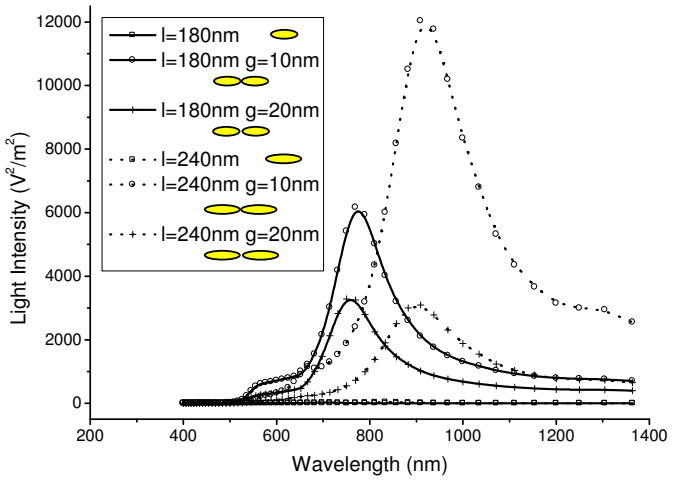

Figure 4.4. Light intensity spectra of spheroid pairs with different lengths and distances.

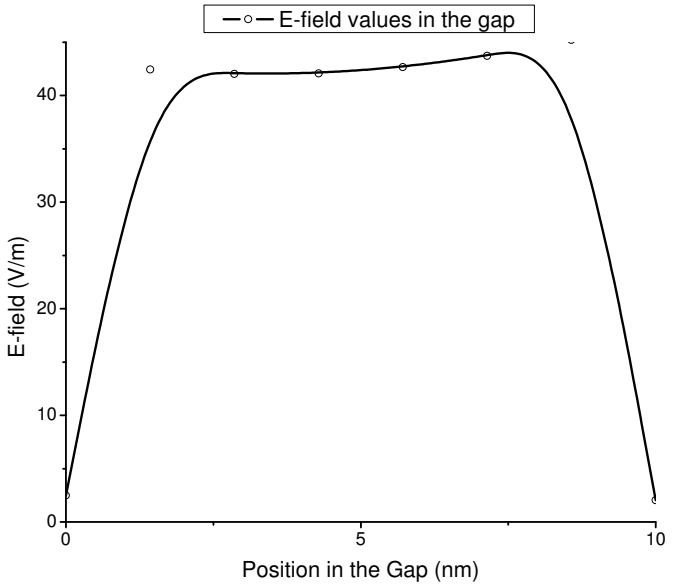

Figure 4.5. *E*-field along the curve between the spheroid pairs.

4.2.2 Optical Resonance Nanoparticle Pairs of Various Shapes

The systematic controllability of the optical properties of the noble metallic nanoparticle pairs has received increasing fundamental and technological interest in recent years. Nevertheless, the published papers usually focused on single type/shape of coupling structures' cases individually and only limited number of tunable factors are proposed. They provided no comprehensive information about how these effects take the role on the optical properties of all the structures. Such effects include the particle's geometry and external substrate and source condictions. Consequently in the next section, our effort is devoted to summarize sufficient "hot-spot" cases covering a number of structures and conduct an innovative and informative study. As shown in Fig. 4.6, Fig. 4.7, Fig. 4.8, and Fig. 4.9, the light intensities of the coupling rod pairs, cylinder pairs, triangle pairs and fan pairs under the influence of different lengths and gap spacing are provided as a synthesis study.

As Fig. 4.4 for spheroids, these figures for the coupling structures of the other shapes also confirm that the light intensity at resonance of two particle pairs is much higher than that of a single particle. In addition, no matter which shape is applied for the nanoparticle pair design, higher intensity is always obtained either with the longer ones assuming the constant gap spacing or more closely placed ones assuming the constant length. This conclusion, especially for the cylinders and triangles in our study, agrees well with that in [130] which explored the optical properties of dipole and bow-tie antennas as a function of the antenna length and gap. For the rods, in

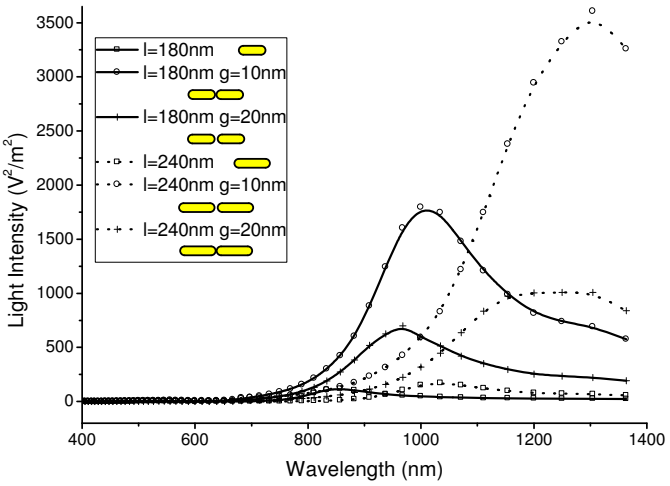

Figure 4.6. Light intensity spectra of rod pairs with different lengths and distances.

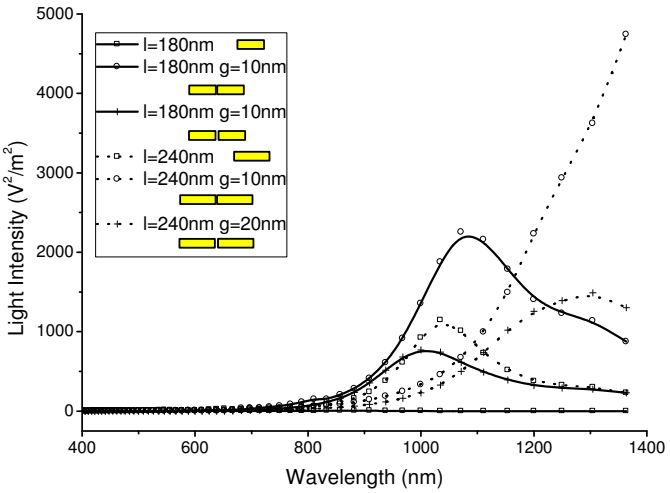

Figure 4.7. Light intensity spectra of cylinder pairs with different lengths and distances.

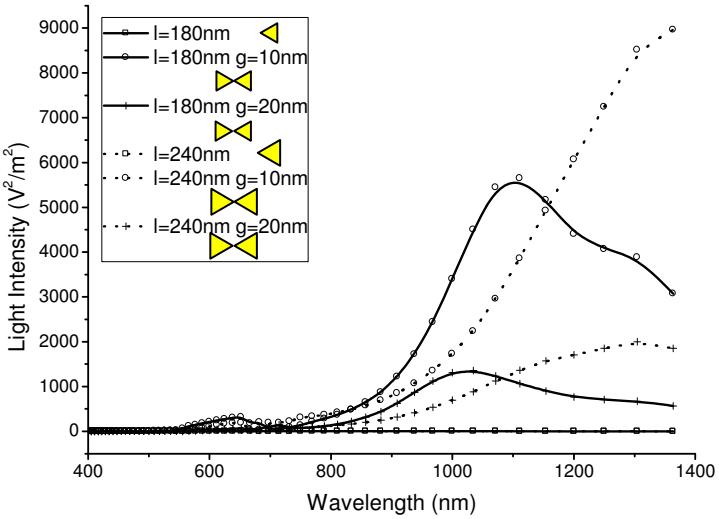

Figure 4.8. Light intensity spectra of triangles pairs with different lengths and distances.

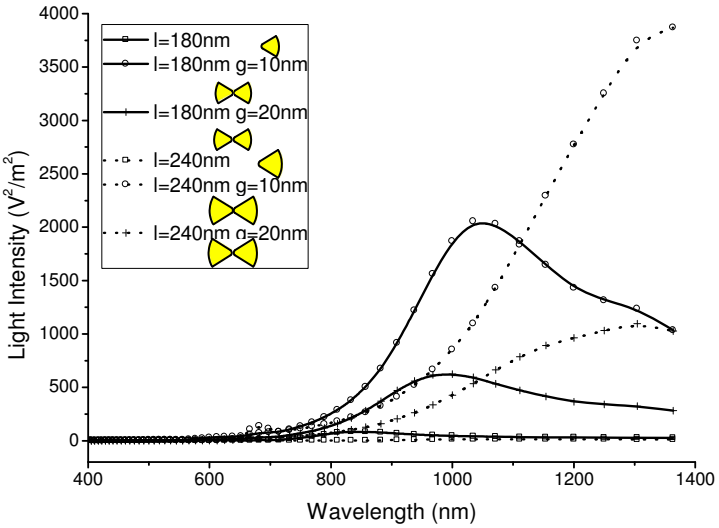

Figure 4.9. Light intensity spectra of fan pairs with different lengths and distances.

the same fashion as the description in [99], this results proved the pair with wider spacing blue shifts the resonance and that with larger length red shifts the resonance in our study.

4.2.3 Optical Resonance of Spheres, Spheroids, Cylinders, Rods, Triangles, and Fans with Constant Length

Fig. 4.10 shows the light intensities of nanoparticle pairs of different shapes with the constant length of 240 nm and spacing of 10 nm under the influence of the shapes. As observed from the figure, the light intensity consistently increases over the visible and infrared range, reaching a peak of more than 3000 unit for all the structures except for the spheroids. Among them, the triangles' intensity rises at the fastest rate. Even through the spheroids' curve decays after the spike occurs around 900 nm in the near-infrared range, its light intensity enhancement performance at resonance is the most pronounced over the considered frequency range. The highest value is 12037 unit, approximately 84 times than that of the cylinders at the same frequency.

4.3 Summary

This chapter states the significance of the unique light confinement and enhancement properties generated by two closely placed nanoparticles of several shapes. This study has taken a major step towards the possible more complex nanoantenna designs in future. One major advantage of this design is that the two nanoparticles is

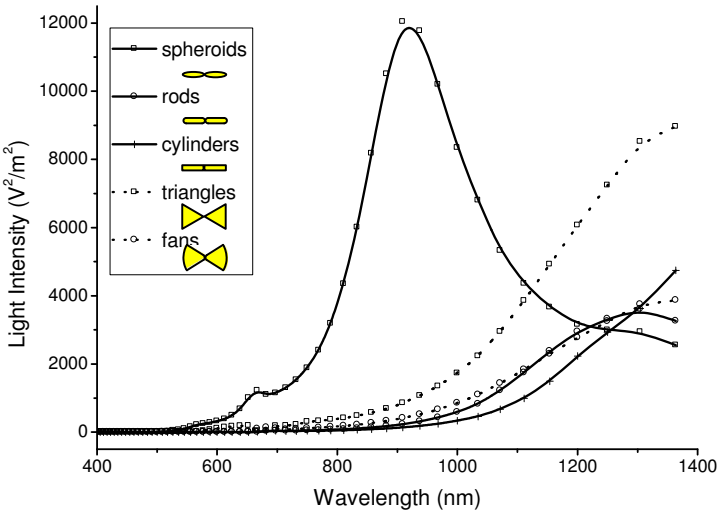

Figure 4.10. Light intensity spectra of different shapes of pairs with the same size.

able to produce more remarkable and adjustable plasmonic resonances than a single nanoparticle when induced by the light. On one hand, there is an accumulation of the energy in the gap region between the two nanoparticles, leading to a considerable enhancement of the near field and an increase in the far-field extinction, and it is much larger than the simple sum of that for individual nanoparticles. For example, the intense light can reach as high as 10^3 times of incident one for our proposed nanospheroid pair. This obvious enhancement phenomenon results from the strengthened interaction and combination of these two nanoparticles. On the other hand, the resonance of coupled pair shows a red-shift behavior in the spectrum compared with that of a single particle. As described by Rechberger in [44] (the structure is spherical nanoparticle pair in this paper, however the same is also true for the other shape nanoparticle pairs at a short distance.), such a coupling effect can be attributed to the dipole-dipole interaction as follows. When illuminated by an oscillating optical field, the resulting plasmon excitations induce and polarize the charge

density of the nanoparticle. Hence each particle individually acts like an oscillating dipole with positive and negative charges distributing on its opposite sides. Because the polarization is parallel to the axis connecting both nanoparticles, the attractive force will be formed between two adjacent nanoparticles. This attractive force will weaken the repulsive forces within each particle and thus result in a correspondingly lower resonance frequency (larger resonant wavelength). In addition to the finding of the notable enhancement, another promising finding is the plasmon resonances of our coupled nanoparticle pair can be tuned over a wide spectral range by changing their geometrical dimensions (like the length and gap). Stronger light intensity and red-shift of resonance can both be obtained through either extending the individual particle length or narrowing the separation between them. These results show good agreement with the current literature. The benefit of the present study is its guideline provided for better adjustment to a satisfying nanoantenna design through parameter optimization. Moreover, the comparable investigation is completed among several types of pair structures. It has demonstrated for the first time that shape effects are also important for the nanoantenna performance when constant length and gap are assumed for the structures. The spheroid pair is capable of offering higher light enhancement at resonance in our studied cases. Furthermore, the substrate effects and source polarization direction effects can be considered in future. Those aspects provide better physical insight and understanding of the coupled nanoparticle pair nanoantenna.

Chapter 5

Bow-tie Nanoantenna and Bow-tie Shaped Aperture Nanoantenna

5.1 Introduction

Among various emerging coupled nanoparticle pair structures as stated in Chapter 1 Section 1.1 and Chapter 4, Section 4.1, the bow-tie antenna consisting of two tip-to-tip triangle slices draw our most attention, because it has shown relative better near-field confinement and enhancement than the other structures [131]. Typical research reults of the bow-tie antenna can be found in [132] for their polarization and gap-dependent scattering response and in [1] for their achievable enhancement multiple (as high as 1000 times) demonstrated by two photon photoluminescence and confined region estimated by FDTD simulation (with the area of 650 nm^2) in quantity. Nowadays, the bow-tie antenna are of interest in a broad range of research

fields [50; 133]. Especially helpful are the findings that the bow-tie nanoantenna has competitive structural advantage so that can be conveniently compatible with surrounding supporting devices. Such applications in which bow-tie nanoantenna plays its important role involve being integrated to the semiconductor laser diode [134] or fabricated at the apex of atomic force microscopy (AFM) tip by focused ion beam (FIB) milling [3]. In this way, the composite system can lead to efficient field enhancement at the outer ends of bow-tie antenna [134] or at the antenna feed gap [18], making it more suitable for spatially-resolved high-resolution chemical and biological imaging and spectroscopy. On the other hand, it is also of interest to investigate the nanometer scale aperture antenna due to their ability to obtain strongly enhanced transmission of light through the holes and wavelength filtering [113]. It is famous for the application in combination with scanning optical microscope (SNOM) to overcome the problem of limited throughput through the transmission, which is especially useful for subwavelength optics [135]. Various of apertures have been explored [136; 137] and the apertures of a number of shapes were particularly designed since they have advantages of both extraordinary optical transmission efficiency and fine nanoscale spatial resolution. Such proposed special shaped apertures contain the C-shaped, H-shaped, and bowtie-shaped ones [138; 139; 140]. These structures' predominance over the other shapes mainly benefits from the waveguide propagation mode confined in the gap between the ridges. As an extension study of aperture structure, evenly distributed aperture array is also available in laboratory [56]. Among various aperture shapes, the bow-tie shaped aperture antenna is shown to be feasible when fabricated on the near-field scanning optical microscope (NSOM) probe to serve as

the aperture probe for the near-field optical imaging [114]. It is also found that the bow-tie nanoaperture has higher optical transmission than the regular rectangular aperture under the same resolution or improved light concentration compared to the rectangular aperture of the same opening area [140; 114]. In this chapter, we suggest the study of the bow-tie antenna together with that of the bow-tie shaped aperture antenna, because they have comparable properties while combined with microscopy in near-field imaging. This idea was also originated from the consideration of treating them as structural correlation (complementary) counterparts, which is probably to own related features. Different from the discussion of the coupling two fan shaped nanoparticles in Chapter 4, Section 4.1, the investigation of the bow-tie nanoantenna in this chapter places additional emphasis on its far-field properties as well as its correlation with the bow-tie aperture nanoantenna. Currently little research has been carried out on the resonance characteristics of both geometrically complementary nanoantennas at the same time. As a result, it is worthwhile to extend such a study in seeking some innovative results. In addition, more meaningful discussions in terms of both the near-field resonance observation (aimed at the experiments for applied optics) and the far-field antenna radiation theory (based on the engineering electromagnetics) are presented in this study. The major antenna parameters responsible for the variation of antenna performance will also be carefully determined. The performance features with adjustable parameters will be provided to add to present literature the direct visualization. Significantly different from present nanoantenna study that was only restricted to independent antenna structure without any matching equipment for guiding the electromagnetic waves (light) like the transmission line,

topics on possible related connection devices are also inclusive. Thus we no longer require simple excitation using the plane wave and it can avoid solving an isolate and one-side problem. Such exploratory study is a favorable attempt for further design and optimization. The configurations of our designed nanoantennas needs further demonstration as follows. The bow-tie nanoantenna as proposed in this work consists of two fan-shaped hollow apertures mounted on a gold thin film. It should be emphasized that the two apertures were jointly contacted in the existing research [140]. But in our present work, the two apertures are separated individually by a film gap contrary to the literature. In view of the evidence shown in Chapter 4 about two components' advantage in the enhancement rather than one, our antenna arrangement is expected to lead to strong inter-aperture coupling. Thus, it is more desirable to enhance its resonance performance. Although the aperture antenna has been pointed out to provide broad band field localization and enhancement regardless of the metals utilized [114], other material like copper may be more economical than gold, we remain the usage of Au to satisfy consistent condition for two complementary geometries. The bow-tie antenna's size is assumed to be the same as that in previously reported studies [131]. Each compositive component has a fan shape with the length of 240 nm and the gap spacing of 20 nm between them. In order to avoid singularity, the apexes of the fans are rounded off with a radius of curvature of 30 nm. The flare angle of the bow-tie antenna is set as 60°. Such bow-tie nanoantenna with a thickness of 60 nm is placed on silicon dioxide substrate with a thickness of 200 nm surrounded by the air. In the same fashion as those parameters for the bow-tie nanoantenna, the aperture nanoantenna has the same length, gap, radius of curvature, and thickness for

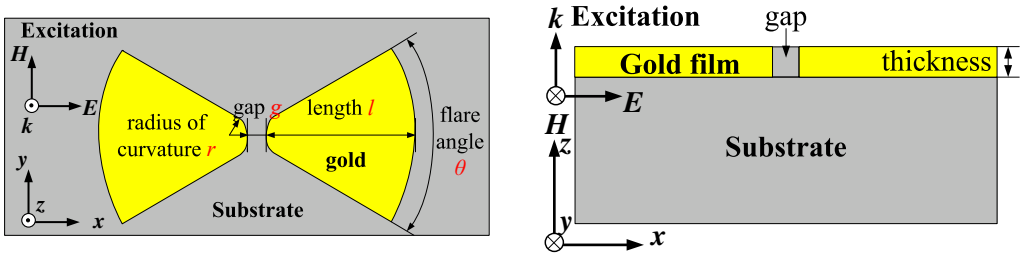

(a) Top view (b) Side view

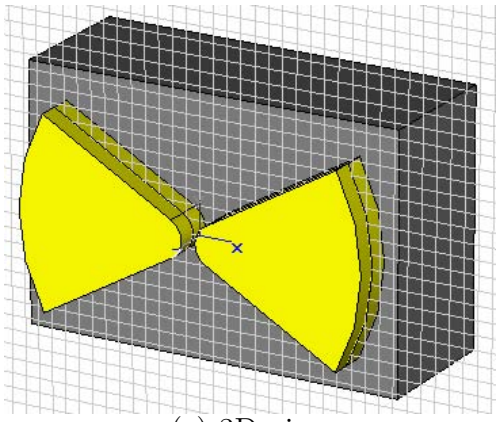

(c) 3D view

Figure 5.1. Scheme of bow-tie nanoantenna.

comparison purpose. The schemes of the designed nanometer scale bow-tie antenna and aperture antenna are given in Figs. 5.1 and 5.2 including their respective (a) top view, (b) side view at the plane y=0, and (c) three-dimensional (3D) view. The main geometric and source parameters of our research interest are provided in the figures, which will be discussed in detail later.

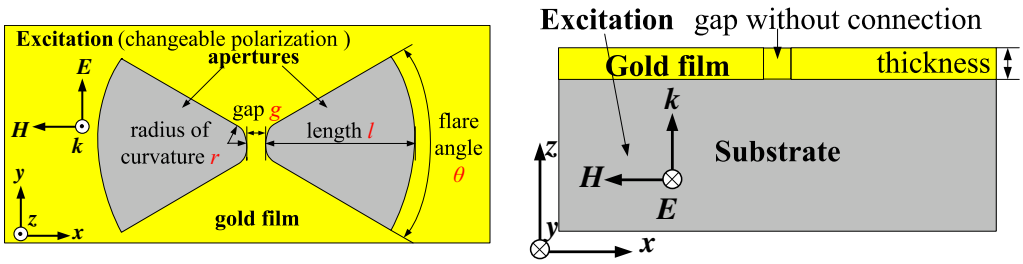

(a) Top view (b) Side view

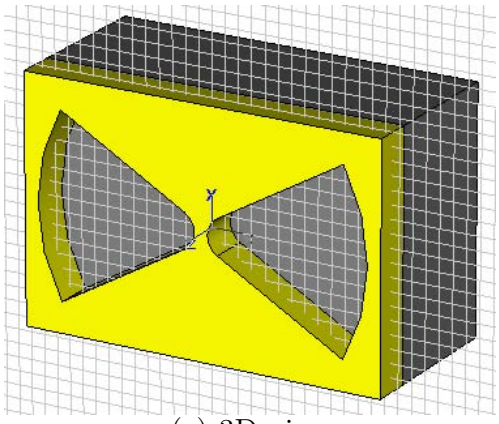

(c) 3D view

Figure 5.2. Scheme of bow-tie aperture nanoantenna.

5.2 Optical Resonant Properties of Bow-tie Nanoantenna Dependent on Geometric Effects

In this section, we considered diverse designs in terms of different radii of curvature r from 10 nm to 80 nm, flare angles θ from 30° to 150°, gap distances g from 10 nm to 40 nm, lengths l from 180 nm to 300 nm, substrate thicknesses t from 20 nm to 200 nm, substrate refractive indices ε from 1 to 3, and materials of four noble metals to achieve a more comprehensive study of the controllable characteristics of the bow-tie nanoantenna. For each effect (or parameter) explained later, we will only change this specific parameter while keep the other parameters constant. Therefore, in this way a comparable study can be carried out.

5.2.1 Tip Design

- Radius of curvature effects

After the calculation, a highly localized field is found inside the gap of the bow-tie antenna, similar as the findings in Chapter 4, Section 4.2.2 for two nanoparticles. This is again due to the surface plasmon excited by the light. Accordingly, the field values are recorded over the frequency range at this spacing between two fan shapes. Fig. 5.3 provides the light intensity spectra of the bow-tie nanoantennas varying with the radius of curvature of the apex angle. Four values for the radii of curvature are

evaluated: 10 nm, 30 nm, 50 nm, and 80 nm. It can be seen from the figure that the bow-tie nanoantenna has two resonances in the spectrum within the visible and near-infrared range. One resonance appears at the red portion of the visible range, while the other one appears in the near-infrared range. The resonances occur around 670 nm in four cases have little difference between each other. They basically remain approximately at the same frequency. But the other resonances occur at around a greater wavelength of 1100 nm have much difference among the four cases. They follow this rule: as the radius of curvature turns larger, the antenna's resonance shifts to the red side of the spectrum. In addition, the bow-tie nanoantenna with a smaller radius of curvature can provide higher light intensity at resonance compared with that of larger ones. The enhancement factor (compared with the incident light) at resonance can be improved from 677.8 to 1161.1 as the radius of curvature decreases from 80 nm to 10 nm. Higher light intensity at resonance achieved by the bow-tie with sharper geometric features can also be attributed to the lightning rod effects.

- Flare angle effects

Similarly, we collect the values and draw the figure for the flare angle's effects on the light intensity for the bow-tie antenna, as shown in Fig. 5.4. Arranged in the descending order, the maximum light intensities of the bow-tie nanoantennas are from those with the flare angles of 30°, 60°, 120°, 150° and 90° in turn. It is suggested that this pheromone can be comprehended in the following way. The sharp degree is acute angle>right angle>obtuse angle, so the nanoantenna with sharpest acute angle of 30° achieves best performance in light intensity enhancement at resonance. This

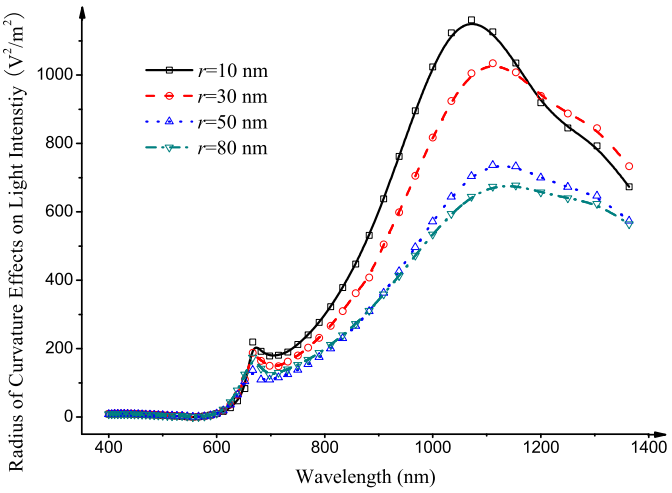

Figure 5.3. Radius of curvature effect on light intensity of the bow-tie nanoantenna.

highest light intensity can be as high as 1094.3 V^2/m^2. The light intensity provided by the nanoantenna with a flare angle of 30° is 2.6 times of that with the flare angle of 90° in their respective resonant cases. As in the discussion on radius of curvature effect, the flare angle effect on the first resonance point (with a smaller wavelength) is not obvious either. Only a very slight trend of shifting to the smaller wavelength is observed as the flare angle increases. But for the second resonance point (with a larger wavelength), the bow-tie nanoantennas' resonance frequencies go higher with increasing flare angles. The detailed values for the resonances are shown in Table 5.1.

5.2.2 Gap and Length Designs

- Gap effects

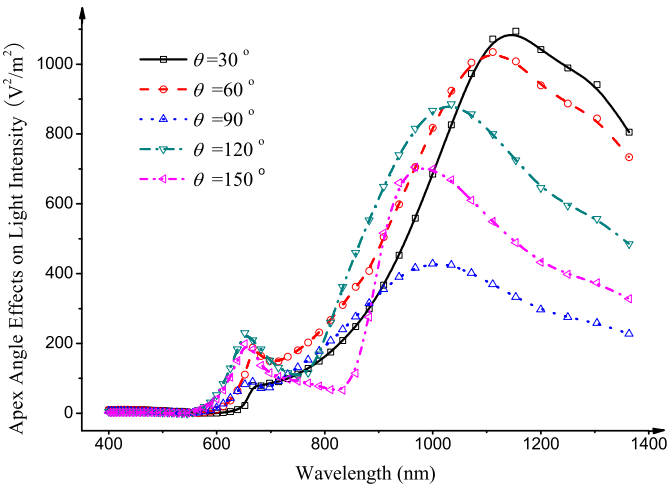

Figure 5.4. Flare angle effect on light intensity of the bow-tie nanoantenna.

Table 5.1. Resonance values for bow-tie nanoantenna under influence by flare angle.

θ **(degree)**	**Resonance 1**		**Resonance 2**	
	Wavelength (nm)	**Light intensity** (V^2/m^2)	**Wavelength** (nm)	**Light intensity** (V^2/m^2)
30	666.7	79.15	1111.1	1094.32
60	666.7	187.83	1111.1	1034.59
90	666.7	89.46	1000	427.98
120	652.2	230.46	1034.5	885.95
150	967.7	705.07	652.2	198.36

In this section, the two components of the bow-tie nanoantenna are placed close or far apart with different spacing. The gap lengths vary from 10 nm to 40 nm with an increment of 10 nm. As seen from Fig. 5.5, it can be found that such spectra obey this law: an antenna arrangement with narrower gap tends to exhibit higher light intensity. The intensity at resonance for nanoantenna with the separation gap of 10 nm is much higher than those with gaps of 10 nm and 40 nm. This high value gained with the gap of 10 nm is 885.9 V^2/m^2, which is more than triple of that in the case with gap of 40 nm. Moreover, the resonance points show a red shift in the spectra as the gap becomes narrower from 40 nm to 10 nm. Such a gap-dependent resonance phenomenon agrees well with the measurement data in [132; 98].

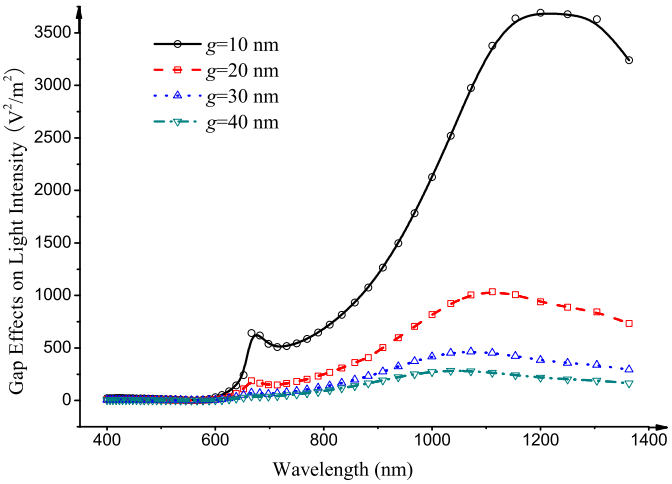

Figure 5.5. Gap effect on light intensity of the bow-tie nanoantenna.

- Length effects

Another geometric effect of our concern is the length of antenna. With the initial design of each component of length 240 nm, the shorter one with 180 nm and the

Table 5.2. Resonance values for bow-tie antenna under influence by length.

l (nm)	Resonance 1		Resonance 2	
	Wavelength (nm)	**Light intensity** (V^2/m^2)	**Wavelength** (nm)	**Light intensity** (V^2/m^2)
180	625	76.2	937.5	976.13
240	666.7	187.83	1111.1	1034.59
300	714.3	323.73	1363.6	1207.36

longer one with 300 nm are investigated. The spectra are given in Fig. 5.6. It can be observed that with a length around 240 nm, the longer antenna possesses higher intensity at resonance as well as a greater wavelength for both resonance points. The data for the resonances are given in Table 5.2.

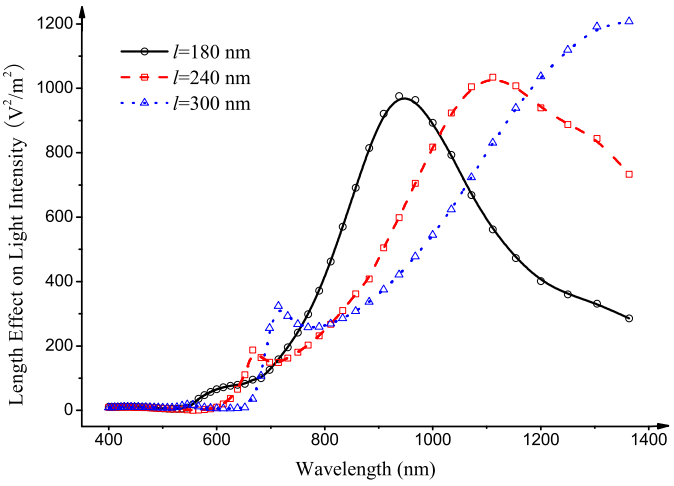

Figure 5.6. Length effect on the light intensity of the bow-tie nanoantenna.

5.2.3 Substrate and Material Analysis

- Substrate thickness effects

In this section, the thickness of the substrate is also taken into account. It varies in the order of thin to thick substrate at different values of 50 nm, 100 nm, 150 nm, and 200 nm when the structure of nanoantenna remains. The results are given in Fig. 5.7. It indicates that the substrate thickness has merely no effect on the resonant frequency. The resonances maintain at the same positions in the spectra. However, the peak light intensity is affected by the substrate thickness. With a thicker substrate, a higher light intensity is exhibited, which is unexpected. The silicon dioxide used as the substrate may couple with the incident light and provide the positive effects on the light enhancement. As for what the mechanism behind this observation is, further investigations on physical insight are desirable, and will be left to the further exploration. The substrate's relative dimension and position compared with the nanoantennas can be varied in future research work. But for convenience in the experiments, the substrate is advised to be neither too thin (less than 10 nm) nor too thick.

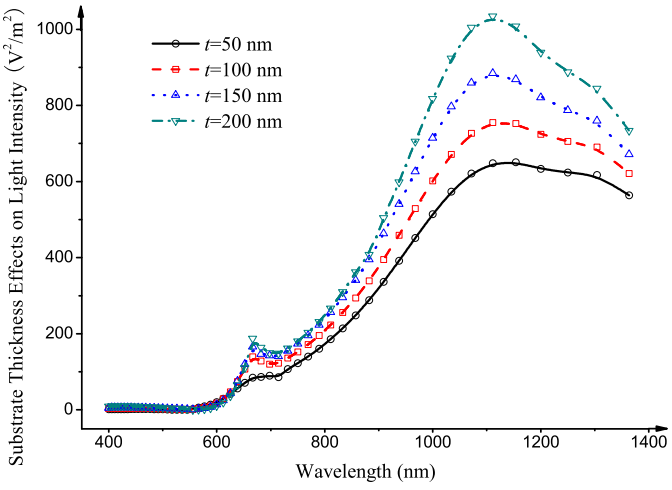

Figure 5.7. Substrate thickness effects on light intensity of the bow-tie nanoantenna.

- Substrate refractive index effects

In a case contrary to the variation of nanoantenna, the variation of its surrounding medium has also been proposed by researchers in [141; 142]. It is proved that the surface plasmon resonance of the coupling nanoparticle pair increases correspondingly with the medium dielectric constant. It exhibits a higher sensitivity to the environment/medium refractive index as compared to an isolated nanoparticle. In our calculation, the substrate's refractive index's impact on light intensity enhancement is also considered. The same antenna is placed on the substrate of identical dimension however with different indices of refraction: 1, 1.5, 2, 2.5, and 3. The light intensities as a function of the wavelength with different substrate's refractive indices are given in Fig. 5.8. This figure shows that as the substrate refractive index increases, the resonance redshifts in the spectra. This show agreements with the results in [143]. The increase in the refractive index n is equivalent to the increase in the dielectric constant of substrate ε because $n = \sqrt{\mu\varepsilon}$. Hence the increase in the overall effective dielectric constant surrounding the nanoparticle result in the redshift of its resonance when it is located on top of a substrate or embeded/immersed in a surrounding medium [92] in comparison to a isolated nanoparticle case without the substrate. This can be adequately explained by the theoretical analysis in Chapter 2, Section 2.2.1. In addition, the peak resonance values slightly grow higher in corresponding case.

- Material effects

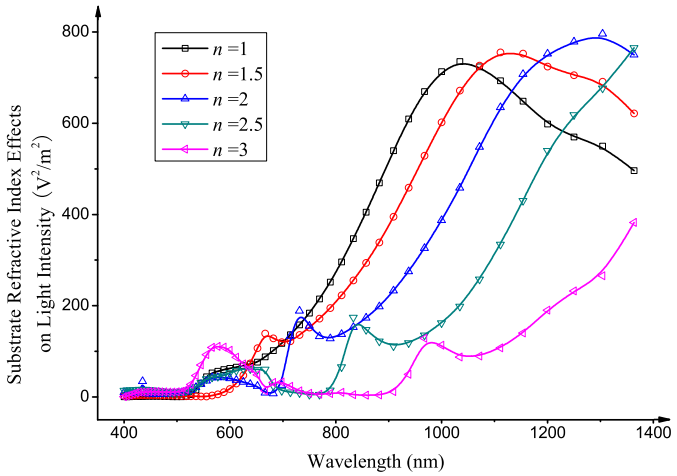

Figure 5.8. Substrate refractive index effects on light intensity of the bow-tie nanoantenna.

In our calculation, the bow-tie nanoantenna designs applying different noble metals are also modelled, including gold, silver, copper and aluminium. Their dielectric constant values are adopted from those in Chapter 1, Section 1.3. Fig. 5.9 shows the light intensity under influence by different noble metals. The results suggest that all the noble metals have apparent enhancement behaviors in our considered frequency region. Except for aluminium, other metals provide quite similar light intensity spectrum, especially for the redder resonance. There's an additional resonance for copper appearing at a larger wavelength, which validity is questionable. Because the data of dielectric constant in [79] are collected from piecewise frequency ranges in different research works, they may have jumps at some values. This may affect the final results of simulation. In addition to the resonance point, the light intensity at resonance is still another interesting topic for material effects. The peak values of light intensity are arranged in the order of metals: silver is better than gold; they are followed by

copper; and the last is aluminium. In practical experiments, for a metallic particle size corresponding to the same deposited mass thickness, gold has lower resonance frequency than silver [92]. The resonances with higher frequencies in our results for gold and silver cases agree with this observation.

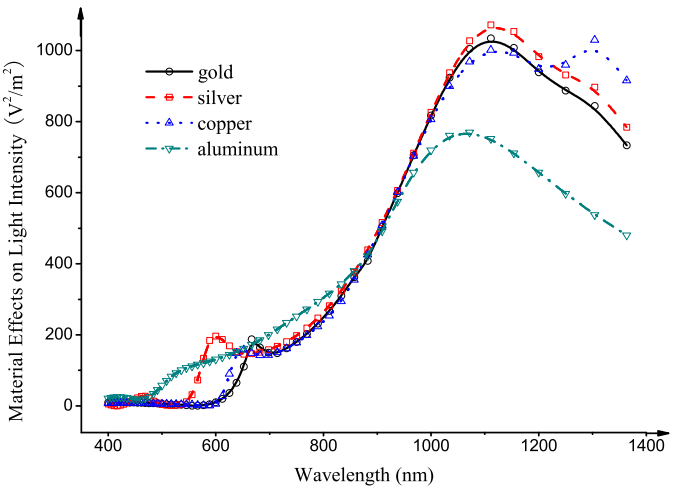

Figure 5.9. Material effects on light intensity of the bow-tie nanoantenna.

5.3 Near-field Resonance and Far-field Radiation of Bow-tie Aperture Nanoantenna

5.3.1 Near-field Resonant Properties

- Effects of source polarization direction

As stated in the beginning of this chapter, fan components of the bow-tie aperture antenna reported in literature were jointly connected as an entire bow-tie shape aper-

ture. Under this structural situation, the E-field of excitation is across its gap, normal to the line connecting both apexes of fan components, which is also the direction applied in the ordinary aperture antenna by feed. However in our study, in order to conduct a comparable study, the case under the source excitation with polarization direction along the line connecting both apexes of fan components is also considered. Thus in the beginning of the discussion on effects on near-field properties of the bow-tie aperture nanoantenna, the effect of the polarization direction of the incident light is theoretically investigated. By keeping the wave propagating in the z-direction associated with the light incident upon the aperture from the substrate side, two cases of polarizations in the x- and y-directions are carefully considered. The results are shown in Fig. 5.10, where the E_x (parallel) and E_y (normal) polarizations are plotted, respectively. The light intensity is calculated and recorded at the origin, *i.e.* the middle of two fan-shaped nanoapertures within the metal. It is found that both cases show a resonant behavior varying with wavelength in the light intensity's spectra. Single resonance occurs in the optical range in the case of the E_x polarization; while two resonances appear in the near infrared range in the case of the E_y polarization. This can be explained by strong interactions between the nanoantenna and the light through plasmon resonance. However, the variation magnitude of the E_x polarization in Fig. 5.10 (a) is much smaller than those of the E_y polarization in Fig. 5.10 (b).

In both cases, there are two apparent differences. On one hand, our simulation results suggest that under the E_x source polarization, the strong field is formed and confined at two outer edges of the nanoapertures; while under the E_y source polar-

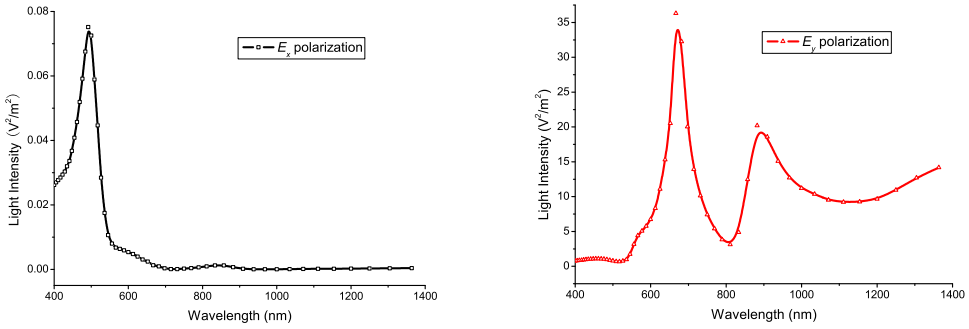

(a) E_x polarization (b) E_y polarization

Figure 5.10. Light intensity of bow-tie aperture nanoantenna under different excitations.

ization, enhancement is found in the area around its inner apexes. The enhancement is obtained due to the lightning rod theory which causes the largest electric field to appear near the sharpest end. The difference of light concentration positions is attributed to different excitation directions. On the other hand, it can be observed from the figures that the E_y polarization is able to achieve much higher light intensity than the E_x polarization at the corresponding wavelengths. That can be accounted for by more effective light excitation induced by the transverse (compared to the aperture longitudinal axis in the x-direction) polarization source similar to the source used in the aperture antenna. The light intensity of our designed aperture nanoantenna can reach as high as 36.3 $\mathrm{V}^2/\mathrm{m}^2$ normalized to the incident one in the latter case. As compared with the results of [141] on the designs with connected aperture, there is still some room to optimize our design to achieve the same level of peak intensity.

- Effects of radius of nanoaperture curvature

Next, the effects of the radius of nanoaperture curvature on the optical resonant properties of the bow-tie aperture nanoantenna are also considered. Fig. 5.11 shows how the light intensity changes with different radii of curvature r: 10 nm, 30 nm, 50 nm, and 70 nm. In each case, the flare angle, length, and gap separation of the aperture nanoantennas are kept unchanged. From Fig. 5.11, it can be observed that as r decreases from 70 nm to 10 nm (*i.e.* the apex of the nanoaperture becomes sharper), the light intensities at two resonances both turn higher. In addition, with a larger radius of curvature, the resonances move toward the larger wavelength side, which means a red-shift in the spectrum. As a result, for preferable stronger enhancement in future studies, the bow-tie aperture nanoantenna can be designed by modest minimizing its inner apexes to meet such a requirement.

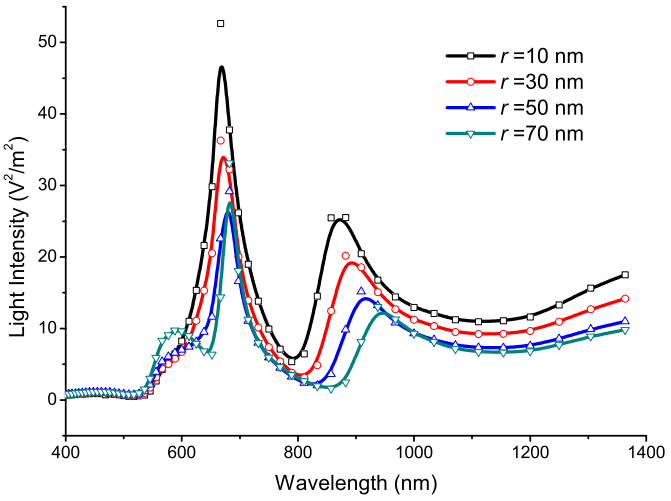

Figure 5.11. Light intensity of bow-tie aperture nanoantenna with different radii of curvature.

- Effects of nanoaperture flare angle

Similarly, the effects of nanoaperture flare angle on the optical resonant properties of bow-tie aperture nanoantenna are demonstrated in detail. The designs vary but a constant radius of curvature 30 nm is kept. The flare angle effects are characterized in several designs with acute angles, right angle and obtuse angles of θ. The simulation results are shown in Fig. 5.12. Except for the light intensity curve for the right angle owning three resonances, all the other curves have two resonances. The peak value at the first resonance is higher than that at the second one for θ of 60° and 120°; while the contrary cases are found for θ of 30° and 150°. In general, both acute angles and obtuse angles provide better enhancement factors at resonance than the right angle. Therefore, an appropriate design is suggested by sharpening its aperture apexes. It is found that all the resonances occur in near infrared range. Moreover, although there is no distinct rule for θ-dependent light intensity enhancement at first resonance, an apparent relationship at second resonance with greater wavelength is shown. A red-shift of this resonance is seen in the optical spectrum with increasing flare angle. The best enhancement achieved by the nanoantanna is as high as 38.91 V^2/m^2 at θ=120° and occurring at a wavelength of 697.7 nm.

In summary, optical properties of the bow-tie aperture nanoantenna is affected by various geometric parameters. Besides, the substrate change also takes an effect on the optical resonances of such antenna. It is reported that the relative permittivity of the dielectric substrate can be altered to tune the resonant wavelength of a nanometric bow-tie aperture[128]. This is an interesting topic for future research.

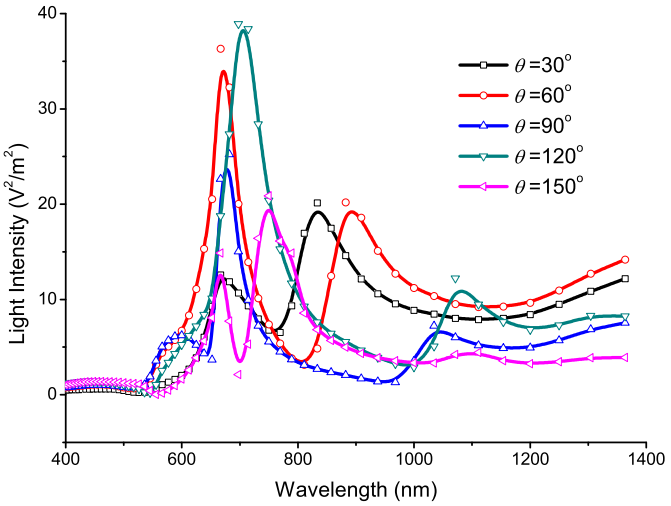

Figure 5.12. Light intensity of bow-tie aperture nanoantenna with different flare angles.

5.3.2 Far-field Radiation Properties

As pointed out in Chapter 2, Section 2.1, the radiation properties of an antenna is very essential. That is also true for our nanoantenna. In this section, we characterize a far-field property of the bow-tie aperture nanoantenna, which is not seen in the present research emphasizing near-field studies based on the optics background. Among several design specifications, the radiation pattern is an important measure in the far-field of the nanoantenna, to what we could see. Besides, the directivity and gain are also of specific interests. Actually, research indicated that the directivity of the radiation pattern of an aperture mounted in real metals is likely to be larger than the theoretical predictions valid for the perfectly conducting plane [144]. In addition, the light transmission through the nanometer scale apertures is another interest topic. It is noted from the diffraction theory developed by Bethe that for a simple circu-

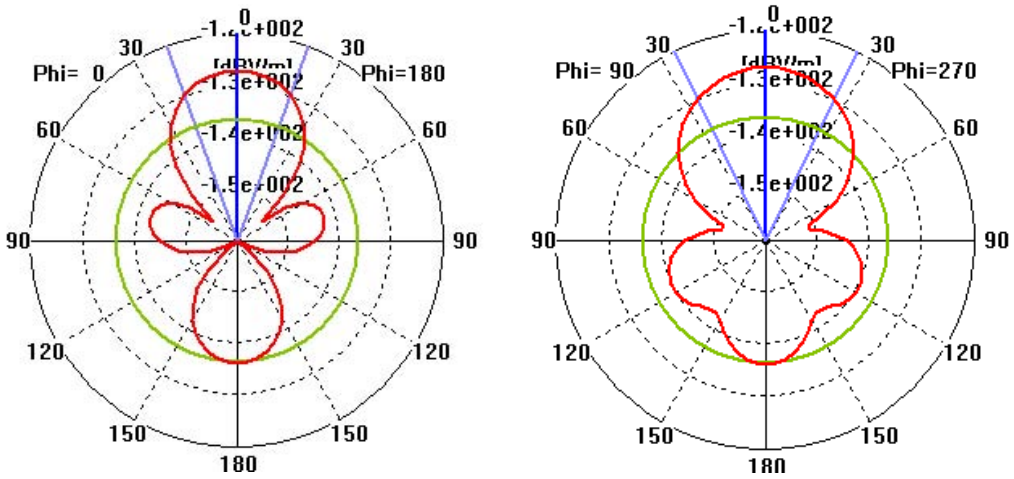

(a) E_θ in $\phi = 0°$ plane (b) E_θ in $\phi = 90°$ plane

Figure 5.13. Field pattern of bow-tie shaped aperture nanoantenna.

lar aperture in an infinitesimally thick perfect conducting plane, the transmittance dramatically reduces as the aperture's dimension decreases [145]. Thus, there exists a demand of understanding both as small focusing spot and high transmittance. It is very difficult, however, to quantify the transmission efficiency in experiments with lab condition restrictions. Furthermore, recent research on the rectangular, circular and bow-tie shaped apertures has shown resonant behaviors in the transmission properties, which was not predicted and addressed [114].

In our far-field computation for the bow-tie aperture nanoantenna, the field patterns in the $\phi = 0°$ plane and $\phi = 90°$ plane are plotted in Fig. 5.13 for the bow-tie shaped aperture nanoantenna with a radius of curvature 30 nm and a flare angle of 60° at a wavelength of 500 nm. The red curve stands for E_θ pattern. The green curve is the magnitude of back lobe. The blue lines are the mark for half power beamwidth. The patterns in our calculation imply that a good directivity is achievable by the bow-tie aperture.

From the figure it is found that the half power beamwidths obtained are 51.8° and 40.2° in both planes, respectively. The following approximation formulation for a directional pattern is used [81]:

$$D = 41253/(\Theta_{1d}\Theta_{2d}), \tag{5.1}$$

where Θ_{1d} and Θ_{2d} stand for the half power beamwidths in degrees in two respective perpendicular planes. The directivity calculated is 19.8, equivalent to 12.97 dB compared with the omnidirectional antenna with directivity of 1. In the same fashion, the gain for antenna satisfies the following empirical equation [81]:

$$G = 30000/(\Theta_{1d}\Theta_{2d}). \tag{5.2}$$

From Eq. (5.2) the gain of nanoantenna calculated is 11.6 dBi. It should be noted that the directivity is obtained by the formulae based on some approximations. Eq. (5.1) suggests one narrow major lobe and very negligible minor lobes. Hence it might be not adequately exact in our case with larger side lobes. Even so, the results could serve as a good reference for nanoantenna designs.

5.4 Results and Discussion on Both Nanoantennas

In this section, a comparison between the bow-tie nanoantenna and the bow-tie aperture nanoantenna is made. All the geometric parameters are the same in both cases: l=240 nm, g=20 nm, r=30 nm, θ=30°, and t=60 nm. The excitation is also the same, with the plane wave polarized in the x-direction and propagating in the z-direction. The near-field value data are collected at a fixed position in the middle of

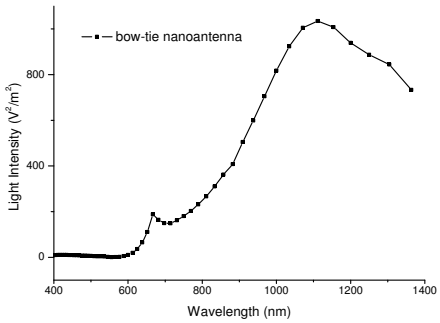

(a) Bow-tie nanoantenna

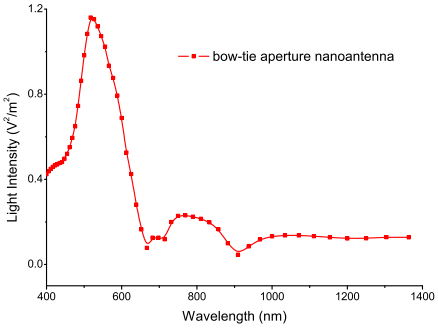

(b) Bow-tie aperture

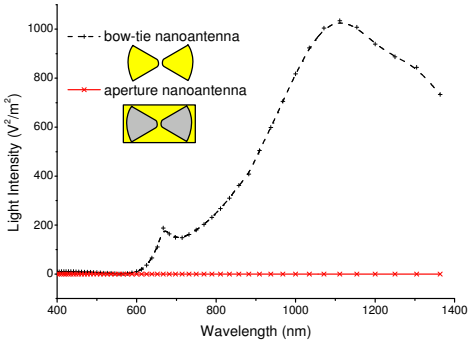

(c) Both nanoantennas

Figure 5.14. Light intensity spectra of bow-tie antenna and complementary aperture antenna.

the gap between the fan shaped components. This can imitate the near-field optical scanning microscope probe used in practical measurement. Fig. 5.14 plots the light intensity spectra of both antennas calculated in the optical range.

As seen from the figure, both antennas' spectra exhibit a resonant behavior in the gap. Although the value for the aperture antenna is much lower than that of the bow-tie antenna at corresponding frequency position, it still shows a fluctuating curve. The bow-tie antenna has two resonances arising at 667 nm and 1111 nm; while the aperture antenna has three resonances. It is found that there are an obvious peak point at 492 nm and two inconspicuous peak points at 789 nm and 833 nm respectively

for the latter antenna. In order to make a comparison between two complementary antennas, the field distributions near them are also simulated, which is shown in Fig. 5.15. In this figure, it is again shown that the bow-tie antenna has advantage of better enhancement in the gap region over the aperture antenna in the near-field region. As stated hereinbefore, the aperture antenna still has its own advantage of high transmitted field intensity in the far field measurement. More differences are considered in our further study. It is noted that the outer side of the aperture antenna shows stronger field than the spacing between the two components. This is due to the excitation direction different from previous research on the aperture antenna [128] (with polarization in the y-direction). For conventional RF aperture antenna with single connective bow-tie aperture, the E-field is located at the gap region along the normal direction to the antenna axis through the feed. But in our structure, the bow-tie aperture is divided into two separate aperture components and the plane wave with x-direction polarization is adopted. Thus the field distribution is different. As discussed in the above section, our purpose is to make equivalent conditions for both bow-tie antenna and aperture antenna, so the source of parallel polarization for the bow-tie antenna is used for aperture antenna instead of that of normal polarization.

In summary, as special cases for coupling nanoparticle pairs, the bow-tie nanoantenna and the bow-tie aperture nanoantenna are proposed together in this chapter. Their near-field optical properties and far-field radiation properties are both investigated. It is found that both antennas can exhibit resonant behavior in the optical and near-infrared regions. The light enhancement sensitive to some geometric effects

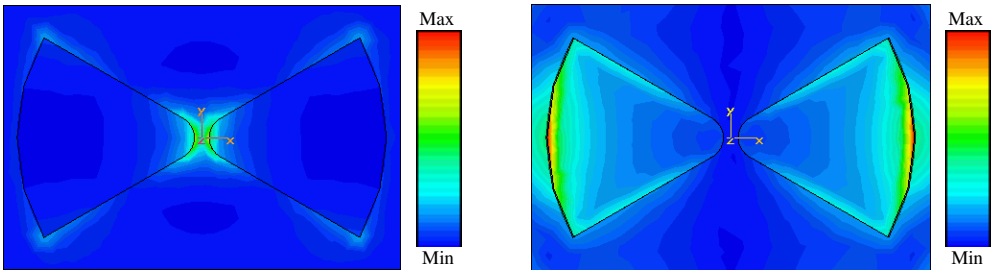

(a) Bow-tie nanoantenna (b) Bow-tie aperture nanoantenna

Figure 5.15. Field comparison between bow-tie antenna and complementary aperture antenna.

for them is determined. The source polarization effects and the substrate thickness effects are also taken into account. Enhancement can occur at different positions on the structures, depending on the polarization directions of incident light. The transverse one can give a better efficiency in enhancement. A nanoantenna with a shaper apex (smaller radius of curvature or smaller flare angle) supports higher light intensity at resonance and usually blue-shifts the resonances at the same time. The far-field patterns are calculated especially for the aperture nanoantenna. The directivity and gain are computed and their physical significance is discussed. Although the concept of enhanced directivity from the nanoantennas has been theoretically explored by researchers [146], quantitive data are provided in the study as an improvement. Under the same excitation conditions, the bow-tie antenna is stronger in light enhancement than the aperture antenna. An important contribution of the present study is that it provides controllable characteristics of nanoantennas, so the parameters can be tunable and adjustable in quantity for a satisfying design needed.

Chapter 6

Nanoantennas of Nanoparticle Chain and Array

6.1 Introduction

In addition to the configurations consisting of single and coupled nanoparticles explained in the last three chapters, the nanoantenna designs of interest also include the nanoparticle chain and array. Such configurations are theoretically demonstrated to be promising, and they are even made possible as the development of nano processing technology. There are the designs consisting of the identical and different nanoparticle components for the chain and array, respectively.

Regarding the chain designs, ordered silver nanoparicles closed arranged in chain were proposed to guide EM energy [147]. They are considered as the plasmon waveguides and considerable related theoretical research emerging subsequently are con-

ducted by Maier [148; 149; 150]. In the meantime, such a periodic chain of metallic nanoparticles is also experimentally demonstrated in comparison with their simulation results [151; 53]. Squeezing of the optical near field along the chain is found using a photon scanning tunneling microscope (PSTM) to be localized between the gold particles. Moreover, dipolar interactions analysis was made in [16] and the results obtained are quite different from previous quasistatic treatments. In addition to such designs made of identical elements, the self-similar elements with progressively decreasing sizes and separations are also suggested to compose the particle chain [152; 153; 154]. They can be treated as the nanolense, where the nanofocus in the gap between the smallest nanospheres is observed.

Regarding the array designs, on one hand, the arrays consisting of identical nanoparticle components are extensively studied in recent years. For instance, a two-dimensional (2D) metal nanodisk array under periodic BC in [54] and an array of finite-length metallic carbon nanotubes in [55] were both theoretically studied; a double-periodic array of pairs of parallel gold nanorods in [155] and an array of coupled gold optical antennas of several shapes lithographicallly defined on the facet of an optical fiber in [12; 99] were fabricated and measured. The nanoshell arrays also draw much interest because they have structural tunability of the plasmon resonances [156] and furthermore support the hybrid junction plasmons that can be tuned into the infrared region of the spectrum [157]. They were theoretically studied using generalized Mie theory [158]. On the other hand, the self-similar array composed of such core-shell nanoparticles is also proposed [159]. Furthermore, the optical Yagi-Uda

antenna consisting of the nanoshell spheres was proposed [160]. Their resonant properties are characterized and controlled by the thickness of spherical shells [161]. Such antenna is well illustrated by Li [160; 162; 163]. However, the shell structure is difficult to realize and control in the practical fabrication process and only one-directional patterns (associated with θ) was considered.

In view of the literature, we propose a chain of nanosheres and nanoellipsoids and the Yagi-Uda antenna constructed by an array of gold spheres in this chapter. In the array case, the resonant elements excited by the incident light act as the optical dipole source in Li's studies. Because the spheres are considered as the dipole elements of Yagi-Uda antenna, our array of spheres are arranged according to the resonance properties of the classic RF Yagi-Uda antenna. Various optical characteristics such as the light field intensity and the power density are studied in the near-field region. The radiation pattern and half-power beamwidth of the antenna in the far-field are illustrated as well. The antenna specifications like gain are calculated using empirical formula.

6.2 Optical Resonant Properties of a Chain of Nanospheres and Nanoellipsoids

Under the help of the dielectric constant calculated in Fig 1.4 in Chapter 2, we consider the case for five spheres in a line with increasing radii ranging from 30 nm to 130 nm. The separation between the two particles is set as the smaller radius value

of two adjacent particles. This condition is the same as that of the ellipsoids. In this case, the separation is set as their minor axis. The long axes are set as 20 to 30 nm larger than the minor axis accordingly. In addition, both chains are aligned in the x-direction and the size of components is incremental along this direction. Fig. 6.1 and Fig. 6.2 show the schemes of the chains of the spheres and ellipsoids for simulations respectively. The unit used to demonstrate the dimension here is nanometer.

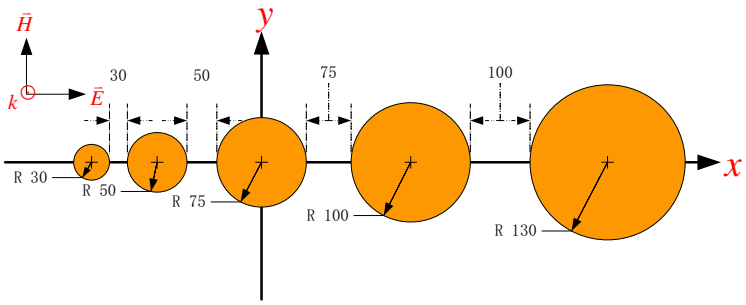

Figure 6.1. Scheme of a chain of nanospheres.

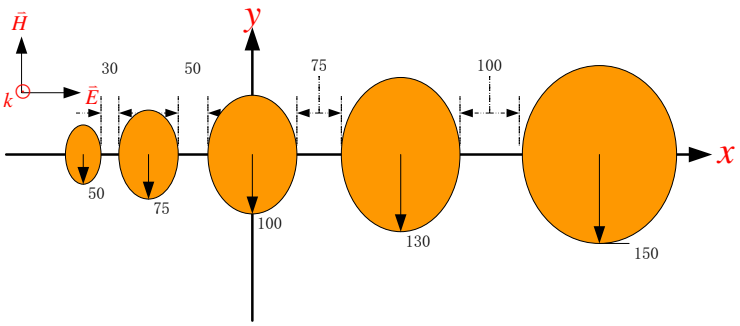

Figure 6.2. Scheme of a chain of nanoellipsoids.

We check the scattering properties of the chain of particles in the reference planes of xoz-plane and yoz-plane, which are respectively the side and the top view of the chains across the particles' aligning direction (*i.e.* the direction of the chain). There are three parameters associated with the EM field quantities of our concern: the electric field vectors, the Poynting vector, and the electric energy density. As we are

using the absolute value for the first two values, so the three parameters become the magnitude of electric field, the power density and the electric energy density. The final simulation results for both chains in terms of corresponding three parameters can be found in Figs. 6.3 to 6.8 at a frequency of 500 THz. They are denoted in the xoy-, xoz-, and yoz-planes in successive order. In each figure, the left-side one denotes the electric field distribution in magnitude; the middle one represents the power flow in magnitude form; and the right-side one stands for the electric energy density. Here a logarithmic scale is used to enhance the figures' contrast. It should be also noted that the yoz-plane here is not exactly the same as the one in Cartesian coordinate. In fact, it is a reference plane across the cross-section of the largest particle parallel to the actual yoz-plane (*i.e.* x=580 nm plane). We mark it as the yoz-plane for convenience.

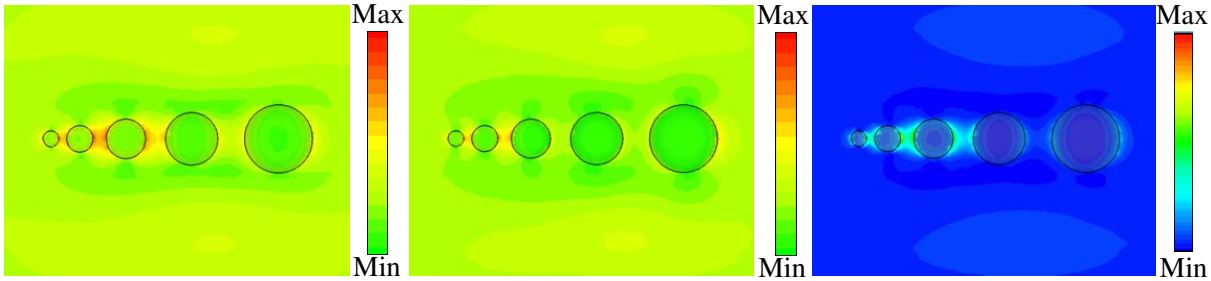

(a) $|E|$-field (b) Power flow (c) Electric energy density

Figure 6.3. Scattering properties of a chain of gold spheres with incremental size in the xoy-plane.

- Light Intensity $|E^2|$

All the left-side figures in the stated six figures give the distribution of the magnitude of the electric field and that can be computed to obtain the light intensity of

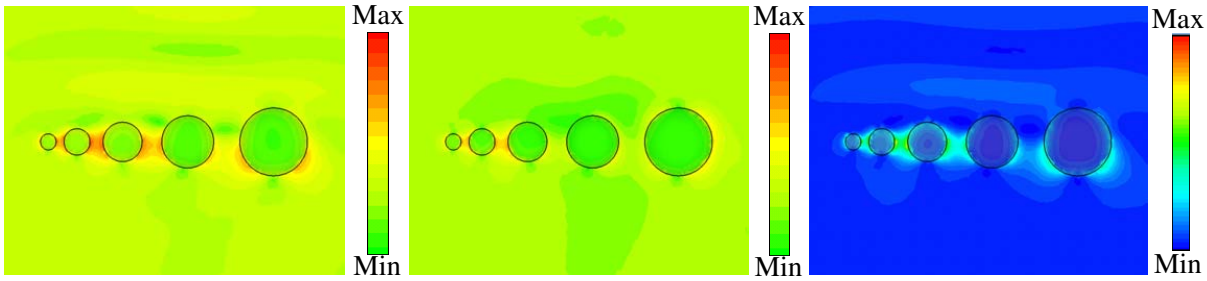

(a) $|E|$-field (b) Power flow (c) Electric energy density

Figure 6.4. Scattering properties of a chain of gold spheres with incremental size in the xoz-plane.

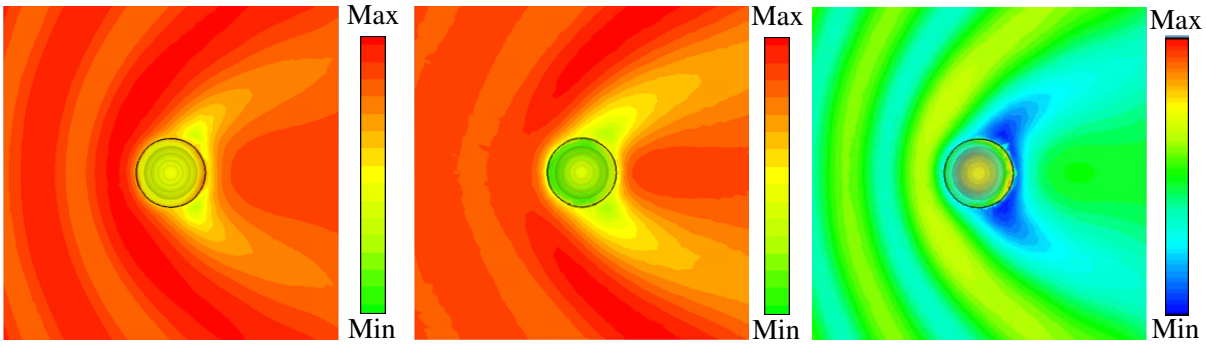

(a) $|E|$-field (b) Power flow (c) Electric energy density

Figure 6.5. Scattering properties of a chain of gold spheres with incremental size in the yoz-plane.

$|E^2|$. For spheres, it can be obtained from the above calculations that the peak value of the light intensity for the five spheres is 163.84 V^2/m^2 in the space, which is attained from 12.8 V/m computed by CST. This value is about 100 times of that of the incident wave (1 V^2/m^2). The peak value is around the edge of the smallest sphere, as shown in Fig. 6.4. In this figure, it can be found that the electric fields around the spheres are stronger than that inside the spheres. In addition, the scattered field has been locally amplified at the area between the spheres. This phenomenon is even obvious in the area between the smallest three particles. This verifies the existence of

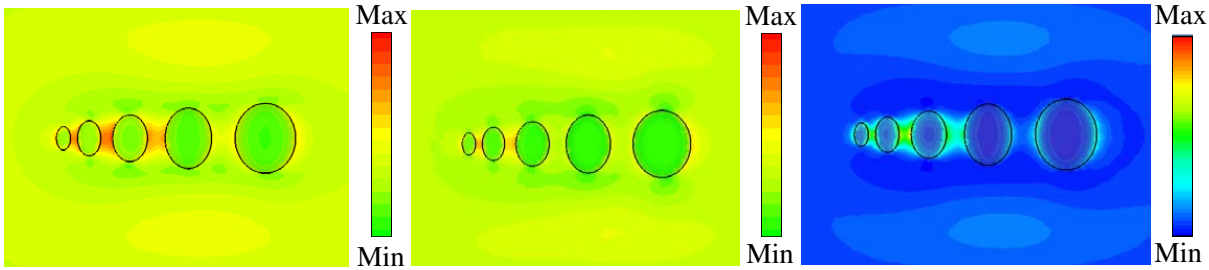

(a) $|E|$-field (b) Power flow (c) Electric energy density

Figure 6.6. Scattering properties of a chain of gold ellipsoids with incremental size in the xoy-plane.

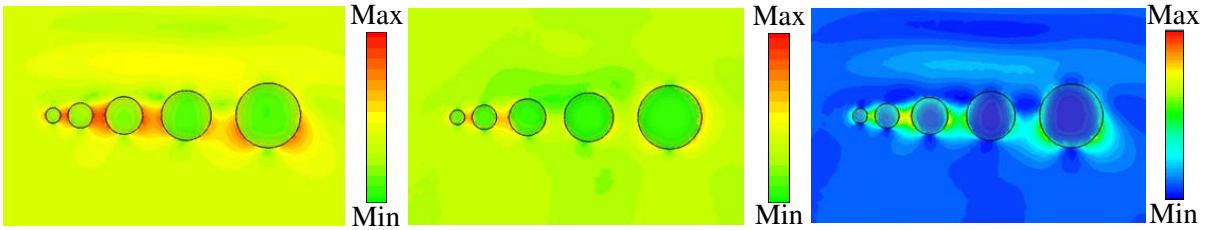

(a) $|E|$-field (b) Power flow (c) Electric energy density

Figure 6.7. Scattering properties of a chain of gold ellipsoids with incremental size in the xoz-plane.

near-field plasmon resonance because this effect becomes weaker when the distance increases, *i.e.* as the spacing between the larger spheres becomes wider, the field between them turn weaker.

For the ellipsoids, the maximum field value is 7.7 V/m and this gives a light intensity of 59.29 V^2/m^2 , which is weaker than that for spheres.

- Power density $|P|$

The central figures show the power density for spheres and spheroids in the mentioned planes. The peak values for the chain of spheres and spheroids are 0.0318

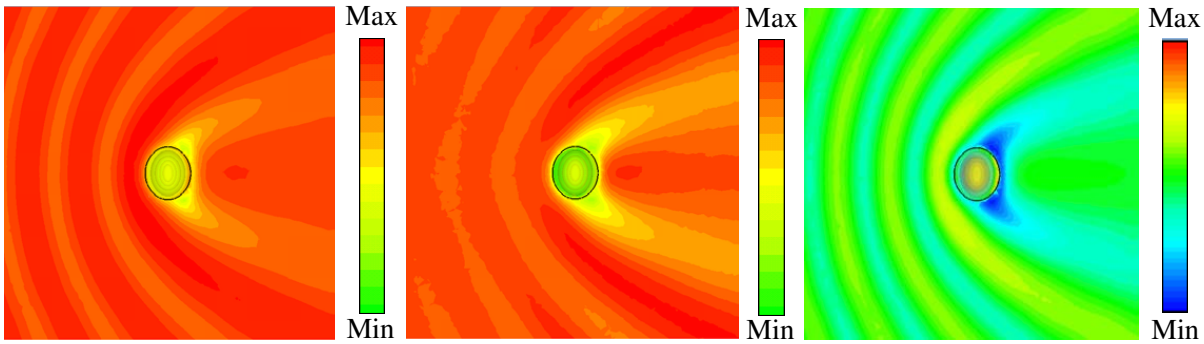

(a) $|E|$-field (b) Power flow (c) Electric energy density

Figure 6.8. Scattering properties of a chain of gold ellipsoids with incremental size in the yoz-plane.

VA/m^2 and 0.0189 VA/m^2 respectively. The value for the ellipsoids is less than that of the spheres, and their ratio is about a half.

- Electric energy density U_e

From the right-side figures in above calculation, it can be obtained that the peak value of the electric energy density for the five spheres and ellipsoids is 7.25363 and 2.60691 respectively (unit is 10^{-10} J/m^3). As shown in these figures, the intensities inside and outside the particles in the xoz-planes and yoz-planes are not uniformly distributed. Fields are focused in the forward direction along the incident light in Fig. 6.4 and Fig. 6.7. This is a dramatically obvious enhancement. In addition, Fig. 6.5 and Fig. 6.8 show that the lateral scattering exists from the chain of the particles. In Fig. 6.3 and Fig. 6.6, the distribution patterns of the parameters considered are symmetric to the x-axis.

The electric energy density was defined in [83] as $U_e(r) = 0.5\varepsilon(r) < E^2(r) >$, where $\varepsilon(r)$ is the permittivity, and $< E^2(r) >$ indicate the temporally averaged field

values. In this case, the densities for homogenous gold particles are proportional to the averaged field value. Generally the distributions agree with the results in [33].

- Comparison between spheres and ellipsoids

In our simulation, the minor axis length of the ellipsoids is the same as the radii of the spheres at the corresponding position for a comparable study. we find that the peak values of the three parameters of the spheres considered are around 2 to 3 times of those of the ellipsoids. In general, the sphere chain give larger values (including the enhancement factor) than the ellipsoid chain.

In this section, the scattering problem of a chain of nanoscale metallic spheres and ellipsoids with incremental size has been studied through theoretical analysis for their field enhancement properties. These chains are able to produce highly localized electromagnetic fields between the nanoparticles. In certain planes, the proposed chain shows backscattering and lateral scattering with respect to the direction of the incident. Generally, the spheres give better enhancement factor than the ellipsoids if the sphere's radii are the same as the ellipsoid's minor axis length. In future work, the case for chains of spheres and ellipsoids with the same volume can be studied for a comparision.

6.3 Optical Yagi-Uda Antenna Using an Array of Gold Nanospheres

6.3.1 Yagi-Uda Antenna Parameters Design Requirements

The Yagi-Uda antenna is a directional antenna widely used in HF, VHF, and UHF ranges (3-3000 MHz). It has the advantage of high directivity. Conventional RF Yagi-Uda antenna consists of a number of linear dipole elements. One of them is energized directly by a feed transmission line; while the others are parasitic radiators including directors and reflectors, whose currents are induced by mutual coupling. The scheme of the RF Yagi-Uda antenna is given in Fig. 6.9. Folded dipole is usually adopted as the feed element. To operate as an endfire array, the lengths of the elements and the separation between them have certain requirements [81]: The driven element is resonant with its length 0.45-0.49λ, whereas the length of the directors will be 0.4-0.45λ, and the lengths of the reflectors are somewhat greater than that of the feed. The separation between the directors is usually 0.3-0.4λ; while that for reflectors is optimum near 0.25λ. The radiation characteristics of interest mainly contain the forward and backward gains, input impedance, bandwidth and so on. The gain of 14.8-17.3 dBi is considered as a typical one.

Since the single plamsonic sphere can be considered as a dipole when excited by light, the idea of organizing the spheres with different dimensions to form the Yagi-Uda antenna components is thus achieved accordingly. In our work, this array of gold

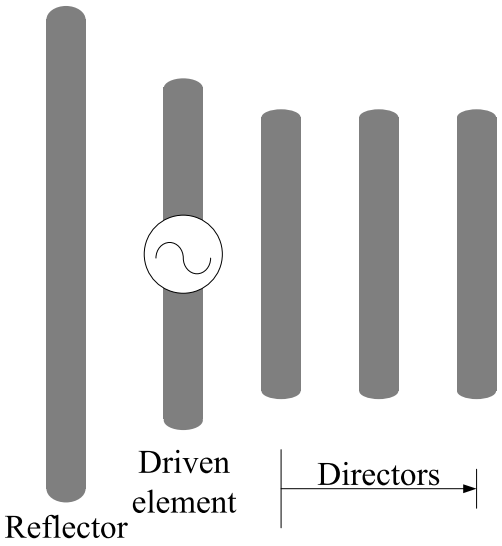

Figure 6.9. Scheme of RF Yagi-Uda antenna consistsing of linear dipoles.

spheres incident by a plane wave is proposed. Such particles can work as induced dipoles which can couple to each other without an additional source. By carefully designing their dimension, they may play the roles of antenna elements like those in a conventional RF Yagi-Uda antenna. The dimensions of the nanoparticles are set, considering the feasibility in the laboratory as explained in Chapter 3, Section 3.1. The "driven element" in this case is denoted by a pair of spheres. They are expected to work at resonance to serve as the energized element in the Yadi-Uda antenna. In addition, other spheres of different size are placed on both sides of the driven nanosphere pair to behave as the parasitic radiators of "reflector" and "directors". The interaction between the spheres makes such an optical Yagi-Uda antenna operate properly. In view of the dimension requirements for the RF Yagi-Uda antenna, we set up our primary model. The sphere dimer with radius of 65 nm is supposed to be the resonant feeder and serve as the "driven element" when excited by light. Lately, the spheres with diameter of 60 nm are found to be resonant when the incident light's

photon energy is 2.27 eV, *i.e.*, the incident light frequency is 547.8 THz and the wavelength λ is 547.6 nm [109]. Under the excitation of light at the same frequency, other sequential six spheres near the sphere dimer aligned in the z-direction (which is the beam direction) are expected to work as the directors. Four spheres (two sphere pairs) in the -z-direction are integrally considered as the reflector. Their positions are carefully arranged as follows. 1) The reflector cannot lie in the middle of the x-direction because it may block some propagating light from completely exposuring to the driven sphere pair and induce insufficient resonance. Therefore the sphere pairs as reflectors are separated with some distance. 2) The directors are not preferably designed as a waveguide formed by two rows of spheres as in [164]. The single sphere is used instead of the sphere pair. For the excitation source, a plane wave with frequency at 547.8 THz, polarized in the x-direction with an electric vector of 1 V/m and propagating in the z-direction in the Cartesian coordinate is utilized. The detailed scheme of the optical Yagi-Uda antenna is shown in Fig. 6.10.

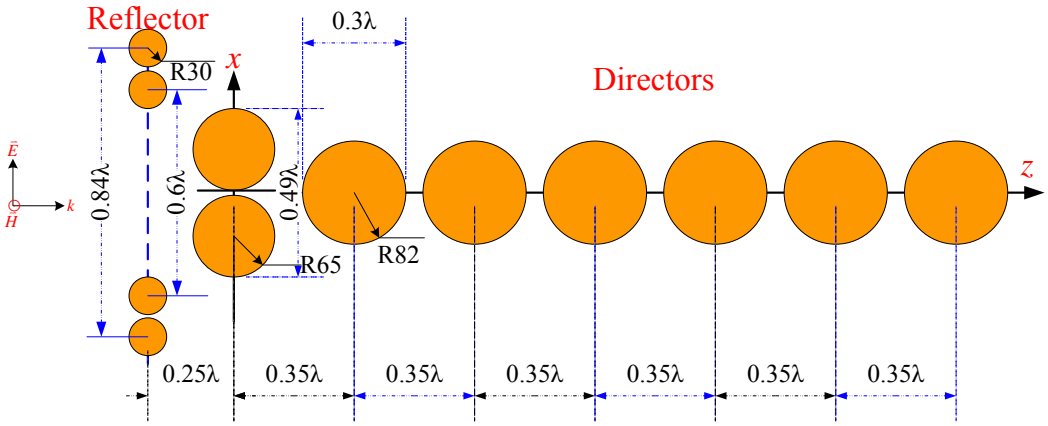

Figure 6.10. Scheme of optical Yagi-Uda antenna consistsing of gold spheres.

6.3.2 Results and Discussion

In this section, the scattering properties of the array in the reference plane of xoz-plane both in the near-field and far-field are evaluated. In the same way as those for the chain study, the parameters of interest referring to the field distributions are determined, including the magnitude of electric field, power density and the electric energy density, which can be found in Fig. 6.11 especially in the transverse xoz-plane for our designed optical Yadi-Uda nanoantenna with five directors. For the far-field radiation properties of antenna, the structure of the directors and reflectors can be also changed to find their influences. Due to the limitation of the existing size of the single sphere and the separation requirements for the Yagi-Uda antenna, the "length" of the non-resonant elements cannot be tunable in a wide range. But we can still change the number of the elements. In our study, the director's number varies from 4 to 6. Similar attempts can be made in future research.

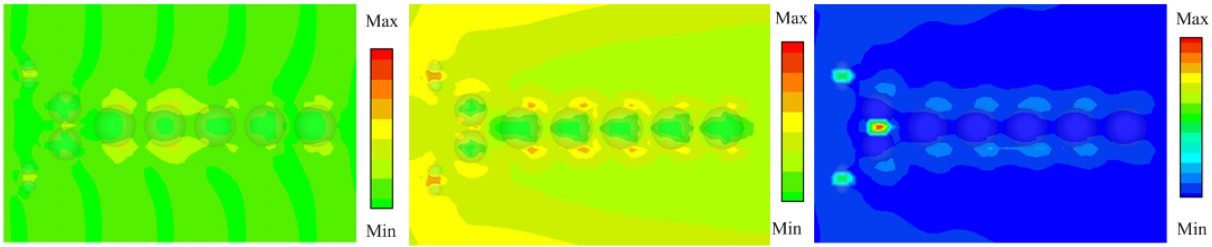

(a) $|E|$-field (b) Power flow (c) Electric energy density

Figure 6.11. Scattering properties of optical Yagi-Uda antenna.

- Light intensity, power density and electric energy density

The left-side figure of Fig. 6.11 depicts the results of the $|E|$ for the spheres in the xoz-plane. From the calculations, it can be obtained that the peak light intensity of the antenna array is 43322.24 V^2/m^2 (computed from E-field of 208.14 V/m), which is about 10^4 times of that of the incident wave. Concentrated fields occur between the feeder spheres, thus they are considered to be near resonance. Similarly the peak values for the power density and electric energy density are observed as 0.3430 VA/m^3 and 1.9885×10^{-7} J/m^3. As shown in these figures, strong resonant fields occur at the spacing between the feeder spheres pairs and the reflector spheres pairs. Both sides of the director spheres also shows stronger fields than the other area around the these spheres. The field distributions in the cross-section of the directors and reflectors, parallel to the xoy-plane, are also recorded. It is found to be similar to that of a dipole antenna. The trend again shows the array to be potentially used as the dipole elements to construct the Yagi-Uda antenna.

- Antenna radiation characteristics

The patterns of the array with four, five and six directors are given in Fig. 6.12, Fig. 6.13, and Fig. 6.14 respectively. The corresponding half-power beamwidths are also marked.

From these figures, we find that this array shows a good directivity in each case. The main beam direction maintains pointing the z-direction, and only the side lobe magnitude varies. The gain and directivity of this antenna are calculated using the approximate formula for practical antenna in Eq. (5.2) and Eq. (5.1). In the present case, $\phi = 90^\circ$ and $\phi = 0^\circ$ planes are chosen as reference planes. After the computation,

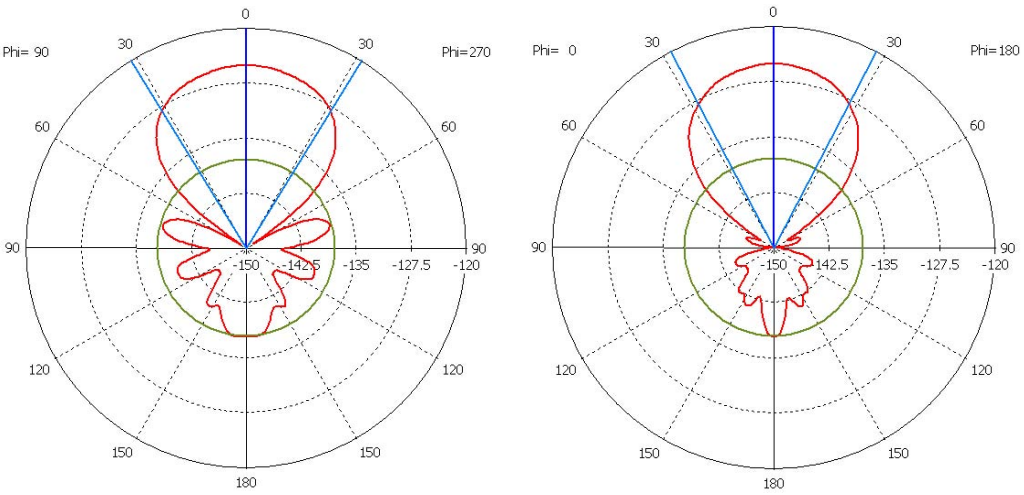

(a) E_θ in $\phi = 90°$ plane (b) E_θ in $\phi = 0°$ plane

Figure 6.12. Radiation patterns of the array with four directors.

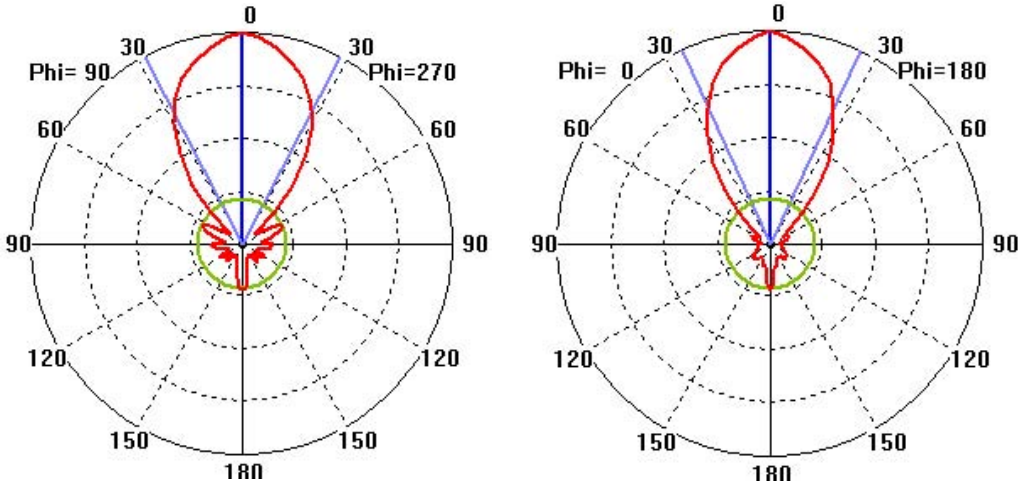

(a) E_θ in $\phi = 90°$ plane (b) E_θ in $\phi = 0°$ plane

Figure 6.13. Radiation patterns of the array with five directors.

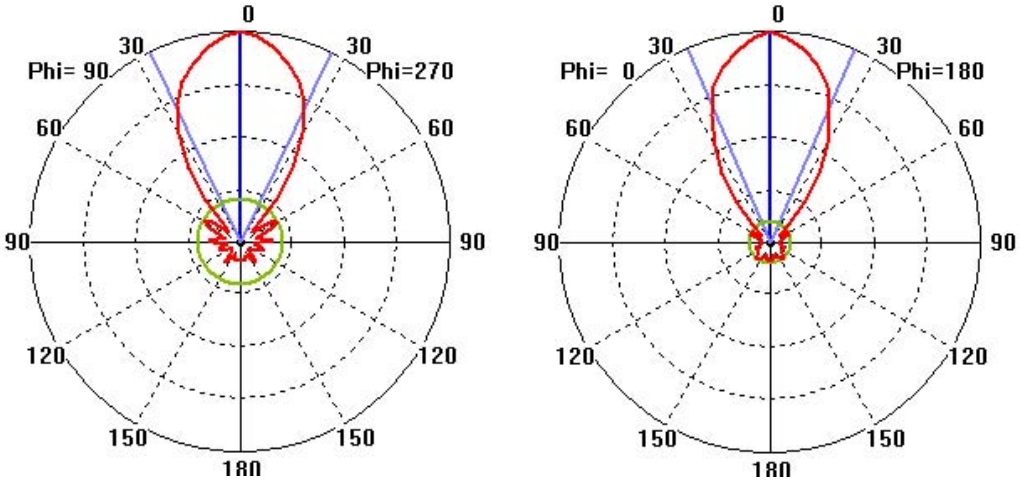

(a) E_θ in $\phi = 90°$ plane (b) E_θ in $\phi = 0°$ plane

Figure 6.14. Radiation patterns of the array with six directors.

Table 6.1. Parameters for arrays with different directors at f=547.8 THz

No. of director	**4**	**5**	**6**
E (V/m)	30.81	31.52	37.24
P (VA/m^2)	0.64	0.058	0.061
main lobe magnitude (V/m)	3.09×10^{-13}	6.55×10^{-10}	7.32×10^{-7}
gain (dBi)	9.34	10.33	10.96
D (dB)	10.72	11.72	12.34

the parameters of main lobe magnitude, gain and directivity are listed together with E-field and power density in Table 6.1. It is clearly seen that such parameters are improved as the number of directors in the array increases. Thus the director element has a positive role in enhancing the optical Yagi-Uda nanoantenna array's gain, which exactly assembles the property of the RF Yagi-Uda antenna.

In addition to the case of the optical Yagi-Uda nanoantennas with different numbers of directors at the same frequency, that for single antennas under excitation at different frequencies f of 400, 500, and 600 THz are also explored, for the structure

Table 6.2. Parameters for arrays of five directors under different frequencies

f **(THz)**	**400**	**500**	**600**
E (V/m)	31.26	237.80	31.52
P (VA/m^2)	0.11	0.34	0.058
U_e (J/m^3)	3.47×10^{-9}	2.79×10^{-7}	4.98×10^{-9}
main lobe magnitude (V/m)	3.63×10^{-7}	9.17×10^{-7}	3.91×10^{-7}
gain (dBi)	7.59	9.43	9.75

with five directors. Various parameters including E-field magnitude E, Power density P, electric energy density U_e, main lobe magnitude, and gain are listed in Table 6.2.

From this table, it can be seen that this array provides the best enhancement performance at 500 THz among three cases, because the highest value of E is gained. But higher gain is reached at a higher frequency.

In this section, an array of gold nanospheres of different dimensions is elaborated arranged to perform the function of Yagi-Uda antenna operating in the optical range. By treating the spheres with different dimensions as the dipole elements with different lengths, they can be especially placed together assembling the conventional RF Yagi-Uda antenna to achieve high directionality and gain enhancement in the preferred direction. Its scattering properties are studied in comparison with the RF Yagi-Uda antenna. In our simulation, radiation patterns of the array of spheres show desirable directivity and is comparable with the RF Yagi-Uda antenna. A gain of about 10 dBi for such an antenna is achieved. By changing the number of "directors" and "reflectors", their influences on the near-field enhancement and far-field radiation properties are evaluated. More directors utilized can lead to better performance. Our results demonstrated here are consistent with those from the conventional RF

Yagi-Uda antenna. Compared with the exiting studies, it has the advantage of flexible adjustability in practice and good compatibility with the other optical devices. The problem of driven element is solved and a simple plane wave is adequate for excitation. Due to the effective coupling among the spheres, such an antenna can be integrated to the optical device like optical fiber. In addition, high transmission in optical circuits can also be achievable in further exploration. As for the variances in the structure arrangement of this antenna array, this awaits further optimization to improve the antenna performance.

Chapter 7

Conclusions and Recommendations for Future Work

7.1 Conclusions

In this dissertation, a theoretical study on the nanoantennas consisting of single and multiple metallic nanoparticles are presented, focusing on their promising optical properties. The nanoantennas operating at optical range have special features of producing giant concentrated and highly localized light with subwavelength enhanced field area. This small dimension of the enhanced light can successfully overcome the diffraction limit, thus realizing the promising light manipulation at nanometer scale. Such a nanoantenna function is shown to be performed by strong localized plasmon resonance induced by the incident light.

In our work, the latest dispersive dielectric constant data reliable for calculating

the antenna's specifications are collected at different frequencies to accurately characterize the optical properties of nanoantennas. Therefore, the deficiencies caused by the inaccurate dielectric constant data characterized by the models in many current studies are addressed. Moreover, the proper calculation approach for exploring nanoantenna is designed to obtain wider frequency response and more efficient usage of the frequency spectrum, which is a remarkable improvement over presently used methods. Based on such an accurate characterization of the dielectric constant and an appropriate method for broadband calculation, various nanoantenna configurations of research interest are particularly designed and analyzed through useful simulations in Chapters 3-6.

The computed results have provided clear evidence that the near-field light enhancement generated by the nanoantennas is closely related to their geometries. For the antenna configuration of a single nanoparticle, its shape, length and volume are all responsible for the optical performance. In general, the nanoparticle with larger length along the incident light's polarization direction offers better near-field enhancement at resonance. For the antenna configuration of the coupling nanoparticle pair, its element length and separation play an important role. Much stronger light than what a single nanoparticle can produce is focused in the middle of two closely placed nanoparticles. Both larger length and narrower spacing have advantages over the other designs in providing the higher light intensity at resonance. These also result in the red-shift of the resonance. In particular, if the elements in the pair are of triangular shape in the bow-tie antenna and the bow-tie aperture antenna cases, an

adequately sharper apex is recommended for improving the design. For the antenna configuration of a chain of spheres and ellipsoids, we find that the spheres exhibits stronger light intensity at about 100 times of incident one. The spheres give higher light intensity than the ellipsoids. These findings provide better interpretation of the near-field properties of kinds of nanoantennas. Other than the geometric effects of an antenna, the effects of its supporting substrate and excitation source are also analyzed in part. It is important to match the wavelength and polarization of the excitation to the nanoantenna under investigation and use the proper substrate materials. Besides the antenna composed by identical elements, a Yagi-Uda antenna made from the nanospheres with different dimensnion is also proposed for the first time for its high directivity and gain. The field distribution, power flow and electric energy density are calculated for better understanding. A key benefit of the present work is to significantly improve current designs of the nanoantennas by comprehensive studies of various factors.

In addition to such properties in the near-field of nanoantennas, the far-field radiation properties are also inclusive in the work. In this way, an alternative explanation of the nanoantenna characterization in engineering sense is offered. To date, there is little comprehensive study looking into the role of nanoantennas's radiation features for possible optical circuit applications. Our study addresses this problem especially according to quantitative analysis. The conventional antenna design specifications such as the field patterns, gain and directivity are demonstrated for the bow-tie nanoantenna and the Yagi-Uda nanoantenna to extend previous work. The roles that

the source and geometry play in determining the nanoantenna's radiation properties are examined to further optimize the antenna design. For the Yagi-Uda nanoantenna, higher gain is achieved under the excitation by the light at a higher frequency. Furthermore, the improvement of the directivity and gain can also result from increasing number of directors employed. Because our structure is easier to control and more convenient to integrate compared with similar studies, it shows potential to be applied in combination with the other optical devices. These findings have taken an important step towards the future optical transmission systems.

In short, compared with current studies on nanoantennas, our study contributes to a more effective and helpful guidance for the nanoantenna's design. The results obtained in our study are very useful because they can be the theoretical basis for improving the nanoantenna designs in future nanoantenna fabrications.

7.2 Recommendations for Future Work

In view of presently obtained research results and the state of arts of nanoantenna research, there is still some space for further research, which is illustrated in detail subsequently.

In the research content aspect, some limitations existing in our current designs require further improvements and extensions. Firstly, the source utilized in our present research topics is of single type by plane wave excitation. In order to develop a systematical study, it would be interesting to apply other kinds of light sources to illuminate

upon nanoantennas. The beam wave is a choice as reported in [117] to control the plasmnoic structures in the near field. Moveover, the fluorescent molecules around the nanoantenna geometries can also constitute the source to excite the nanoantenna resonance modes [165]. Thus other forms of driven sources can be applied to our nanoantenna configurations as an extension of the present work.

Secondly, the configurations of investigated nanoantennas in this work are limited to simple particle components. The design of the structures originate from their counterparts of the RF antenna in some helpful applications. However, there are still many other sophisticated RF antennas possessing of exciting characteristics for our design references. It is meaningful if some designs can be transferred from the RF range to the optical range, although not all designs are applicable at higher frequencies. The transformation should be based on close examination of basic principles behind and credible feasibility assessment. In future, there is a need to explore more kinds of nanoantennas effective for the optical applications.

Thirdly, regarding the optical Yagi-Uda antenna, its configuration needs further improvement for a better performance. In our work, the proposal of the resonant spheres excited by light is constructive. But the reflectors in the system may partially interfere with its illuminance toward the driven elements, causing inadequate utilization of given light source. Better arranged designs should be developed while the convenience in regulating components' resonance based on the nanoantenna configuration should be considered as well.

Fourthly, rather than solving only antenna individually, it will be interesting to

take into account its connecting or light guiding devices based on the consideration of optical transmission system. Recently, the nanoantennas can be fabricated on the facet of optical fibre [12] and semiconductor laser diode [131]. It is challenging to model such a system in theory and investigate their overall functions. A possible route is provided where an optical fibre can be treated as the circular waveguide, then the problem of waveguide and antenna can be solved as a simplified model. In addition, the nanoantenna as an component of device integration have potential applications in both emission and detection devices that can be studied together with the nanoantennas. Multi-disciplines' knowledge can enhance our understanding and design, including chemistry, physics, bioengineering, optics, and electrical engineering. For example, it may help to better establish suitable local environments for the emitter in optoelectronics and sensor in biological or medical imaging. Growing demand of interdisciplinary research will provide new perspective to the nanoantennas research in these areas.

In the method aspect, in order to launch an in-depth investigation, there is a need to explore other theoretical approaches suitable for the nanoantenna problems especially for the complex array's case. As introduced in Chapter 2, the proposal of circuit model of the nanoparticle array to derive analytical solutions [54] has drawn our attention. The nanocircuit elements were used in [166]. Therefore, another possible avenue of future work is to investigate the equivalent circuit of our particle chain and array.

After the nanoantenna design is theoretically optimized to reach satisfactory per-

formance, it is suggested to carry out further research on the fabrication and experiments for the designed nano-system proposed. Related nanoprocessing knowledge and techniques are thus needed.

Bibliography

[1] P. J. Schuck, D. P. Fromm, A. Sundaramurthy, G. S. Kino, and W. E. Moerner, "Improving the mismatch between light and nanoscale objects with gold bowtie nanoantennas," *Phys. Rev. Lett.*, vol. 94, no. 1, p. 17402, 2005.

[2] K. B. Crozier, A. Sundaramurthy, G. S. Kino, and C. F. Quate, "Optical antennas: resonators for local field enhancement," *J. Appl. Phys.*, vol. 94, pp. 4632–4642, 2003.

[3] J. N. Farahani, D. W. Pohl, H. J. Eisler, and B. Hecht, "Single quantum dot coupled to a scanning optical antenna: a tunable superemitter," *Phys. Rev. Lett.*, vol. 95, p. 017402, 2005.

[4] S. I. Bozhevolnyi and T. Søndergaard, "General properties of slow-plasmon resonant nanostructures: nano-antennas and resonators," *Phys. Rev. Lett.*, vol. 91, p. 253902, 2003.

[5] P. Muhlschlegel, H. J. Eisler, O. J. F. Martin, B. Hecht, and D. Pohl, "Resonant optical antennas," *Science*, vol. 308, no. 5728, p. 1607, 2005.

[6] B. Hecht, P. Muhlschlegel, *et al.*, "Prospects of resonant optical antennas for nano-analysis," *CHIMIA International Journal for Chemistry*, vol. 60, no. 11, pp. 765–769, 2006.

[7] E. S. Barnard, J. White, A. Chandran, and M. L. Brongersma, "Spectral properties of plasmonic resonator antennas," *Opt. Express*, vol. 16, pp. 16 529–16 537, 2008.

[8] P. Biagioni, J. S. Huang, L. Duò, M. Finazzi, and B. Hecht, "Cross resonant optical antenna," *Phys. Rev. Lett.*, vol. 102, no. 25, p. 256801, 2009.

[9] K. Kneipp, Y. Wang, *et al.*, "Single molecule detection using surface-enhanced Raman scattering (SERS)," *Phys. Rev. Lett.*, vol. 78, no. 9, pp. 1667–1670, 1997.

[10] S. Khn, U. Håkanson, L. Rogobete, and V. Sandoghdar, "Enhancement of single-molecule fluorescence using a gold nanoparticle as an optical nanoantenna," *Phys. Rev. Lett.*, vol. 97, p. 017402, 2006.

[11] F. Neubrech, A. Pucci, *et al.*, "Resonant plasmonic and vibrational coupling in a tailored nanoantenna for infrared detection," *Phys. Rev. Lett.*, vol. 101, no. 15, p. 157403, 2008.

[12] E. J. Smythe, M. D. Dickey, *et al.*, "Optical Antenna Arrays on a Fiber Facet for In Situ Surface Enhanced Raman Scattering Detection," *Nano Lett.*, vol. 9, no. 3, p. 1132, 2009.

[13] A. Kinkhabwala, Z. Yu, *et al.*, "Large single-molecule fluorescence enhancements produced by a bowtie nanoantenna," *Nature Photonics*, vol. 3, no. 11, pp. 654–657, 2009.

[14] T. H. Taminiau, F. D. Stefani, F. B. Segerink, and N. F. V. Hulst, "Optical antennas direct single-molecule emission," *Nature Photonics*, vol. 2, no. 4, pp. 234–237, 2008.

[15] J. Petschulat, D. Cialla, *et al.*, "Doubly resonant optical nanoantenna arrays for polarization resolved measurements of surface-enhanced Raman scattering," *Opt. Express*, vol. 18, pp. 4184–4197, 2010.

[16] W. H. Weber and G. W. Ford, "Propagation of optical excitations by dipolar interactions in metal nanoparticle chains," *Phys. Rev. B*, vol. 70, no. 12, p. 125429, 2004.

[17] T. Kalkbrenner, U. Håkanson, *et al.*, "Optical microscopy via spectral modifications of a nanoantenna," *Phys. Rev. Lett.*, vol. 95, no. 20, p. 200801, 2005.

[18] J. N. Farahani, H. J. Eisler, *et al.*, "Bow-tie optical antenna probes for single-emitter scanning near-field optical microscopy," *Nanotechnology*, vol. 18, p. 125506, 2007.

[19] R. M. Bakker, V. P. Drachev, H. K. Yuan, and V. M. Shalaev, "Enhanced transmission in near-field imaging of layered plasmonic structures," *Phys. Rev. Lett.*, vol. 91, p. 227402, 2003.

[20] L. Zhou, Q. Gan, F. J. Bartoli, and V. Dierolf, "Direct near-field optical imaging of UV bowtie nanoantennas," *Opt. Express*, vol. 17, pp. 20 301–20 306, 2009.

[21] K. Kneipp, H. Kneipp, I. Itzkan, R. R. Dasari, and M. S. Feld, "Ultrasensitive chemical analysis by Raman spectroscopy," *Chem. Rev*, vol. 99, no. 10, pp. 2957–2976, 1999.

[22] H. Wang, C. T. Chong, and L. Shi, "Optical antennas and their potential applications to 10 terabit/in 2 recording," in *Proceedings of Optical Data Storage Topical Meeting*, 2009, pp. 16–18.

[23] D. P. Fromm, A. Sundaramurthy, A. Kinkhabwala, *et al.*, "Exploring the chemical enhancement for surface-enhanced Raman scattering with Au bowtie nanoantennas," *J. Chem. Phys.*, vol. 124, p. 061101, 2006.

[24] M. A. Cooper, "Optical biosensors in drug discovery," *Nat. Rev. Drug Discov.*, vol. 1, no. 7, pp. 515–528, 2002.

[25] A. J. Haes and R. P. V. Duyne, "A nanoscale optical biosensor: sensitivity and selectivity of an approach based on the localized surface plasmon resonance spectroscopy of triangular silver nanoparticles," *J. Am. Chem. Soc.*, vol. 124, no. 35, pp. 10 596–10 604, 2002.

[26] W. L. Barnes, A. Dereux, and T. W. Ebbesen, "Surface plasmon subwavelength optics," *Nature*, vol. 424, no. 6950, pp. 824–830, 2003.

[27] N. Engheta, "Circuits with light at nanoscales: Optical nanocircuits inspired by metamaterials," *Science*, vol. 317, no. 5845, p. 1698, 2007.

[28] M. Abe and T. Suwa, "Surface plasma resonance and magneto-optical enhancement in composites containing multicore-shell structured nanoparticles," *Phys. Rev. B*, vol. 70, no. 23, p. 235103, 2004.

[29] A. Ahmadi, S. Ghadarghadr, and H. Mosallaei, "An optical reflectarray nanoantenna: The concept and design," *Opt. Express*, vol. 18, pp. 123–133, 2010.

[30] J. Li and N. Engheta, "Subwavelength plasmonic cavity resonator on a nanowire with periodic permittivity variation," *Phys. Rev. B*, vol. 74, no. 11, p. 115125, 2006.

[31] M. D. Malinsky, K. L. Kelly, G. C. Schatz, and R. P. V. Duyne, "Chain length dependence and sensing capabilities of the localized surface plasmon resonance of silver nanoparticles chemically modified with alkanethiol self-assembled monolayers," *J. Am. Chem. Soc.*, vol. 123, no. 7, pp. 1471–1482, 2001.

[32] A. Mohammadi, F. Kaminski, V. Sandoghdar, and M. Agio, "Spheroidal nanoparticles as nanoantennas for fluorescence enhancement," *International Journal of Nanotechnology*, vol. 6, no. 10, pp. 902–914, 2009.

[33] C. Li, G. W. Kattawar, P. W. Zhai, and P. Yang, "Electric and magnetic energy density distributions inside and outside dielectric particles illuminated by a plane electromagnetic wave," *Opt. Express*, vol. 13, pp. 4554–4559, 2005.

[34] E. E. N. V. A. Podolskiy, A. K. Sarychev and V. M. Shalaev, "Light manipulation with plasmonic nanoantennas," in *Proceedings of IEEE Antennas amd Propagation Society international Symposium*, vol. 2, 2004, pp. 1915–1918.

[35] F. Neubrech, T. Kolb, *et al.*, "Resonances of individual metal nanowires in the infrared," *Appl. Phys. Lett.*, vol. 89, p. 253104, 2006.

[36] V. A. Podolskiy, A. K. Sarychev, E. E. Narimanov, and V. M. Shalaev, "Resonant light interaction with plasmonic nanowire systems," *J. Optic. A*, vol. 7, p. S32, 2005.

[37] G. Y. Slepyan, M. V. Shuba, S. A. Maksimenko, and A. Lakhtakia, "Theory of optical scattering by achiral carbon nanotubes and their potential as optical nanoantennas," *Phys. Rev. B*, vol. 73, no. 19, p. 195416, 2006.

[38] T. H. Taminiau, R. J. Moerland, F. B. Segerink, L. Kuipers, and N. F. van Hulst, "[lambda]/4 Resonance of an Optical Monopole Antenna Probed by Single Molecule Fluorescence," *Nano Lett.*, vol. 7, pp. 28–33, 2007.

[39] T. H. Taminiau, F. B. Segerink, and N. F. van Hulst, "A monopole antenna at optical frequencies: single-molecule near-field measurements," *IEEE Trans. Antennas Propag.*, vol. 55, no. 11 Part 1, pp. 3010–3017, 2007.

[40] T. H. Taminiau, F. B. Segerink, R. J. Moerland, L. Kuipers, and N. F. van Hulst, "Near-field driving of a optical monopole antenna," *J. Optic. A*, vol. 9, pp. S315–S321, 2007.

[41] Z. Chen, X. Li, A. Taflove, and V. Backman, "Backscattering enhancement of light by nanoparticles positioned in localized optical intensity peaks," *Appl. Opt.*, vol. 45, no. 4, pp. 633–638, 2006.

[42] K. L. Kelly, E. Coronado, L. L. Zhao, and G. C. Schatz, "The optical properties of metal nanoparticles: the influence of size, shape, and dielectric environment," *J. Phys. Chem. B*, vol. 107, no. 3, pp. 668–677, 2003.

[43] J. J. Mock, M. Barbic, D. R. Smith, D. A. Schultz, and S. Schultz, "Shape effects in plasmon resonance of individual colloidal silver nanoparticles," *J. Chem. Phys.*, vol. 116, p. 6755, 2002.

[44] W. Rechberger, A. Hohenau, *et al.*, "Optical properties of two interacting gold nanoparticles," *Optics Communications*, vol. 220, no. 1-3, pp. 137–141, 2003.

[45] A. V. Kildishev, W. Cai, *et al.*, "Negative refractive index in optics of metal-dielectric composites," *J. Opt. Soc. Am. B*, vol. 23, no. 3, pp. 423–433, 2006.

[46] E. Cubukcu, E. A. Kort, K. B. Crozier, and F. Capasso, "Plasmonic laser antenna," *Appl. Phys. Lett.*, vol. 89, p. 093120, 2006.

[47] L. Gunnarsson, T. Rindzevicius, *et al.*, "Confined plasmons in nanofabricated single silver particle pairs: experimental observations of strong interparticle interactions," *J. Phys. Chem. B*, vol. 109, no. 3, pp. 1079–1087, 2005.

[48] T. Atay, J. H. Song, and A. V. Nurmikko, "Strongly interacting plasmon nanoparticle pairs: from dipole-dipole interaction to conductively coupled regime," *Nano Lett.*, vol. 4, no. 9, pp. 1627–1632, 2004.

[49] K. H. Su, Q. H. Wei, *et al.*, "Interparticle coupling effects on plasmon resonances of nanogold particles," *Nano Lett.*, vol. 3, no. 8, pp. 1087–1090, 2003.

[50] A. Sundaramurthy, P. J. Schuck, *et al.*, "Toward nanometer-scale optical photolithography: utilizing the near-field of bowtie optical nanoantennas," *Nano Lett.*, vol. 6, no. 3, pp. 355–360, 2006.

[51] S. Lal, S. Link, and N. J. Halas, "Nano-optics from sensing to waveguiding," *Nature photonics*, vol. 1, no. 11, pp. 641–648, 2007.

[52] A. J. Haes, S. Zou, G. C. Schatz, and R. P. V. Duyne, "Nanoscale optical biosensor: short range distance dependence of the localized surface plasmon resonance of noble metal nanoparticles," *J. Phys. Chem. B*, vol. 108, no. 22, pp. 6961–6968, 2004.

[53] L. A. Sweatlock, S. A. Maier, H. A. Atwater, J. J. Penninkhof, and A. Polman, "Highly confined electromagnetic fields in arrays of strongly coupled Ag nanoparticles," *Phys. Rev. B*, vol. 71, no. 23, p. 235408, 2005.

[54] D. A. Genov, A. K. Sarychev, V. M. Shalaev, and A. Wei, "Resonant field enhancements from metal nanoparticle arrays," *Nano Lett.*, vol. 4, pp. 153–158, 2004.

[55] J. Hao and G. W. Hanson, "Electromagnetic scattering from finite-length metallic carbon nanotubes in the lower IR bands," *Phys. Rev. B*, vol. 74, no. 3, p. 35119, 2006.

[56] Z. J. Zhang, R. W. Peng, *et al.*, "Plasmonic antenna array at optical frequency made by nanoapertures," *Appl. Phys. Lett.*, vol. 93, p. 171110, 2008.

[57] S. A. Maier, M. L. Brongersma, *et al.*, "Plasmonics-A route to nanoscale optical devices," *Adv. Mater.*, vol. 13, no. 19, pp. 1501–1505, 2001.

[58] C. F. Bohren and D. R. Huffman, *Absorption and scattering of light by small particles*. New York: John Wiley & Sons, 1983.

[59] R. M. Bakker, "Optical nanoantennae: Enhanced electromagnetic fields and enhanced fluorescence," Ph.D. dissertation, Purdue University, 2008.

[60] M. C. Beard and C. A. Schmuttenmaer, "Using the finite-difference time-domain pulse propagation method to simulate time-resolved THz experiments," *J. Chem. Phys.*, vol. 114, p. 2903, 2001.

[61] J. T. K. II, E. Sánchez, and X. S. Xie, "Design of near-field optical probes with optimal field enhancement by finite difference time domain electromagnetic simulation," *J. Chem. Phys.*, vol. 116, pp. 10 895–10 901, 2002.

[62] S. K. Gray and T. Kupka, "Propagation of light in metallic nanowire arrays: Finite-difference time-domain studies of silver cylinders," *Phys. Rev. B*, vol. 68, no. 4, p. 45415, 2003.

[63] M. Futamata, Y. Maruyama, and M. Ishikawas, "Local electric field and scattering cross section of Ag nanoparticles under surface plasmon resonance by finite difference time domain method," *J. Phys. Chem. B*, vol. 107, no. 31, pp. 7607–7617, 2003.

[64] A. K. Azad, Y. Zhao, W. Zhang, and M. He, "Effect of dielectric properties of metals on terahertz transmission subwavelength hole arrays," *Opt. Lett.*, vol. 31, no. 17, pp. 2637–2639, 2006.

[65] K. Y. Jung, F. L. Teixeira, and R. M. Reano, "Au/SiO_2 Nanoring Plasmon Waveguides at Optical Communication Band," *J. Lightwave Technol.*, vol. 25, no. 9, pp. 2757–2765, 2007.

[66] C. Hafner, "Drude model replacement by symbolic regression," *J. Comput. Theor. Nanosci.*, vol. 2, pp. 88–98, 2005.

[67] R. Qiang, R. L. Chen, and J. Chen, "Modeling electrical properties of gold films at infrared frequency using FDTD method," *Int. J. Infrared Millimet. Waves*, vol. 25, no. 8, pp. 1263–1270, 2004.

[68] R. J. Zhu, J. Wang, and G. F. Jin, "Mie scattering calculation by FDTD employing a modified Debye model for Gold material," *Optik-International Journal for Light and Electron Optics*, vol. 116, no. 9, pp. 419–422, 2005.

[69] R. Qiang, J. Chen, *et al.*, "Modelling of infrared bandpass filters using three-dimensional FDTD method," *Electron. Lett.*, vol. 41, p. 914, 2005.

[70] H. Gai, J. Wang, and Q. Tian, "Modified Debye model parameters of metals applicable for broadband calculations," *Appl. Opt.*, vol. 46, pp. 2229–2233, 2007.

[71] H. Ehrenreich and H. R. Philipp, "Optical properties of Ag and Cu," *Phys. Rev.*, vol. 128, no. 4, pp. 1622–1629, 1962.

[72] P. B. Johnson and R. W. Christy, "Optical constants of the noble metals," *Phys. Rev. B*, vol. 6, pp. 4370–4379, 1972.

[73] M. A. Ordal, L. L. Long, *et al.*, "Optical properties of the metals Al, Co, Cu, Au, Fe, Pb, Ni, Pd, Pt, Ag, Ti, and W in the infrared and far infrared," *Appl. Opt.*, vol. 22, no. 7, pp. 1099–1119, 1983.

[74] K. Y. Jung and F. L. Teixeira, "Multispecies ADI-FDTD algorithm for nanoscale three-dimensional photonic metallic structures," *IEEE Photonics Technology Letters*, vol. 19, no. 8, pp. 586–588, 2007.

[75] A. D. Rakic, A. B. Djurisic, J. M. Elazar, and M. L. Majewski, "Optical properties of metallic films for vertical-cavity optoelectronic devices," *Appl. Opt.*, vol. 37, pp. 5271–5283, 1998.

[76] A. Vial, A. Grimault, D. Macías, D. Barchiesi, and M. L. de La Chapelle, "Improved analytical fit of gold dispersion: Application to the modeling of extinction spectra with a finite-difference time-domain method," *Phys. Rev. B*, vol. 71, p. 085416, 2005.

[77] G. Schiderand, J. R. Krenn, *et al.*, "Plasmon dispersion relation of Au and Ag nanowires," *Phys. Rev. B*, vol. 68, no. 15, p. 155427, 2003.

[78] F. J. González, J. Alda, J. Simón, J. Ginn, and G. Boreman, "The effect of metal dispersion on the resonance of antennas at infrared frequencies," *Infrared Physics & Technology*, vol. 52, no. 1, pp. 48–51, 2009.

[79] E. D. Palik and G. Ghosh, *Handbook of optical constants of solids*. Academic press, New York, 1998.

[80] A. Alù and N. Engheta, "Input impedance, nanocircuit loading, and radiation tuning of optical nanoantennas," *Phys. Rev. Lett.*, vol. 101, no. 4, p. 43901, 2008.

[81] C. A. Balanis, *Antenna Theory: Analysis and Design*, The 2nd ed. New York: John Wiley & Sons, 1997.

[82] M. L. Brongersma and P. G. Kik, *Surface plasmon nanophotonics*. The Netherlands: Springer Verlag, 2007.

[83] J. D. Jackson, *Classical Electrodynamics*, The 2nd ed. New York: Wiley, 1999.

[84] H. Wang, "Tunable plasmonic nanostructures: from fundamental nanoscale optics to surface-enhanced spectroscopies," Ph.D. dissertation, Rice University, 2007.

[85] U. Kreibig and M. Vollmer, *Optical properties of metal clusters*. Berlin: Springer, 1995.

[86] G. Mie, "Articles on the optical characteristics of turbid tubes, especially colloidal metal solutions," *Ann. Phys*, vol. 25, no. 3, pp. 377–445, 1908.

[87] A. L. Aden and M. Kerker, "Scattering of electromagnetic waves from two concentric spheres," *J. Appl. Phys.*, vol. 22, p. 1242, 1951.

[88] J. A. Kong, *Electromagnetic Wave Theory*. EMW Publishing, Cambridge, MA, 2000.

[89] M. Meier and A. Wokaun, "Enhanced fields on large metal particles: dynamic depolarization," *Opt. Lett.*, vol. 8, no. 11, pp. 581–583, 1983.

[90] H. Kuwata, H. Tamaru, K. Esumi, and K. Miyano, "Resonant light scattering from metal nanoparticles: Practical analysis beyond Rayleigh approximation," *Appl. Phys. Lett.*, vol. 83, pp. 4625–2627, 2003.

[91] S. A. Maier, *Plasmonics: fundamentals and applications*. Springer Verlag, 2007.

[92] S. Pillai, K. R. Catchpole, T. Trupke, and M. A. Green, "Surface plasmon enhanced silicon solar cells," *J. Appl. Phys.*, vol. 101, p. 093105, 2007.

[93] D. Derkacs, S. H. Lim, P. Matheu, W. Mar, and E. T. Yu, "Improved performance of amorphous silicon solar cells via scattering from surface plasmon polaritons in nearby metallic nanoparticles," *Appl. Phys. Lett.*, vol. 89, p. 093103, 2006.

[94] M. N. O. Mattew and O. Sadiku, *Numerical techniques in electromagnetics*. CRC Press Boca Raton, FL, 2000.

[95] D. M. Sullivan, *Electromagnetic simulation using the FDTD method*. IEEE press New York, 2000.

[96] A. Taflove, S. C. Hagness, *et al.*, *Computational electrodynamics: the finite-difference time-domain method*. Artech House Norwood, MA, 1995.

[97] R. F. Harrington, *Field computation by moment methods*. Wiley-IEEE Press, 1993.

[98] A. Sundaramurthy, K. B. Crozier, *et al.*, "Field enhancement and gap-dependent resonance in a system of two opposing tip-to-tip Au nanotriangles," *Phys. Rev. B*, vol. 72, no. 16, p. 165409, 2005.

[99] E. J. Smythe, E. Cubukcu, and F. Capasso, "Optical properties of surface plasmon resonances of coupled metallic nanorods," *Opt. Express*, vol. 15, pp. 7439–7447, 2007.

[100] C. Hafner, X. Cui, A. Bertolace, and R. Vahldieck, "Frequency-domain simulations of optical antenna structures," in *Proceedings of SPIE*, vol. 6617, 2007, p. 66170E.

[101] C. Rockstuhl, M. G. Salt, and H. P. Herzig, "Application of the boundary-element method to the interaction of light with single and coupled metallic nanoparticles," *J. Opt. Soc. Am. A*, vol. 20, no. 10, pp. 1969–1973, 2003.

[102] L. N. Illyashenko-Raguin, "Analysis of channel plasmon-polariton nanoantennas based on a meshless boundary integral equation approach," in *Proceedings of SPIE*, vol. 6987, 2008, p. 69870X.

[103] L. Novotny, R. X. Bian, and X. S. Xie, "Theory of nanometric optical tweezers," *Phys. Rev. Lett.*, vol. 79, no. 4, pp. 645–648, 1997.

[104] R. M. Bakker, A. Boltasseva, *et al.*, "Near-field excitation of nanoantenna resonance," *Opt. Express*, vol. 15, pp. 13 682–13 688, 2007.

[105] M. W. Knight and N. J. Halas, "Nanoshells to nanoeggs to nanocups: optical properties of reduced symmetry core–shell nanoparticles beyond the quasistatic limit," *New Journal of Physics*, vol. 10, p. 105006, 2008.

[106] G. Shvets, S. Trendafilov, J. B. Pendry, and A. Sarychev, "Guiding, focusing, and sensing on the subwavelength scale using metallic wire arrays," *Phys. Rev. Lett.*, vol. 99, no. 5, p. 53903, 2007.

[107] J. S. Huang, T. Feichtner, P. Biagioni, and B. Hecht, "Impedance matching and emission properties of nanoantennas in an optical nanocircuit," *Nano Lett.*, vol. 9, no. 5, pp. 1897–1902, 2009.

[108] M. H. Chowdhury, S. K. Gray, J. Pond, C. D. Geddes, K. Aslan, and J. R. Lakowicz, "Computational study of fluorescence scattering by silver nanoparticles," *J. Opt. Soc. Am. B*, vol. 24, no. 9, pp. 2259–2267, 2007.

[109] S. E. Sburlan, L. A. Blanco, and M. Nieto-Vesperinas, "Plasmon excitation in sets of nanoscale cylinders and spheres," *Phys. Rev. B*, vol. 73, p. 035403, 2006.

[110] C. R. Simovski, A. J. Viitanen, and S. A.Tretyakov, "Resonator mode in chains of silver spheres and its possible application," *Phys. Rev. E*, vol. 72, no. 6, p. 66606, 2005.

[111] G. H. Chan, J. Zhao, E. M. Hicks, G. C. Schatz, and R. P. V. Duyne, "Plasmonic properties of copper nanoparticles fabricated by nanosphere lithography," *Nano Lett.*, vol. 7, no. 7, pp. 1947–1952, 2007.

[112] A. Mohammadi, V. Sandoghdar, and M. Agio, "Gold, copper, silver and aluminum nanoantennas to enhance spontaneous emission," *J. Comput. Theor. Nanosci.*, vol. 6, pp. 2024–2030, 2009.

[113] C. Genet and T. W. Ebbesen, "Light in tiny holes," *Nature*, vol. 445, no. 7123, pp. 39–46, 2007.

[114] L. Wang and X. Xu, "High transmission nanoscale bowtie-shaped aperture probe for near-field optical imaging," *Appl. Phys. Lett.*, vol. 90, p. 261105, 2007.

[115] R. M. Bakker, H. K. Yuan, *et al.*, "Enhanced localized fluorescence in plasmonic nanoantennae," *Appl. Phys. Lett.*, vol. 92, p. 043101, 2008.

[116] C. E. Webb and J. D. C. Jones, *Handbook of Laser Technology and Applications: Laser design and laser systems.* Philadelphia, 2004.

[117] G. Volpe, S. Cherukulappurath, R. J. Parramon, G. Molina-Terriza, and R. Quidant, "Controlling the Optical Near Field of Nanoantennas with Spatial Phase-Shaped Beams," *Nano Lett.*, vol. 9, no. 10, pp. 3608–3611, 2009.

[118] L. B. Scaffardi, N. Pellegri, O. D. Sanctis, and J. O. Tocho, "Sizing gold nanoparticles by optical extinction spectroscopy," *Nanotechnology*, vol. 16, pp. 158–163, 2005.

[119] K. C. Vernon, A. M. Funston, C. Novo, D. E. Gomez, P. Mulvaney, and T. J. Davis, "Influence of Particle- Substrate Interaction on Localized Plasmon Resonances," *Nano Lett.*, vol. 10, no. 6, pp. 2080–2086, 2010.

[120] T. R. Jensen, M. L. Duval, *et al.*, "Nanosphere lithography: effect of the external dielectric medium on the surface plasmon resonance spectrum of a periodic array of silver nanoparticles," *J. Phys. Chem. B*, vol. 103, no. 45, pp. 9846–9853, 1999.

[121] P. F. Liao and A. Wokaun, "Lightning rod effect in surface enhanced Raman scattering," *J. Chem. Phys.*, vol. 76, p. 751, 1982.

[122] R. Jin, Y. W. Cao, C. A. Mirkin, K. L. Kelly, G. C. Schatz, and J. G. Zheng, "Photoinduced conversion of silver nanospheres to nanoprisms," *Science*, vol. 294, no. 5548, p. 1901, 2001.

[123] J. J. Mock, D. R. Smith, and S. Schultz, "Local refractive index dependence of plasmon resonance spectra from individual nanoparticles," *Nano Lett.*, vol. 3, no. 4, pp. 485–491, 2003.

[124] P. K. Jain and M. A. El-Sayed, "Noble metal nanoparticle pairs: Effect of medium for enhanced nanosensing," *Nano Lett.*, vol. 8, no. 12, pp. 4347–4352, 2008.

[125] J. P. Kottmann and O. J. F. Martin, "Retardation-induced plasmon resonances in coupled nanoparticles," *Opt. Lett.*, vol. 26, no. 14, pp. 1096–1098, 2001.

[126] H. Tamaru, H. Kuwata, H. T. Miyazaki, and K. Miyano, "Resonant light scattering from individual Ag nanoparticles and particle pairs," *Appl. Phys. Lett.*, vol. 80, p. 1826, 2002.

[127] P. K. Jain, W. Huang, M. A. El-Sayed, and P. Nordlander, "On the universal scaling behavior of the distance decay of plasmon coupling in metal nanoparticle pairs: a plasmon ruler equation," *Nano Lett.*, vol. 7, pp. 2080–2088, 2007.

[128] H. Gai, J. Wang, and Q. Tian, "Tuning the resonant wavelength of a nanometric bow-tie aperture by altering the relative permittivity of the dielectric substrate," *J. Nanophotonics*, vol. 1, no. 013555, p. 013555, 2007.

[129] J. Merlein, M. Kahl, *et al.*, "Nanomechanical control of an optical antenna," *Nature Photonics*, vol. 2, no. 4, pp. 230–233, 2008.

[130] H. Fischer and O. J. F. Martin, "Engineering the optical response of plasmonic nanoantennas," *Opt. Express*, vol. 16, pp. 9144–9154, 2008.

[131] E. Cubukcu, N. Yu, *et al.*, "Plasmonic Laser Antennas and Related Devices," *IEEE J. Sel. Topics Quantum Electron.*, vol. 14, no. 6, pp. 1448–1461, 2008.

[132] D. P. Fromm, A. Sundaramurthy, P. J. Schuck, G. Kino, and W. E. Moerner, "Gap-dependent optical coupling of single bowtie nanoantennas resonant in the visible," *Nano Lett.*, vol. 4, no. 5, pp. 957–961, 2004.

[133] R. D. Grober, R. J. Schoelkopf, and D. E. Prober, "Optical antenna: Towards a unity efficiency near-field optical probe," *Appl. Phys. Lett.*, vol. 70, p. 1354, 1997.

[134] N. Yu, E. Cubukcu, L. Diehl, *et al.*, "Bowtie plasmonic quantum cascade laser antenna," *Opt. Express*, vol. 15, no. 20, pp. 13 272–13 281, 2007.

[135] T. Thio, H. J. Lezec, *et al.*, "Giant optical transmission of sub-wavelength apertures: physics and applications," *Nanotechnology*, vol. 13, p. 429, 2002.

[136] E. X. Jin and X. Xu, "Plasmonic effects in near-field optical transmission enhancement through a single bowtie-shaped aperture," *Appl. Phys. B*, vol. 84, pp. 3–9, 2006.

[137] E. X. Jin and X. Xu, "Obtaining super resolution light spot using surface plasmon assisted sharp ridge nanoaperture," *Appl. Phys. Lett.*, vol. 86, p. 111106, 2005.

[138] X. Shi, L. Hesselink, and R. L. Thornton, "Ultrahigh light transmission through a C-shaped nanoaperture," *Opt. Lett.*, vol. 28, no. 15, pp. 1320–1322, 2003.

[139] X. Eric and X. Xu, "Finitte-difference time-domain studies on optical transmission through planar nano-apertures in a metal film," *Japanese Journal of Applied Physics*, vol. 43, no. 1, pp. 407–417, 2004.

[140] L. Wang, S. M. Uppuluri, E. X. Jin, and X. Xu, "Nanolithography using high transmission nanoscale bowtie apertures," *Nano Lett.*, vol. 6, no. 3, pp. 361–364, 2006.

[141] J. Xu, J. Wang, and Q. Tian, "Design and analysis of bow tie aperture with strong near-field enhancement effect," in *Proceedings of SPIE*, vol. 5635, 2005, p. 284.

[142] A. Curry, G. Nusz, A. Chilkoti, and A. Wax, "Substrate effect on refractive index dependence of plasmon resonance for individual silver nanoparticles observed using darkfield microspectroscopy," *Opt. Express*, vol. 13, no. 7, pp. 2668–2677, 2005.

[143] W. A. Murray, B. Auguié, and W. L. Barnes, "Sensitivity of Localized Surface Plasmon Resonances to Bulk and Local Changes in the Optical Environment," *J. Phys. Chem. C*, vol. 113, no. 7, pp. 5120–5125, 2009.

[144] E. Popov, M. Nevière, *et al.*, "Single-scattering theory of light diffraction by a circular subwavelength aperture in a finitely conducting screen," *J. Opt. Soc. Am. A*, vol. 24, no. 2, pp. 339–358, 2007.

[145] H. A. Bethe, "Theory of diffraction by small holes," *Phys. Rev.*, vol. 66, no. 7-8, pp. 163–182, 1944.

[146] A. Alù and N. Engheta, "Enhanced directivity from subwavelength infrared/optical nano-antennas loaded with plasmonic materials or metamaterials," *IEEE Trans. Antennas Propag.*, vol. 55, no. 11, p. 3027, 2007.

[147] M. Quinten, A. Leitner, J. R. Krenn, and F. R. Aussenegg, "Electromagnetic energy transport via linear chains of silver nanoparticles," *Opt. Lett.*, vol. 23, no. 17, pp. 1331–1333, 1998.

[148] S. A. Maier, P. G. Kik, *et al.*, "Local detection of electromagnetic energy transport below the diffraction limit in metal nanoparticle plasmon waveguides," *Nature Materials*, vol. 2, no. 4, pp. 229–232, 2003.

[149] S. A. Maier, P. G. Kik, and H. A. Atwater, "Optical pulse propagation in metal nanoparticle chain waveguides," *Phys. Rev. B*, vol. 67, no. 20, p. 205402, 2003.

[150] S. A. Maier, P. G. Kik, and H. A. Atwater, "Observation of coupled plasmon-polariton modes in au nanoparticle chain waveguides of different lengths: Estimation of waveguide loss," *Appl. Phys. Lett.*, vol. 81, no. 9, pp. 1714–1716, 2002.

[151] J. R. Krenn, A. Dereux, *et al.*, "Squeezing the optical near-field zone by plasmon coupling of metallic nanoparticles," *Phys. Rev. Lett.*, vol. 82, no. 12, pp. 2590–2593, 1999.

[152] K. R. Li, M. I. Stockman, and D. J. Bergman, "Self-similar chain of metal nanospheres as an efficient nanolens," *Phys. Rev. Lett.*, vol. 91, no. 22, p. 227402, 2003.

[153] K. Li, M. I. Stockman, and D. J. Bergman, "Enhanced second harmonic generation in a self-similar chain of metal nanospheres," *Phys. Rev. B*, vol. 72, p. 153401, 2005.

[154] Z. P. Li, Z. L. Yang, and H. X. Xu, "Comment on "self-similar chain of metal nanospheres as an efficient nanolens"," *Phys. Rev. Lett.*, vol. 97, no. 7, p. 079701, 2006.

[155] V. M. Shalaev, W. Cai, *et al.*, "Negative index of refraction in optical metamaterials," *Opt. Lett.*, vol. 30, no. 24, pp. 3356–3358, 2005.

[156] E. Prodan and P. Nordlander, "Structural tunability of the plasmon resonances in metallic nanoshells," *Nano Lett.*, vol. 3, no. 4, pp. 543–547, 2003.

[157] H. Wang, J. Kundu, and N. J. Halas, "Plasmonic Nanoshell arrays combine surface-enhanced vibrational spectroscopies on a single substrate," *Angew. Chem. Int. Edn*, vol. 46, no. 47, pp. 9040–9044, 2007.

[158] A. O. Pinchuk and G. C. Schatz, "Collective surface plasmon resonance coupling in silver nanoshell arrays," *Appl. Phys. B*, vol. 93, no. 1, pp. 31–38, 2008.

[159] J. Li and N. Engheta, "Self-similar optical antenna arrays composed of multiple core-shell plasmonic nanoparticles," in *Proceedings of 2007 IEEE Antennas and Propagation Society International Symposium*, 2007, pp. 3388–3391.

[160] J. Li, A. Salandrino, and N. Engheta, "Shaping light beams in the nanometer scale: A Yagi-Uda nanoantenna in the optical domain," *Phys. Rev. B*, vol. 76, no. 24, p. 245403, 2007.

[161] H. F. Hofmann, T. Kosako, and Y. Kadoya, "Design parameters for a nano-optical Yagi–Uda antenna," *New J. Phys.*, vol. 9, p. 217, 2007.

[162] J. Li, A. Salandrino, and N. Engheta, "Optical spectrometer at the nanoscale using optical Yagi-Uda nanoantennas," *Phys. Rev. B*, vol. 79, no. 19, p. 195104, 2009.

[163] J. Li, "Theory of optical nanoantennas and arrays based on surface plasmon resonance of plasmonic nanoparicles," Ph.D. dissertation, University of Pennsylvania, 2007.

[164] A. J. Viitanen and S. A. Tretyakov, "Metawaveguides formed by arrays of small resonant particles over a ground plane," *J. Opt. A: Pure Appl. Opt.*, vol. 7, p. S133, 2005.

[165] P. Anger, P. Bharadwaj, and L. Novotny, "Enhancement and quenching of single-molecule fluorescence," *Phys. Rev. Lett.*, vol. 96, no. 11, p. 113002, 2006.

[166] A. Alù and N. Engheta, "Tuning the scattering response of optical nanoantennas with nanocircuit loads," *Nature photonics*, vol. 2, no. 5, pp. 307–310, 2008.

Curriculum Vitae

WU YU-MING

Education

2002-2006	Harbin Institute of Technology, Harbin, China B. Eng. degree, Communication Engineering
2006-2010	National Univ. of Singapore, Singapore Ph.D. degreee, Electrical and Computer Engineering

Experience

2009-2010	National University of Singapore, Singapore Graduate Assistant

Honors and Awards

2006-2010	NUS Graduate Scholarship
2010	Invited talk in 2010 Asia-Pacific EMC Symposium and EMC-Zurich (APEMC2010)
2009	Shortlisted in Asia-Pacific Microwave Conference (APMC) Student Paper Contest
2009	IEEE Regional 10 Student Paper Contest, 2nd Position
2006	Outstanding Graduate, Heilongjiang Province, China
2005	China CNPC-Scholarship, China Petroleum and Chemical Corporation
2002-2006	Undergraduate Scholarship, HIT
2003,2005	Outstanding Student, HIT

Activities

Student Member	IEEE, AP, MTT and Photonics Societies, 2005-Present